Lawrence Berkeley National Laboratory
LBL Publications

Title
Axions at the meV crossroads: theory, cosmology, astrophysics, and experiments

Permalink
https://escholarship.org/uc/item/7mb0k407

Journal
Journal of Cosmology and Astroparticle Physics, 2026(07)

Authors
Cicoli, Michele
D'Eramo, Francesco
Luzio, Luca Di
et al.

Publication Date
2026-07-01

DOI
10.1088/1475-7516/2026/07/060

Copyright Information
This work is made available under the terms of a Creative Commons Attribution License, available at https://creativecommons.org/licenses/by/4.0/

Peer reviewed

eScholarship.org Powered by the California Digital Library
University of California

Journal of Cosmology
and Astroparticle
Physics

SISSA

PAPER • OPEN ACCESS

Axions at the meV crossroads: theory, cosmology, astrophysics, and experiments

To cite this article: Michele Cicoli *et al* JCAP07(2026)060

View the article online for updates and enhancements.

You may also like

- Direct detection of dark matter—APPEC committee report
Julien Billard, Mark Boulay, Susana Cebrián et al.
- Physics beyond colliders at CERN: beyond the Standard Model working group report
J Beacham, C Burrage, D Curtin et al.
- Physics potential of the International Axion Observatory (IAXO)
E. Armengaud, D. Attié, S. Basso et al.

This content was downloaded from IP address 108.75.79.166 on 16/11/2026 at 23:41

Journal of Cosmology and Astroparticle Physics
An IOP and SISSA journal

Received: March 21, 2026
Revised: May 15, 2026
Accepted: May 25, 2026
Published: July 16, 2026

Axions at the meV crossroads: theory, cosmology, astrophysics, and experiments

Michele Cicoli,[a,b] **Francesco D'Eramo**,[c,d] **Luca Di Luzio**,[d] **Damiano F.G. Fiorillo**,[e,f] **Maurizio Giannotti**,[g,h,i,*] **Alicia Gomez**,[j] **Diego Guadagnoli**,[k] **Mathieu Kaltschmidt**,[g,h] **Bradley J. Kavanagh**,[l] **Alessandro Lella**,[c,d] **Giuseppe Lucente**,[m] **David J.E. Marsh**,[n] **Federico Mescia**,[o] **Alessandro Mirizzi**,[p,q,*] **Javier Redondo**,[g,h] **Nicole Righi**,[r,s] **Jaime Ruz**,[t] **Ken'ichi Saikawa**,[u] **Elisa Todarello**,[v,w,x] **Edoardo Vitagliano**[c,d] **and Su-Yang Xu**[y]

[a] *Dipartimento di Fisica e Astronomia, Università di Bologna, via Irnerio 46, 40126 Bologna, Italy*
[b] *INFN, Sezione di Bologna, viale Berti Pichat 6/2, 40127 Bologna, Italy*
[c] *Dipartimento di Fisica e Astronomia, Università degli Studi di Padova, Via Marzolo 8, 35131 Padova, Italy*
[d] *Istituto Nazionale di Fisica Nucleare (INFN), Sezione di Padova, Via Marzolo 8, 35131 Padova, Italy*
[e] *Istituto Nazionale di Fisica Nucleare (INFN), Sezione di Napoli, Complesso Universitario di Monte Sant'Angelo, Via Cintia, 80126 Napoli, Italy*
[f] *Gran Sasso Science Institute, Viale F. Crispi 7, L'Aquila, 67100, Italy*
[g] *Departamento de Física Teórica, Universidad de Zaragoza, C. de Pedro Cerbuna 12, 50009 Zaragoza, Spain*
[h] *Centro de Astropartículas y Física de Altas Energías, Universidad de Zaragoza, C. de Pedro Cerbuna 12, 50009 Zaragoza, Spain*
[i] *Department of Chemistry and Physics, Barry University, 11300 NE 2nd Ave., Miami Shores, FL 33161, U.S.A.*
[j] *Centro de Astrobiología, INTA-CSIC, Ctra. Torrejón-Ajalvir km.4, Torrejón de Ardoz, 28850, Madrid, Spain*
[k] *LAPTh, Université Savoie Mont-Blanc et CNRS, 74941 Annecy, France*
[l] *Instituto de Física de Cantabria (IFCA, UC-CSIC), Av. de Los Castros s/n, 39005 Santander, Spain*
[m] *SLAC National Accelerator Laboratory, 2575 Sand Hill Rd, Menlo Park, CA 94025, U.S.A.*
[n] *Physics Department, King's College London, Strand, London WC2R 2LS, U.K.*

*Corresponding author.

© 2026 The Author(s). Published by IOP Publishing Ltd on behalf of Sissa Medialab. Original content from this work may be used under the terms of the Creative Commons Attribution 4.0 licence. Any further distribution of this work must maintain attribution to the author(s) and the title of the work, journal citation and DOI.

https://doi.org/10.1088/1475-7516/2026/07/060

JCAP07(2026)060

[o] *Istituto Nazionale di Fisica Nucleare, Laboratori Nazionali di Frascati, 00044 Frascati, Italy*
[p] *Dipartimento Interuniversitario di Fisica "Michelangelo Merlin", Via Amendola 173, 70126 Bari, Italy*
[q] *Istituto Nazionale di Fisica Nucleare – Sezione di Bari, Via Orabona 4, 70126 Bari, Italy*
[r] *Scuola Normale Superiore, Piazza dei Cavalieri 7, 56126 Pisa, Italy*
[s] *INFN, Sezione di Pisa, Largo Bruno Pontecorvo 3, 56127 Pisa, Italy*
[t] *Fakultät für Physik, Technische Universität Dortmund, D-44221 Dortmund, Germany*
[u] *Institute for Theoretical Physics, Kanazawa University, Kakuma-machi, Kanazawa, Ishikawa 920-1192, Japan*
[v] *Leinweber Institute for Theoretical Physics, University of California, Berkeley, CA 94720, U.S.A.*
[w] *Theoretical Physics Group, Lawrence Berkeley National Laboratory, Berkeley, CA 94720, U.S.A.*
[x] *Università degli Studi di Torino, via P. Giuria 1, I–10125 Torino, Italy*
[y] *Department of Chemistry and Chemical Biology, Harvard University, MA 02138, U.S.A.*

E-mail: mgiannotti@unizar.es, Alessandro.Mirizzi@ba.infn.it

Abstract: The meV mass range has emerged as a focal point in axion physics, where advances in theory, cosmology, astrophysics, and experimental techniques converge. Axions in this mass range are theoretically well motivated, can arise in ultraviolet-complete models, and can have significant cosmological impacts as dark matter or dark radiation. In parallel, their efficient production in stellar and supernova environments provides powerful astrophysical probes. Here, we provide a comprehensive overview of meV axions across these domains, highlighting both established results and open questions. We discuss the theoretical underpinnings of meV axions, their cosmological and astrophysical signatures, and the diverse experimental strategies — ranging from helioscopes and haloscopes to quasiparticle systems and large-volume Cherenkov detectors — that aim to explore this regime. The convergence of these approaches emphasizes the pivotal role of the meV mass range for axion discovery in the coming years, identifying meV axions as a key probe for testing beyond-Standard-Model physics. This review document is the direct outcome of the discussions at the dedicated workshop "The meV Mass Axion Frontier: Challenges and Opportunities", held at Laboratori Nazionali di Frascati (IT) on 27–28 October 2025, and organized by the EU funded COST Action *"Cosmic WISPers in the Dark Universe: Theory, astrophysics, and experiments"* (CA21106, https://www.cost.eu/actions/CA21106). Its aim is to provide an overview of current efforts in meV axion research, their motivations, and the research goals that animate the community involved in this search.

Keywords: core-collapse supernovae, dark matter experiments, dark matter theory

ArXiv ePrint: 2603.18167

JCAP07(2026)060

Contents

1 Introduction 1

2 meV axions model building 3
- 2.1 Axion quality problem 5
- 2.2 meV axions from string theory 7

3 meV axions as cold dark matter 15

4 meV axions as dark radiation 19
- 4.1 Thermal production of axions 20
- 4.2 Dark radiation as a cosmological consequence 22
- 4.3 Thermal axions: what's next? 23

5 meV axions astrophysics 24
- 5.1 Axion production in dense nuclear media 24
- 5.2 Axion conversion in astrophysical magnetic fields 26
- 5.3 Supernova axions in large-volume Cherenkov detectors 28

6 meV axions experiments 34
- 6.1 Extending axion mass sensitivity in CAST 35
- 6.2 Axion mass-scanning strategy of BabyIAXO 37
- 6.3 Post-discovery strategies for axion mass determination 38
- 6.4 Pushing the haloscope searches towards the meV range: The CADEx experiment 40
- 6.5 meV axion quasiparticles 42

7 Discussion and conclusions 46

A List of acronyms 51

JCAP07(2026)060

1 Introduction

More than a decade ago, ref. [1] articulated the case for the "meV mass frontier" of axion physics. That work drew attention to the fact that axions with masses of a few meV — lying just below the astrophysical sensitivity threshold set by stellar cooling arguments — occupy a uniquely interesting region of parameter space for QCD axions. The original motivation was rooted in the intriguing hint that white-dwarf (WD) cooling rates could be explained by axion emission with an electron coupling $g_{ae} \sim 10^{-13}$, corresponding to decay constants $f_a \sim 5 \times 10^9\,\text{GeV}$ and masses $m_a \sim \mathcal{O}(\text{meV})$. While the detection prospects for the diffuse supernova axion background appeared daunting, ref. [1] emphasised that next-generation helioscopes could realistically probe this regime, thereby establishing the meV mass range as an experimentally accessible target. Since then, the physics case for meV axions has strengthened considerably across multiple fronts, from theoretical developments to cosmological considerations and astrophysical observations.

On the theoretical side, developments in string phenomenology have revealed that meV-scale QCD axions can emerge in large classes of ultraviolet-complete scenarios. In type IIB models with stabilised moduli, meV QCD axions can be realised as either closed string

axions associated to blow-up cycles [2–5], or as open string axions on sequestered branes at singularities [6–9]. When the QCD axion is a closed string, its decay constant is typically of order the string scale, resulting in a pre-inflationary scenario with a non-linearly realised Peccei-Quinn (PQ) symmetry. In models with a relatively small number of Kähler moduli, the QCD axion decay constant can take a large range of values with a statistical logarithmic preference for higher values [4]. Interestingly, when instead the number of Kähler moduli is very large, the requirement to trust the low-energy theory does not allow for large decay constants, resulting in an upper bound on the QCD axion mass around the meV range [10, 11]. On the other hand, if the QCD axion is an open string, its decay constant is suppressed with respect to the string scale, leaving the possibility to realise a post-inflationary scenario. Concurrently, field-theoretic approaches to the PQ quality problem — the requirement that PQ-breaking operators be highly suppressed to preserve the solution to the strong CP problem — favour relatively low values of f_a, again pointing towards meV masses as theoretically preferred.

From the cosmological perspective, meV axions occupy a distinctive niche. They are too heavy to constitute the dominant cold dark matter component via the standard misalignment mechanism with $\mathcal{O}(1)$ initial angles, yet they remain viable dark matter candidates under alternative production scenarios such as large-misalignment tuning, kinetic misalignment, or post-inflationary dynamics with domain-wall number $N_{\rm DW} > 1$. Simultaneously, thermal production in the early Universe renders meV axions a natural target for precision cosmology: future cosmic microwave background (CMB) experiments, including the Simons Observatory, will achieve sensitivity to the contribution of thermal axions to the effective number of relativistic species, $\Delta N_{\rm eff}$, precisely in the mass range where astrophysical probes currently set the strongest bounds.

Astrophysical constraints themselves have undergone significant refinement. Observations of neutron-star cooling now provide limits competitive with the classical supernova 1987A bound, placing the current sensitivity at $m_a \lesssim 10$–20 meV for KSVZ-type models. The theoretical understanding of axion emission from dense nuclear matter — including the role of nucleon spin fluctuations, pionic processes, and in-medium modifications — has matured, clarifying both the robustness and the residual uncertainties of these bounds. Furthermore, novel detection strategies have emerged: axion-to-photon conversion in the magnetic fields of supernova progenitor stars could yield detectable gamma-ray bursts from the next Galactic core-collapse event, offering a direct probe of meV-scale couplings complementary to laboratory experiments.

Perhaps most significantly, the experimental landscape has been transformed. The roadmap from CAST to BabyIAXO and ultimately IAXO represents a coherent helioscope programme capable of systematically scanning the meV mass range through buffer-gas techniques, with sensitivity extending to the QCD axion band. High-frequency haloscope concepts, such as CADEx, are pushing resonant-cavity searches towards the 100 μeV–meV regime, while broadband approaches offer complementary coverage. A particularly exciting development is the recent experimental discovery of axion quasiparticles in topological antiferromagnets, which exhibit masses $m_\Theta \sim 0.1$–1 meV set by intrinsic material scales. These condensed-matter analogues not only validate the underlying axion electrodynamics

JCAP07(2026)060

but also open new avenues for resonant dark-matter detection at meV frequencies through axion–polariton hybridisation, with tunability provided by external magnetic fields.

The convergence of these diverse approaches motivated the workshop "The meV Mass Axion Frontier: Challenges and Opportunities", held at Laboratori Nazionali di Frascati (IT) on 27–28 October 2025 (https://agenda.infn.it/event/48801/) and organized by the EU funded COST Action *"Cosmic WISPers in the Dark Universe: Theory, astrophysics, and experiments"* (CA21106, https://www.cost.eu/actions/CA21106). The workshop played a central role in fostering interdisciplinary discussions across theory, cosmology, astrophysics, and experimental techniques, clarifying the key challenges and opportunities in this mass range, and establishing a coherent roadmap for the field. The present review emerges directly from these discussions and aims to present the meV axion as a coherent, cross-validated research programme. In section 2, we survey the theoretical underpinnings that single out this mass range, including field-theoretic approaches to the PQ quality problem and top-down string constructions. We then turn to the cosmological roles of meV axions: Section 3 discusses their viability as cold dark matter candidates under various production scenarios, while section 4 addresses their contribution to dark radiation, covering thermal production mechanisms (section 4.1), observational consequences (section 4.2), and future prospects (section 4.3). In section 5, we review astrophysical probes of meV-scale axions, focusing on axion production in dense nuclear media (section 5.1), axion–photon conversion in astrophysical magnetic fields (section 5.2), and searches for supernova axions in large-volume Cherenkov detectors (section 5.3), with supernovae and neutron stars providing both stringent constraints and promising discovery opportunities. Section 6 outlines the diverse experimental strategies converging on this parameter space: helioscope searches with CAST (section 6.1) and the upcoming BabyIAXO (section 6.2), post-discovery mass determination techniques (section 6.3), high-frequency haloscope searches with CADEx (section 6.4), and axion quasiparticle detection in topological materials (section 6.5). Finally, in section 7 we present our conclusions. A comprehensive list of acronyms employed in this review can be found in appendix A.

The central message is that the meV frontier has matured from a theoretically motivated target into a well-defined experimental programme. Multiple independent approaches — spanning particle physics, cosmology, astrophysics, and condensed-matter physics — now probe overlapping regions of parameter space, offering the prospect of robust, cross-validated discovery or exclusion. The coming decade promises to subject the meV QCD axion hypothesis to decisive tests, making this mass range one of the most compelling targets in the broader search for physics beyond the Standard Model (SM).

2 meV axions model building

Before discussing specific theoretical motivations that point towards the meV range, we briefly recall the basic field-theoretic ingredients of QCD axion model building. A QCD axion arises from a spontaneously broken global $\mathrm{U}(1)_{\mathrm{PQ}}$ symmetry whose associated pseudo-Nambu–Goldstone boson couples anomalously to QCD. At energies below the PQ-breaking

JCAP07(2026)060

scale, the axion effective Lagrangian reads (see e.g. [12])

$$\mathcal{L}_a = \frac{1}{2}(\partial_\mu a)^2 + \frac{\alpha_s}{8\pi}\frac{a}{f_a}G^a_{\mu\nu}\tilde{G}^{a\mu\nu} + \frac{\alpha}{8\pi}C^0_{a\gamma}\frac{a}{f_a}F_{\mu\nu}\tilde{F}^{\mu\nu} + \sum_f \frac{\partial_\mu a}{2f_a}C^0_f\,\bar{f}\gamma^\mu\gamma_5 f + \dots\,, \tag{2.1}$$

where $\tilde{G}^a{}_{\mu\nu} = \frac{1}{2}\epsilon_{\mu\nu\rho\sigma}G^{a\,\rho\sigma}$ ($\epsilon_{0123} = +1$), and similarly for the electromagnetic field strength, $C^0_{a\gamma} = E/N$ is fixed by the ratio of electromagnetic and color anomalies of the PQ current, while the coefficients C^0_f depend on the PQ charges of the SM fermions. After QCD confinement, the axion mixes with the neutral pseudoscalar mesons and obtains a mass

$$m_a \simeq 5.7\ \text{meV}\left(\frac{10^9\ \text{GeV}}{f_a}\right), \tag{2.2}$$

up to small uncertainties from light-quark masses and higher-order chiral effects [13]. Thus, the meV mass range corresponds to an axion decay constant around $f_a \sim 10^9$–$10^{10}\,\text{GeV}$, close to the region where stellar cooling, helioscope searches, thermal production, and several model-building considerations become simultaneously relevant.

Two benchmark classes of ultraviolet (UV) completions are commonly used to organise the phenomenology. In KSVZ models [14, 15], the PQ anomaly is generated by heavy vector-like quarks, while ordinary SM fermions are not charged under $\text{U}(1)_{\text{PQ}}$ at tree level. As a result, the axion couplings to electrons arise from loop effects. In DFSZ models [16, 17], instead, the SM fermions and two Higgs doublets carry PQ charges, and the axion has tree-level derivative couplings to ordinary matter. These differences have important phenomenological consequences. For instance, the electron coupling is typically suppressed in hadronic KSVZ models, while it is present at tree level in DFSZ models. This distinction is directly relevant for stellar cooling bounds and for the interpretation of helioscope searches. Similarly, the nucleon couplings depend on both the UV PQ charges and the model-independent contribution induced by axion-meson mixing, which is crucial for supernova and neutron-star constraints.

At low energies, the axion-photon interaction is conventionally written as

$$\mathcal{L}_{a\gamma} = -\frac{1}{4}g_{a\gamma}aF_{\mu\nu}\tilde{F}^{\mu\nu} = g_{a\gamma}\mathbf{E}\cdot\mathbf{B}, \qquad g_{a\gamma} = \frac{\alpha}{2\pi f_a}\left(\frac{E}{N} - 1.92(4)\right), \tag{2.3}$$

where the second term is the model-independent contribution from axion mixing with neutral mesons [18, 19]. The ratio E/N is therefore one of the key model-building quantities controlling the location of a QCD axion model in the $(m_a, g_{a\gamma})$ plane. While $E/N = 0$ (8/3) in KSVZ (DFSZ) models, different values of E/N are possible in specific UV completions. Phenomenological selection criteria have been proposed to single out "preferred" models [20–23], which define the so-called QCD axion band.

A similar interplay between model-independent and UV contributions holds for the derivative couplings to low-energy matter fields,

$$\mathcal{L}_{a\Psi} = \sum_\Psi \frac{\partial_\mu a}{2f_a}C_\Psi\,\bar{\Psi}\gamma^\mu\gamma_5\Psi, \tag{2.4}$$

where $\Psi = e, p, n, \dots$ and the low-energy coefficients C_Ψ include both UV contributions (including running effects [24–29]) and, in the case of nucleons, infrared corrections induced

JCAP07(2026)060

by QCD. These couplings control many of the thermal production rates discussed in section 4, as well as the astrophysical emission processes reviewed in section 5. In particular, the axion-electron coupling drives production in electron-rich stellar plasmas, while axion-nucleon couplings determine emission from dense nuclear matter in supernovae and neutron stars.

The cosmological implications of a QCD axion also depend on the thermal history of PQ symmetry breaking. If the PQ symmetry is broken before or during inflation and is not restored afterwards, the observable Universe contains a single initial value of the axion field. In this pre-inflationary scenario, the relic abundance depends on the initial misalignment angle [30–32], and isocurvature perturbations can impose strong constraints on high-scale inflation. In contrast, if PQ breaking occurs after inflation, different Hubble patches choose different initial axion angles and a network of global strings and domain walls forms [33–45]. The decay of these topological defects gives an additional contribution to the axion relic abundance, and the viability of the scenario depends crucially on the domain-wall number $N_{\rm DW}$. Models with $N_{\rm DW} = 1$ are cosmologically safe, while stable domain walls for $N_{\rm DW} > 1$ would overclose the Universe unless the degeneracy among vacua is lifted [46] or the cosmological history is modified.

These standard ingredients provide the baseline framework for axion model building. Within this framework, the meV range is not tied to a single UV realisation: it can arise in hadronic or DFSZ-like models, in variants with suppressed or enhanced photon and fermion couplings (see e.g. [20, 21, 47–54]), and in both pre- and post-inflationary cosmologies. In the following subsection we focus on one specific model-building motivation for the meV range, namely the PQ quality problem, which tends to favour relatively low values of f_a in several field-theoretic constructions.

2.1 Axion quality problem

The axion solution to the strong CP problem [55–58], while elegant and potentially testable, raises the puzzling question of the origin of the PQ symmetry. In quantum field theories, global symmetries are not considered fundamental but are rather seen as accidental, as e.g. in the familiar cases of strong isospin or baryon number. While some axion models [14–17] impose an effective $\mathrm{U}(1)_{\rm PQ}$ symmetry "by hand", a robust PQ theory should preferably generate this symmetry in an automatic way [59]. Furthermore, the PQ symmetry needs to be of very "high quality", since even a tiny explicit breaking of the $\mathrm{U}(1)_{\rm PQ}$ from the ultraviolet (UV) completion would spoil the PQ solution to the strong CP problem, raising the so-called PQ quality problem [59–64]. To quantify the latter, consider a PQ-breaking effective operator of the type

$$V_{\text{PQ-break}} = -e^{i\delta}\frac{\Phi^n}{\Lambda_{\rm UV}^{n-4}} + \text{h.c.}\,, \tag{2.5}$$

with $n > 4$. Here, δ denotes a generic phase, $\Lambda_{\rm UV}$ is some UV scale like the Planck mass and $\Phi = \frac{f_a}{\sqrt{2}}e^{ia/f_a}$ is a complex scalar, with the radial mode integrated out and the angular mode a/f_a given by the axion field. The induced axion potential then reads

$$V_{\text{PQ-break}} = -\frac{1}{2^{n/2-1}}\frac{f_a^n}{\Lambda_{\rm UV}^{n-4}}\cos\left(\frac{na}{f_a} + \delta\right)\,. \tag{2.6}$$

JCAP07(2026)060

In general, the phase of this potential, parameterized by δ, does not need to be aligned with the CP-conserving minimum of the QCD potential at $a = 0$. Therefore, we generically expect δ to be $\mathcal{O}(1)$. The balance between $V_{\rm PQ-break}$ and the standard QCD axion potential, $V_{\rm QCD} = \frac{1}{2} f_a^2 m_a^2 (a/f_a)^2 + \mathcal{O}((a/f_a)^4)$, yields an axion vacuum expectation value (VEV) displaced from zero, that is

$$\theta_{\rm eff} \equiv \langle a/f_a \rangle \simeq -\frac{n \Lambda_{\rm UV}^{4-n} f_a^n \sin\delta}{2^{\frac{n}{2}-1} f_a^2 m_a^2}\,, \tag{2.7}$$

where we took into account the approximation $\theta_{\rm eff} \ll 1$. Taking for instance $\sin\delta = 1$, $\Lambda_{\rm UV} = M_{\rm Pl}$ and $f_a = 10^8\,{\rm GeV}$, the nEDM bound $|\theta_{\rm eff}| \lesssim 10^{-10}$ translates into $n \geq 9$. Therefore, the original question "why is $\theta_{\rm QCD}$ small?" is traded for "why PQ-breaking operators are highly suppressed?".

Different approaches to the PQ quality problem have been proposed so far. It is useful to classify them in three categories:

1. *Low-scale f_a*

   For $f_a \sim 10^3\,{\rm GeV}$, only $n > 5$ is required in order not to generate a too large $\theta_{\rm eff}$ from eq. (2.7). From this perspective, the original Weinberg-Wilczek model [57, 58] would have been perfectly natural, since in the absence of SM-singlet fields, the first gauge invariant PQ-breaking operator that one can write in the scalar potential features $n = 6$. Over the years, the increasingly lower bounds on f_a let the PQ quality problem emerge and worsen. It is, however, possible to modify the standard QCD relation between m_a and f_a such that $m_a \gtrsim 10$ MeV (see e.g. [65, 66]), in which case the conventional astrophysical constraints on f_a can be avoided. Such heavy axion models feature an axion decay constant of the order of $10^{4\div5}\,{\rm GeV}$, thus improving on the PQ quality problem.

2. *$U(1)_{\rm PQ}$ as an accidental symmetry*

   A prevalent strategy involves extending the Standard Model (SM) gauge symmetry, using either continuous or discrete local symmetries that are exact in the UV regime, so that the PQ symmetry arises as an accidental global symmetry, and is eventually broken by some higher-order effective operators (see, for example, refs. [67–81]).

   This mechanism provides a robust solution, independent of the specific UV completion. It requires, however, non-trivial model building, characterised by an integer parameter that matches the dimension n of the PQ-breaking operator. Considerations of minimality and simplicity favour low values of n, which in turn imply relatively small values of f_a, close to the boundary of astrophysical limits. Consequently, meV-scale axions emerge as the most favourable scenarios for addressing the PQ-quality problem within field-theoretical four-dimensional models.

3. *Extra-dimensional axions*

   Axions may also arise as zero modes of higher dimensional forms in string theory compactifications [82] or, more in general, in models with extra dimensions [83–85].

JCAP07(2026)060

In this context, the PQ shift symmetry is inherited from a higher-dimensional gauge symmetry and it is exact at perturbative level. Non-perturbative contributions to the axion potential are exponentially suppressed, and so extra-dimensional axions (when calculable) can offer a structural solution to the PQ quality problem.

2.2 meV axions from string theory

The existence of axions in field theory is motivated by the PQ solution to the strong-CP problem, but they have natural and elegant realisations in string theory which is currently one of the most well-developed approaches to a UV-complete theory of quantum gravity. Antisymmetric p-form gauge potentials in 10 dimensions give rise, after compactification, to 4-dimensional pseudo-scalar fields enjoying an (approximate) continuous shift symmetry, typically broken to a discrete one by non-perturbative effects. These modes are called *closed string axions*. String compactifications feature also branes wrapping internal cycles and supporting QCD-like gauge theories. In these scenarios a global PQ U(1) symmetry can arise at low energy as the remnant of a higher dimensional anomalous gauge symmetry, and the phases of U(1) charged modes behave as axions. These are named *open string axions*. The periodicity, decay constant and interactions of both closed and open string axions are set by the geometry and topology of the internal space, making axions sensitive probes of the UV completion.

From the top-down point of view, different scenarios with meV axions seem to be possible. In fact, meV axions can arise in various corners of the string landscape, either as closed or open string modes, with an intermediate scale decay constant which can be around the string scale or much smaller, resulting in the possibility to reproduce both the pre- and post-inflationary scenario. Conversely, the potential discovery of a meV axion would provide valuable information about the ultraviolet structure of the theory, the size of extra dimensions, and the nature of moduli stabilisation, thereby offering a rare opportunity to use low-energy axion physics as a probe of string theory.

2.2.1 meV axions as closed strings

Axions arise ubiquitously in the closed string sector from dimensional reduction of p-form gauge fields, C_p, over internal p-cycles Σ_p. Their phenomenological properties are set by moduli stabilisation which determines their mass spectrum and couplings. Moduli stabilisation is therefore a crucial prerequisite for trusting any attempt to build phenomenologically viable axion models. Given that type IIB is the perturbative corner of string theory where moduli stabilisation is best understood, the majority of string axion models have been constructed in this context. In type IIB the most promising examples are C_4 axions:

$$\theta^i = \int_{\Sigma_4^{(i)}} C_4 \qquad i = 1, \cdots, h^{1,1}\,, \tag{2.8}$$

where $h^{1,1}$ is the number of Kähler moduli, $T^i = \tau^i + \mathrm{i}\,\theta^i$, with τ^i the volume of the i-th 4-cycle $\Sigma_4^{(i)}$ in units of the string length $\ell_s = 2\pi\sqrt{\alpha'}$:

$$\tau^i = \mathrm{Vol}\left(\Sigma_4^{(i)}\right)\, \ell_s^{-4}\,. \tag{2.9}$$

JCAP07(2026)060

The kinetic terms of the Kähler moduli are determined by the Kähler metric:

$$\mathcal{L}_{\rm kin} = K_{i\bar{j}}\partial_\mu T^i \partial^\mu \overline{T}^{\bar{j}} = \frac{1}{4}\frac{\partial^2 K}{\partial\tau^i \partial\tau^j}\left(\partial_\mu \tau^i \partial^\mu \tau^j + \partial_\mu \theta^i \partial^\mu \theta^j\right), \tag{2.10}$$

where the tree-level Kähler potential K depends on the Calabi-Yau (CY) volume $\mathcal{V}$ as:

$$K = -2\ln \mathcal{V} = -2\ln\left(\frac{1}{6}k_{ijk}t^i t^j t^k\right) \qquad \tau_i = \frac{1}{2}k_{ijk}t^j t^k\,. \tag{2.11}$$

In the previous expression k_{ijk} are the CY intersection numbers and t^i denote 2-cycle moduli.

In type IIB models, QCD-like non-Abelian gauge theories with chiral matter arise naturally on magnetised D7-branes wrapped around 4-cycles [86–89]. In particular, the gauge kinetic function $\mathfrak{f}^a$ associated to the D7-stack wrapped around the a-th 4-cycle is set by T^a, $\mathfrak{f}^a = T^a$. This induces a natural axion-like coupling for θ^a of the form:

$$\mathcal{L} \supset \theta^a \,\mathrm{Tr}\,(F_a \wedge F_a) + \tau^a \,\mathrm{Tr}\,(F_a \wedge \star F_a)\,. \tag{2.12}$$

Note that the gauge coupling is controlled by τ^a since $\alpha_a^{-1} = \mathrm{Re}(\mathfrak{f}^a) = \tau^a$.

The scalar potential receives D- and F-term contributions which depend on the Kähler potential K and the superpotential W as follows:

$$V_D = \sum_b \frac{1}{\tau_b}\left(\sum_k \hat{q}_k^{(b)}|\phi_k|^2 - \xi_b\right)^2 \qquad V_F = e^K\left[K^{i\bar{j}}\left(W_i + W K_i\right)\left(\overline{W}_{\bar{j}} + \overline{W}K_{\bar{j}}\right) - 3|W|^2\right]. \tag{2.13}$$

The sum on b is over all U(1) factors, $\hat{q}_k^{(b)}$ is the charge under $\mathrm{U}(1)_b$ of the k-th open string mode ϕ_k, and the Fayet-Iliopoulos (FI) term ξ_b reads (see appendix A of [90]):

$$\xi_b = -q_i^{(b)}\frac{\partial K}{\partial \tau_i} \qquad q_i^{(b)} = \int_{\Sigma_4^{(b)}} \hat{D}_i \wedge \mathcal{F}^{(b)}\,, \tag{2.14}$$

where $q_i^{(b)}$ is the charge under $\mathrm{U}(1)_b$ of the i-th Kähler modulus, $\mathcal{F}^{(b)}$ is the gauge flux on the b-th D7-stack, and $\hat{D}_i$ is the i-th element of a basis of harmonic $(1,1)$-forms.

At leading order, the D-term potential is minimised supersymmetrically at $V_D = 0$. It is worth pointing out that V_D does not depend on the axions but plays a crucial role in determining which axions are eaten by anomalous U(1) gauge bosons. In fact, focusing for illustrative purpose on a single matter field ϕ and a single Kähler modulus τ charged under $\mathrm{U}(1)_b$, the Abelian gauge boson becomes massive by absorbing a combination of the open string axion ζ, which is the phase of $\phi = |\phi|\, e^{\mathrm{i}\zeta}$, and the closed string axion θ, that is the supersymmetric partner of τ. The mass of $\mathrm{U}(1)_b$ can be written schematically as [90]:

$$m^2_{\mathrm{U}(1)_b} \simeq \tau_b^{-1}\left(f^2_{\rm op} + f^2_{\rm cl}\right), \tag{2.15}$$

where $f_{\rm op}$ and $f_{\rm cl}$ denote, respectively, the open and closed string axion decay constants given by (for $q^{(b)} \simeq \hat{q}^{(b)}$):

$$f^2_{\rm op} = \langle|\phi|\rangle^2 \simeq \left|\frac{\partial K}{\partial \tau}\right| \qquad \text{and} \qquad f^2_{\rm cl} \simeq \frac{\partial^2 K}{\partial \tau^2}\,. \tag{2.16}$$

JCAP07(2026)060

If $f_{\rm op} \gg f_{\rm cl}$, the combination of axions eaten by $\mathrm{U}(1)_b$ is mostly given by ζ, while if $f_{\rm op} \ll f_{\rm cl}$, the eaten axion is mostly θ [91]. The magnitude of $f_{\rm op}$ relative to $f_{\rm cl}$ is a function of the Kähler moduli that remain flat after D-term stabilisation.

The minimisation of the F-term potential is essential to address three important issues for axion phenomenology:

1. To determine the ratio $f_{\rm op}/f_{\rm cl}$ which establishes which axions are not eaten by anomalous U(1)'s, and so survive in the low-energy theory. If τ is fixed at large values, $\tau \gg 1$, as in the case of D7-branes wrapped around 4-cycles in the geometric regime, the surviving axion is θ. If, instead, τ shrinks to zero size, $\tau \to 0$, as for the case of D3-branes at a CY singularity, the role of the QCD axion is played by ζ.

2. To fix the ratio between the axion mass m_θ and the saxion mass m_τ. Being pseudo-scalars with spin dependent couplings, the axions do not mediate any long-range force between unpolarised bodies. This is however not the case for the saxions which naturally couple with Planckian strength to ordinary matter. The non-observation of fifth-forces sets a lower bound on m_τ of the order $m_\tau \gtrsim \mathcal{O}(0.1)$ meV [92]. Cosmology gives yet a much more stringent bound from the requirement of decaying before BBN, $m_\tau \gtrsim \mathcal{O}(30)\,\mathrm{TeV}$ [93–95]. Thus, to avoid the case where axions are necessarily very heavy, F-term fixing has to create a hierarchy between m_θ and m_τ of the form $m_\theta \ll m_\tau$.

3. To reproduce the value of the QCD coupling at the cut-off scale, $\alpha_{\rm QCD}^{-1}(\Lambda_{\rm UV}) = \tau_{\rm QCD}$, and, at the same time, an meV mass for the QCD axion with an intermediate scale decay constant, $f_{\rm QCD} \simeq 5 \times 10^9\,\mathrm{GeV}$. Note that, in 4D string models, the UV cut-off is set by the overall volume $\mathcal{V}$ and, for purely local cycles, it corresponds to the string scale, $M_s \simeq M_p/\sqrt{\mathcal{V}}$, while for cycles with homology representatives both locally and in the bulk, it is given by the winding scale, $M_{\rm W} \simeq M_p/\mathcal{V}^{1/3}$ [96].

The first realisation of a closed string QCD axion at the meV scale with F-term moduli stabilisation has been proposed in [2] and, later on, D-term stabilisation has been included in [3]. The idea is to consider the C_4-axion $\theta_{\rm QCD}$ associated to a blow-up cycle with volume $\tau_{\rm QCD}$ and wrapped by D7-branes which realise QCD. Knowing that $\alpha_{\rm QCD}^{-1}(90\,\mathrm{GeV}) \simeq 8.5$, one can work out $\tau_{\rm QCD} = \alpha_{\rm QCD}^{-1}(\Lambda_{\rm UV})$ using RG running. Given that blow-up cycles are local, we shall consider $\Lambda_{\rm UV} \simeq M_s$. As we will see, M_s sets the scale of the QCD axion decay constant, which has therefore to be intermediate to reproduce an meV axion. In turn, this fixes also the gravitino mass that gives a scale of supersymmetry breaking around a few tens of TeV. Thus, performing RG running in the SM up to a few tens of TeV, and then in the MSSM up to an intermediate scale, one finds $\tau_{\rm QCD} \sim 20$.

The simplest CY volume including also a bulk cycle with volume τ_b looks like:

$$\mathcal{V} = \tau_b^{3/2} - \tau_{\rm QCD}^{3/2} \simeq \tau_b^{3/2} \qquad \text{for} \qquad \tau_b \gg \tau_{\rm QCD}\,. \tag{2.17}$$

Eq. (2.16) applied to our case would give:

$$\left(\frac{f_{\rm op}}{f_{\rm QCD}}\right)^2 \simeq \frac{\partial K}{\partial \tau_{\rm QCD}} \left(\frac{\partial^2 K}{\partial \tau_{\rm QCD}^2}\right)^{-1} \sim \tau_{\rm QCD} \sim 20 \quad \Rightarrow \quad f_{\rm op} \gg f_{\rm QCD}\,, \tag{2.18}$$

JCAP07(2026)060

implying that $\theta_{\rm QCD}$ is not eaten by any anomalous U(1). Moreover the QCD axion decay constant is not fixed uniquely by $\alpha_{\rm QCD}^{-1}$ since:

$$f_{\rm QCD}^2 \simeq \frac{\partial^2 K}{\partial \tau_{\rm QCD}^2} \simeq \frac{M_p^2}{\mathcal{V}\sqrt{\tau_{\rm QCD}}} \simeq \left(\frac{M_s}{\alpha_{\rm QCD}^{-1/4}}\right)^2 . \tag{2.19}$$

If $M_s \sim 10^{10}\,{\rm GeV}$ for $\mathcal{V} \sim 10^{15}$, one then obtains indeed $f_{\rm QCD} \sim 5 \times 10^9\,{\rm GeV}$ for $\alpha_{\rm QCD}^{-1} \sim 20$. Let us make two observations. The first is that $f_{\rm QCD}$ is tight to the string scale, and so any realisation of cosmic inflation in 4 dimensions features inevitably a Hubble scale below the PQ breaking scale, $H_{\rm inf} < f_{\rm QCD}$. This leads to a typical post-inflationary scenario where $H_{\rm inf}$ is upper bounded by isocurvature constraints due to the oscillations of the light axion during inflation. The second observation is that the axion decay constant would not be decoupled from the QCD gauge coupling if one tried to realise the QCD axion with θ_b. In fact, in the case of a bulk cycle, one would obtain:

$$f_{\theta_b}^2 \simeq \frac{\partial^2 K}{\partial \tau_b^2} \simeq \left(\frac{M_p}{\tau_b}\right)^2 \simeq \left(\frac{M_p}{\alpha_b^{-1}}\right)^2 , \tag{2.20}$$

which would give $f_{\theta_b} \sim 10^{16}\,{\rm GeV}$ for $\alpha_{\rm QCD}^{-1} \sim 45$ which is the right QCD coupling for a higher string scale, $M_s \sim M_p/\tau_b^{3/4} \sim 5 \times 10^{16}\,{\rm GeV}$.

Having established that $\theta_{\rm QCD}$ is a promising meV axion candidate, it remains to show that the F-terms potential has indeed a minimum at $\mathcal{V} \sim 10^{15}$ and $\tau_{\rm QCD} \sim 20$, and that the moduli mass spectrum around this vacuum does not lead to any cosmological moduli problem (CMP) for the saxions. Such a large value of the CY volume can be achieved in LVS models where $\mathcal{V}$ is stabilised at exponentially large values in terms of the string coupling $g_s \ll 1$ as $\mathcal{V} \sim e^{c/g_s} \gg 1$ [97, 98], where c is an $\mathcal{O}(1)$ parameter that depends on the details of the underlying microscopic construction.

Note that, contrary to closed string axions θ^i which enjoy perturbatively exact shift symmetries, the saxionic component τ^i of any Kähler modulus $T^i = \tau^i + {\rm i}\,\theta^i$ is not protected by any symmetry. Hence, if perturbative effects dominate over non-perturbative ones, $\tau_{\rm QCD}$ can be much heavier than $\theta_{\rm QCD}$, resulting in $m_{\theta_{\rm QCD}} \sim \mathcal{O}({\rm meV}) \ll m_{\tau_{\rm QCD}} \gtrsim \mathcal{O}(30)\,{\rm TeV}$. However in LVS models the main contribution to the potential of blow-up modes arises typically from non-perturbative corrections to W due to the extended no-scale cancellation of loop corrections to K [99]. This results in very heavy axions associated to blow-up cycles. The situation is, however, more subtle for blow-up modes wrapped by the QCD stack of branes due to the well-known tension between non-perturbative effects and chirality [100]. In fact, as we have seen, in this case $T_{\rm QCD}$ gets a non-zero charge $q_{\rm QCD}$ under an anomalous U(1). Thus, any non-perturbative corrections to W, to be gauge invariant, has to depend also on the open string modes ϕ with charge $\hat{q}_{\rm QCD}$:

$$W \supset A\,\phi^n\,e^{-2\pi T_{\rm QCD}} \qquad \text{with} \qquad n = q_{\rm QCD}/\hat{q}_{\rm QCD}\,. \tag{2.21}$$

As can be seen from (2.16), D-term stabilisation fixes $|\phi|^2 \sim \sqrt{\tau_{\rm QCD}}/\mathcal{V} \ll 1$, introducing an extra $\mathcal{V}$ suppression factor in (2.21) which makes this term negligible. Therefore $\tau_{\rm QCD}$ can be stabilised by contributions to the scalar potential which do not depend on $\theta_{\rm QCD}$. These

JCAP07(2026)060

are loop corrections to K and supersymmetry breaking effects of order the gravitino mass $m_{3/2} \sim W_0\, M_p/\mathcal{V}$ (where W_0 is the $\mathcal{O}(10)$ flux superpotential [101]) [4, 7]:

$$V(\tau_{\rm QCD}) = m_{3/2}^2|\phi|^2 + \frac{c_{\rm loop}}{\mathcal{V}^3\sqrt{\tau_{\rm QCD}}} \simeq \frac{W_0^2}{\mathcal{V}^3}\left(c_{\rm D}\sqrt{\tau_{\rm QCD}} + \frac{c_{\rm loop}}{\sqrt{\tau_{\rm QCD}}}\right), \tag{2.22}$$

where we have substituted $|\phi|$ in terms of $\tau_{\rm QCD}$ using D-term stabilisation, and $c_{\rm D}$ and $c_{\rm loop}$ are $\mathcal{O}(1)$ coefficients which depend, respectively, on 2-form and 3-form gauge flux quanta. This potential has a minimum at $\langle\tau_{\rm QCD}\rangle \simeq c_{\rm loop}/c_{\rm D}$ which can easily lie around $\langle\tau_{\rm QCD}\rangle \sim 20$. Moreover, it gives a mass to $\tau_{\rm QCD}$ of order $m_{\tau_{\rm QCD}} \sim m_{3/2} \sim \mathcal{O}(50)\,\text{TeV}$ for $W_0 \sim \mathcal{O}(10)$, while leaving $\theta_{\rm QCD}$ as a flat direction. A similar result can be obtained also if $\langle|\phi|\rangle = 0$ for geometries where $\tau_{\rm QCD}$ intersects another local blow-up cycle with volume $\tau_{\rm int}$. In that case, $V_D = 0$ if the FI-term vanishes, corresponding to stabilising $\tau_{\rm int}$ in terms of $\tau_{\rm QCD}$ which, in turn, can then be fixed by string loops at subleading order [3, 5, 86].

This model seems to provide an attractive meV QCD axion with $f_{\rm QCD} \sim 5\times 10^9\,\text{GeV}$, the correct QCD coupling and a saxion above the CMP bound, $m_{\tau_{\rm QCD}} \sim \mathcal{O}(50)\,\text{TeV}$ [2]. However it faces a severe challenge associated to the decay of the volume mode after BBN due to the smallness of its mass, $m_{\tau_b} \sim M_p/\mathcal{V}^{3/2} \sim \mathcal{O}(1)\,\text{MeV}$. In order to make τ_b heavy enough to avoid any CMP, one would need to focus on vacua with a smaller value of $\mathcal{V}$, $\mathcal{V} \lesssim 10^8$. This lower bound would then restrict the possible values of the QCD axion decay constant, using (2.19), to the window $10^{13}\,\text{GeV} \lesssim f_{\rm QCD} \lesssim 10^{16}\,\text{GeV}$, where the upper bound comes from the condition to trust the α' expansion that, for models with small $h^{1,1}$, can be estimated as $\mathcal{V}^{-1/3} \lesssim 0.1$. This conclusion might seem to forbid an meV-scale QCD axion, unless the CMP is solved via a late time dilution mechanism or a suppressed initial misplacement of τ_b from the minimum of its potential. In this case, the CY volume could be safely as large as $\mathcal{V} \sim 10^{15}$, resulting in $f_{\rm QCD} \sim 5\times 10^9\,\text{GeV}$.

Given that different values of $\mathcal{V}$ yield different values of $f_{\rm QCD}$, it is interesting to investigate the statistical distribution of the QCD axion decay constant in the type IIB flux landscape moving along trajectories in the field space which correspond to stabilised vacua. This analysis has been performed in [4] by varying flux quanta at fixed $h^{1,1}$, finding a mild logarithmic preference for larger decay constants of the form $N(f_{\rm QCD}) \sim \ln(f_{\rm QCD}/M_p)$, where $N(f_{\rm QCD})$ counts the number of flux vacua for a given $f_{\rm QCD}$.

A complementary statistical approach has been taken in [10, 11] which derived numerically the distribution of the axion decay constants fixing a point in moduli space and varying $h^{1,1}$ by changing geometries within the largest known ensemble of CY manifolds given by the Kreuzer-Skarke database [102]. In this construction, a CY threefold is built as a complex 3-dimensional hypersurface in a complex 4-dimensional ambient toric variety, and the largest number of Kähler moduli is $h^{1,1} = 491$. The decay constants of all axions are estimated by the eigenvalues of the kinetic matrix using the software CYTools [103], and their distribution turns out to be approximately log-normal with a decreasing mean value as $h^{1,1}$ increases (a similar trend has been found also in more general F-theory models [104]). In particular, $f_{\rm QCD} \lesssim \mathcal{O}(10^{10})\,\text{GeV}$ for $h^{1,1} \gtrsim \mathcal{O}(400)$, showing that, at large $h^{1,1}$, the lower bound on the mass of a closed string QCD axion lies exactly around the meV scale.

JCAP07(2026)060

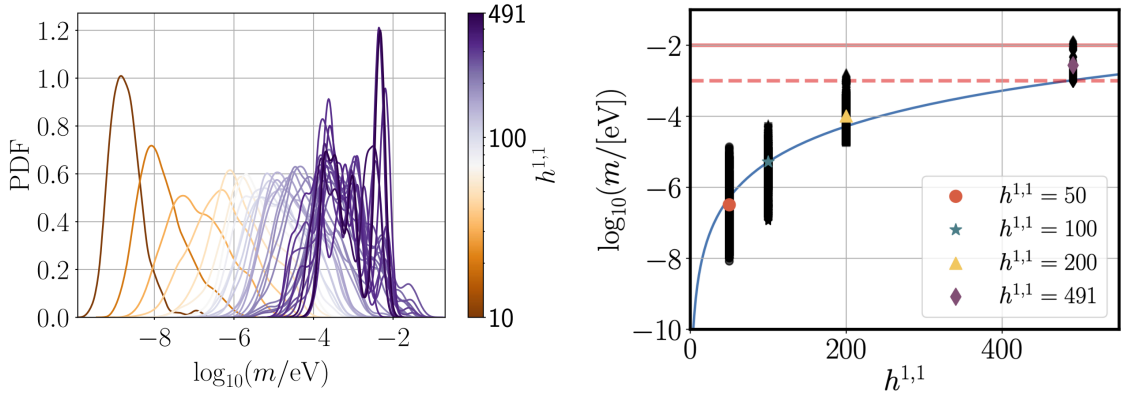


Figure 1. QCD axion mass, at random points along a ray from the tip of the SKC, for different values of $h^{1,1}$ in type IIB CY models. *Left.* Probability distribution on the QCD axion mass colour coded by $h^{1,1}$. Distributions move towards meV for $h^{1,1} \gtrsim 200$ (Reproduced from [108]. CC BY 4.0). *Right.* QCD axion mass as a function of $h^{1,1}$. Coloured dots denote the average in the bin, the line denotes a power law assuming $\mathcal{V} \sim (h^{1,1})^5$. The horizontal solid line is the current limit from SN1987A, and the dotted line is the projection for the next galactic supernova (Reproduced from [109]. The Author(s). CC BY 4.0).

The point in moduli space considered in [10, 11] is the tip of the stretched Kähler cone (SKC), corresponding to the minimal value of all 2-cycle moduli t^i which allows to control α' corrections to the EFT. Ref. [105] found that this requirement can be translated into an $h^{1,1}$-dependent lower bound on the overall volume of the form $\mathcal{V} \gtrsim 10^{-3.4}(h^{1,1})^{7.2}$. Intuitively, this is due to the fact that, as $h^{1,1}$ increases, the conditions which define the Kähler cone also increase, making the cone narrower, and so moving the tip of the SKC farther from the origin. For $h^{1,1} \gtrsim 400$, one would indeed obtain $\mathcal{V} \gtrsim 10^{15}$ which, as we have seen above, is in the right ballpark to realise an meV-scale QCD axion using a C_4-axion associated to a rigid blow-up mode. Figure 1 shows the distribution of the QCD axion mass evaluated at points that reproduce the correct UV QCD coupling and are randomly selected along a ray originating from the tip of the SKC. The QCD axion mass increases as a power law with $h^{1,1}$, and starts to have support near the meV scale for $h^{1,1} \gtrsim 200$. At the largest value of $h^{1,1} = 491$, the QCD axion mass appears to be distributed around 1 meV. It is interesting to observe that the distribution barely goes above 10 meV: these string theory models appear largely unconstrained by the SN1987A neutrino burst limits [106, 107], but are within reach of other meV phenomenology.

Let us stress that these results are valid at the tip of the SKC (or along a ray generated from the tip) but one could also analyse the distribution of the axion decay constants when moving deeper inside the Kähler cone. An indication of the outcome of this study comes from the analysis of [4] which implies a mild statistical preference for an meV-scale QCD axion compared to larger masses, when considering all allowed values of f_{QCD} at very large $h^{1,1}$. To have a complete understanding of the statistical distribution of f_{QCD} in the entire flux landscape, one should combine this result with the distribution at small $h^{1,1}$, counting the number of different vacua which depends on $h^{1,2}$ and the number of topologically inequivalent CY geometries. This is still an open question, due also to the difficulty to stabilise explicitly all

JCAP07(2026)060

the moduli at large $h^{1,1}$ without a CMP (see however [110] for an attempt to fix an arbitrary number of moduli perturbatively at exponentially large $\mathcal{V}$). The PQ quality is, however, in general exponentially good at large $h^{1,1}$ due to the large number of shift symmetries and the presence of axions much lighter than the QCD axion [111]. Different phenomenological aspects of axion physics at large $h^{1,1}$ have been studied in [112, 113].

Let us finally comment that for axion-like particles (ALP) not tied to QCD, the relation between mass and decay constant is less constrained. For C_4-axions associated to bulk cycles τ_b, ALP decay constants and masses exhibit parametric scalings of the schematic form $f_{\rm ALP} \sim M_p/\tau_b$ and $m_{\rm ALP} \sim e^{-kM_p/f_{\rm ALP}}\, M_p$, where k is an $\mathcal{O}(1)$ coefficient which depends on the instanton order at which the ALP becomes massive. These relations indicate that meV ALPs tend to be associated with very large decay constants, potentially as high as $f_a \sim 10^{16}\,\text{GeV}$. Conversely ALPs with intermediate scale decay constants (as would be the case for an meV-scale QCD axion) are effectively massless. Moreover, when considering mass eigenstates, these ALPs tend to couple to the visible sector extremely weakly [4], and so might be effectively invisible to many experimental probes. A more promising case is the one of C_4-axions associated to small moduli τ_s which intersect the rigid 4-cycle supporting the QCD stack of branes [3]. In this case, the ALP can couple to the visible sector more strongly with decay constant $f_{\rm ALP} \sim M_s \sim M_p/\sqrt{\mathcal{V}}$ which can be at an intermediate scale for the same value of $\mathcal{V}$ that yields an meV-scale QCD axion. On the other hand, the ALP mass, scaling as $m_{\rm ALP} \sim e^{-k\tau_s}\, M_p$, can take a large range of values since it is very sensitive to the specific values of k and τ_s.

2.2.2 meV axions as open strings

D3-branes at del Pezzo singularities are a common way to realise chiral non-Abelian gauge theories like QCD [6, 114–117]. The singularity is obtained via the collapse of a del Pezzo divisor, $\tau_{\rm dP} \to 0$, induced dynamically by moduli stabilisation. In these models there is always an anomalous U(1) factor that acquires a Stückelberg mass by absorbing the closed string axion $\theta_{\rm dP}$ that is the supersymmetric partner of $\tau_{\rm dP}$. The role of the QCD axion is therefore played by an open string mode [6–9, 91, 118]. Being localised at a singularity, the visible sector is in general sequestered from supersymmetry breaking sourced by fluxes in the bulk [119, 120], resulting in an axion decay constant which is suppressed with respect to the string scale. Thanks to this property, one can realise an meV axion without a CMP for any saxion. Moreover, one can also reproduce, at the same time, the correct QCD coupling which for D3-branes is set by the dilaton S, $\alpha_{\rm QCD}^{-1} = \text{Re}(S) = g_s^{-1}$.

Let us see this picture more in detail. The Kähler potential expanded around the del Pezzo singularity reads:

$$K = -2\ln\mathcal{V} + \frac{\tau_{\rm dP}^2}{\mathcal{V}}\,. \tag{2.23}$$

Thus, D-term fixing leads to:

$$|\phi|^2 \simeq \xi \simeq \frac{\partial K}{\partial \tau_{\rm dP}} \simeq \frac{\tau_{\rm dP}}{\mathcal{V}} \simeq \tau_{\rm dP}\, M_s^2\,. \tag{2.24}$$

JCAP07(2026)060

This relation can be interpreted as fixing $\tau_{\rm dP}$ in terms of the open string mode $|\phi|$ whose F-term potential receives supersymmetry breaking contributions of the form:

$$V_F(|\phi|) = c_2\, m_0^2\, |\phi|^2 + c_3\, A\, |\phi|^3 + \mathcal{O}(|\phi|^4)\,, \tag{2.25}$$

where c_2 and c_3 are $\mathcal{O}(1)$ coefficients while the soft scalar mass m_0 and the trilinear coupling A scale with the CY volume, respectively, as $m_0^2 \sim M_p^2/\mathcal{V}^{p_2}$ and $A \sim M_p/\mathcal{V}^{p_3}$. If $c_2 > 0$, the minimum lies at $\langle|\phi|\rangle = 0$ which implies $\tau_{\rm dP} = 0$, ensuring that the del Pezzo divisor shrinks down to zero size dynamically. However there is no breaking of the PQ symmetry. If, instead, the soft mass is tachyonic, i.e. $c_2 < 0$, the PQ symmetry is broken at the scale:

$$f_\zeta = \langle|\phi|\rangle \simeq \frac{M_p}{\mathcal{V}^{p_2-p_3}} \qquad \Rightarrow \qquad \langle\tau_{\rm dP}\rangle \simeq \frac{1}{\mathcal{V}^{2(p_2-p_3)-1}}\,. \tag{2.26}$$

The value of $|\phi|$ sets the decay constant of the open string phase ζ, $f_\zeta \sim \langle|\phi|\rangle$, which should be compared with the decay constant of the closed string axion $\theta_{\rm dP}$:

$$f_{\theta_{\rm dP}}^2 \simeq \frac{\partial^2 K}{\partial \tau_{\rm dP}^2} \sim \frac{M_p^2}{\mathcal{V}} \sim M_s^2\,. \tag{2.27}$$

The powers p_2 and p_3 can take different values depending on model building details [119, 120]. In the absence of sequestering where all soft terms are of order the gravitino mass, they are $p_2 = 2$ and $p_3 = 1$. On the other hand, when the visible sector is sequestered, they can be either $p_2 = 3$ and $p_3 = 2$, or $p_2 = 4$ and $p_3 = 2$. Let us consider each case separately:

$$\begin{aligned}
&(1)\ p_2 = 2 \quad p_3 = 1: && f_\zeta \simeq \frac{M_p}{\mathcal{V}} \ll f_{\theta_{\rm dP}} \simeq \frac{M_p}{\sqrt{\mathcal{V}}} && m_0 \simeq \frac{M_p}{\mathcal{V}} && \langle\tau_{\rm dP}\rangle \simeq \frac{1}{\mathcal{V}} \ll 1\,,\\
&(2)\ p_2 = 3 \quad p_3 = 2: && f_\zeta \simeq \frac{M_p}{\mathcal{V}} \ll f_{\theta_{\rm dP}} \simeq \frac{M_p}{\sqrt{\mathcal{V}}} && m_0 \simeq \frac{M_p}{\mathcal{V}^{3/2}} && \langle\tau_{\rm dP}\rangle \simeq \frac{1}{\mathcal{V}} \ll 1\,,\\
&(3)\ p_2 = 4 \quad p_3 = 2: && f_\zeta \simeq \frac{M_p}{\mathcal{V}^2} \ll f_{\theta_{\rm dP}} \simeq \frac{M_p}{\sqrt{\mathcal{V}}} && m_0 \simeq \frac{M_p}{\mathcal{V}^2} && \langle\tau_{\rm dP}\rangle \simeq \frac{1}{\mathcal{V}^3} \ll 1\,.
\end{aligned}$$

Note that in all cases $f_\zeta \ll f_{\theta_{\rm dP}}$, implying that the eaten axion is indeed $\theta_{\rm dP}$, and the value of the del Pezzo modulus is $\langle\tau_{\rm dP}\rangle \ll 1$, ensuring that this 4-cycle is in the singular regime. In the first two cases, reproducing an meV axion with $f_\zeta \sim 5\times 10^9\,$GeV, requires $\mathcal{V} \sim 10^8$ which gives $M_s \sim 10^{14}\,$GeV, and high scale soft terms around $m_0 \sim m_{3/2} \sim 10^{10}\,$GeV for case (1), and $m_0 \sim 10^6\,$GeV for case (2). Note that in both cases the model does not suffer from any CMP since the mass of the volume mode is $m_{\tau_b} \sim M_p/\mathcal{V}^{3/2} \sim 10^6\,$GeV. Case (3) instead can reproduce an meV axion for $\mathcal{V} \sim 10^4$, which correlates with $M_s \sim 10^{16}\,$GeV, $m_0 \sim 10^{10}\,$GeV and $m_{\tau_b} \sim 10^{12}\,$GeV.

It is worth pointing out that in all cases the decay constant of the open string axion is suppressed with respect to the string scale, allowing for the possibility to realise a standard post-inflationary scenario with $f_\zeta \ll H_{\rm inf}$. Due to the absence of any CMP, this model seems more promising to realise an meV axion. The main challenge is however the control over the EFT around the singularity, in particular the form of perturbative corrections to the Kähler potential, as well as potential sources of desequestering due to moduli redefinitions [96].

JCAP07(2026)060

3 meV axions as cold dark matter

Relic axions can be produced thermally by particle reactions initiated by the primordial plasma or by a number of non-thermal processes. Today, the former would have momenta of the order of the temperature of the Universe, $T \sim 2.3 \times 10^{-4}\,\mathrm{eV}$, smaller than a meV. However, they would have become non-relativistic late enough in the history of the Universe to behave as "hot" dark matter or dark radiation for most cosmological observables. The next generations of precision cosmological surveys will sharpen our measurements of ΛCDM parameters and could reveal a number of surprises in observables like the power spectrum of fluctuations or N_{eff}, cf. section 4 for a complete discussion.

In the following, we will discuss non-thermally produced QCD axion cold dark matter. We focus on vanilla cosmology, assuming radiation-domination (RD) started at temperatures $T_{\mathrm{RH}} \gg \mathrm{GeV}$. Depending on the timing of the PQ symmetry breaking, either before or after inflation, the dominant production mechanisms are the misalignment mechanism or axion production from the decay of topological defects. The characteristic momentum of the ensued axions is tied to the Hubble scale, which is suppressed by factors of T/M_{Planck} with respect to the temperature, making them perfect candidates for CDM. In the pre-inflationary scenario, the "standard" misalignment mechanism for *untuned* initial conditions far from $\theta_0 \simeq (2n+1)\pi$, with $n \in \mathbb{Z}$, predicts the observed CDM yield to be on the per-mil level [121],

$$\frac{\Omega_a h^2}{0.12} \simeq 2.7 \times 10^{-3} \theta_i^2 \left(\frac{\mathrm{meV}}{m_a}\right)^{1.17}. \tag{3.1}$$

The yield can be significantly increased by a few effects. In the *large misalignment angle* (LMA) scenario [122], the initial angle θ_i is very close to the top of the potential, $\theta \approx \pi$, delaying the onset of axion oscillations, see figure 2 (left). Assuming the $-\chi_T \cos\theta$ potential motivated by the dilute instanton gas approximation (DIGA) and following the standard calculation, see e.g. [123], one needs $\theta_0 - \pi \sim 10^{-32}$ for $m_a = 6$ meV axions to be dark matter.

Such a finely tuned result is very easy to invalidate after taking into account fluctuations. Adiabatic perturbations might not spoil the prediction, but isocurvature fluctuations are potentially enhanced and very constrained [124]. Since the latter are controlled by the inflationary expansion rate H_I, imposing a lower bound on H_I gives us an upper bound on the CDM abundance as a function of axion mass as shown in figure 2.

In the *kinetic misalignment* (KM) scenario [126], the axion field at GeV temperatures still has some residual velocity from its non-trivial history during the early Universe. The onset of oscillations, which happens at a time t_1 given by $m_a(t_1) = H(t_1)$ in the standard misalignment case, is delayed until the kinetic energy drops below the potential energy and the field is "trapped" by the QCD potential. Axions with meV masses require a very significant velocity and delay of the trapping with respect to the standard $\dot\theta_1 = 0$ case to account for a sizable fraction of the CDM abundance,

$$\Omega_a h^2 \simeq 0.12 \left(\frac{\mathrm{meV}}{m_a}\right)^{1.176} \frac{\dot\theta_1/H_1}{545}. \tag{3.2}$$

Adiabatic (and potentially isocurvature) fluctuations become $\mathcal{O}(1)$ for the large velocities required in the meV region due to non-linearities [127]. This affects the relic density calculation,

JCAP07(2026)060

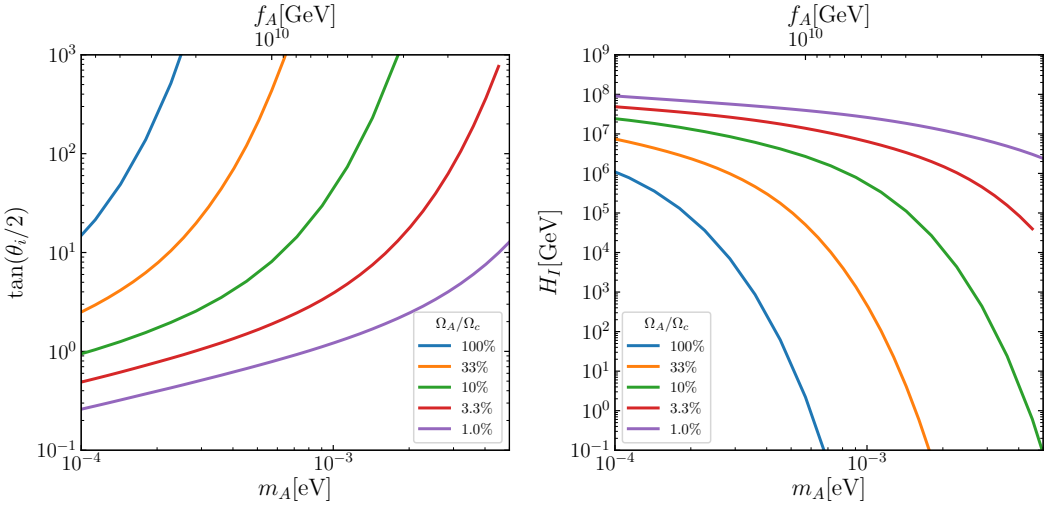


Figure 2. *Left.* Value of the initial misalignment angle required to obtain different fractions of axion cold dark matter. *Right.* Upper bound on the CDM abundance of meV axions in the LMA scenario as a function of the inflationary rate H_I. Reproduced from ref. [125]. © 2019 IOP Publishing Ltd and Sissa Medialab. All rights reserved.

but not as radically as in the LMA case [128]. In the extreme cases of the misalignment mechanism relevant for the meV axion scenario discussed here, the nonlinear dynamics can give rise to interesting phenomena with direct implications for experiments, such as the formation of axion miniclusters, which are typically considered a distinctive feature of post-inflationary axions, cf. refs. [129, 130].

In the post-inflationary scenario, the evolution of the resulting cosmic string network releases axions as string loops collapse, oscillate and intersect. The energy radiated by the network, quantified by the *string tension* μ, is enhanced by the large gradient energy near the axion strings, which is proportional to $\ell \equiv \log d_H/d_c$, the logarithm of the ratio of the typical inter-string distance $\sim H^{-1}$ and the inverse string core size $\sim f_a^{-1}$ which at around the QCD scale is $f_a/H \approx 10^{30}$, or $\ell \approx 70$.

The axion radiation from strings is measured as the instantaneous emission spectrum $\mathcal{F}$, which in the scaling regime is expected to follow a power-law $\mathcal{F} \sim k^{-q}$, with spectral index q between IR and UV cut-offs limited by causality (parameterized by a multiple of the Hubble scale, $x_0 H$) and the string core size ($\sim f_a^{-1}$), respectively. The absolute normalisation is proportional to the string length per Hubble patch ξ. The resulting density of axions has been the subject of a longstanding debate, which has been revived in the last decade, with the hope of settling it with state-of-the-art numerical simulations [36–45].

Most groups simulate the axion field as the angular degree of freedom of a complex scalar field ϕ with potential $V_{\rm PQ} \sim \lambda\left(|\phi|^2 - v^2\right)^2$. Current high-performance computing (HPC) clusters have limited the hierarchy of scales to a $\mathcal{O}(1)$ fraction of the grid size, typically $N^3 = (16k)^3$ or less grid sites for regular grids and up to effectively $N^3 = (262k)^3$ using Adaptive Mesh Refinement (AMR) [43]. A clever model with two complex scalars with charges $q_{1,2}$ under a vector field is able to simulate strings with much higher "effective" tensions, $\mu \sim (q_1^2 + q_2^2)$, using the same regular grids [131–133]. The results can be summarized as

JCAP07(2026)060

follows. The string length parameter ξ shows an attractor-like behavior whose fixed point increases with ℓ [36, 134, 135]. Simulations with fixed ℓ confirm the dependence and allow us to interpret the evolution as a tracking solution where ξ approaches a growing moving target $\xi(\ell)$ [133]. This behavior has been established up to $\ell \sim 9$ but is expected to plateau at some level, because in the $\ell \to \infty$ limit, global strings are expected to evolve as Nambu-Goto (NG) strings with renormalised tension, which are insensitive to the value of ℓ. However, the plateau could be very large. Early NG simulations find $\xi \sim 13$ [136] and recent ones $\xi \sim 4$ [132, 137]. Extrapolating the simulations of ref. [41] leads to $\xi \sim 7(3)$. The lower cut-off parameter, x_0, has been found to depend on this value [41], which can make a difference if large ξ values are assumed at the physical values of $\ell \sim 70$.

The most relevant parameter for the final abundance is q, which controls whether many $k \sim H$ ($q > 1$) or few $k \sim f_a$ ($q < 1$) axions are emitted by strings. Some theoretical expectations can be drawn based on simulations of Nambu-Goto strings coupled to a Kalb-Ramond field $B_{\mu\nu}$, which plays the role of the axion via the duality $\nabla\theta_\mu \sim \nabla_{[\nu} B_{\rho\sigma]}$ in four spacetime dimensions [138, 139]. Long strings radiate low energy axions and loops lead to $q \sim 4/3$ except in some cases like the circular loop, $q \approx 1$. Thus, one expects $q \gtrsim 1$ and a significant enhancement of the axion abundance. On the other hand, some authors argue that $q = 1$ is the correct expectation for global strings [40, 43, 45]. Network simulations show either $q \simeq 1$ [40, 43] or $q < 1$ with a linearly increasing trend with ℓ approaching $q \sim 1$ [36, 38, 41, 42]. The results appear to be compatible at the moment, given that the first AMR simulation [40] did not use initial conditions in the attractor but slightly underdense, which increases q [41]. The same applies to the updated results from an even larger AMR simulation of the same group [43]. The attractor simulations extrapolate well linearly to $q > 1$ at $\ell \sim 70$ but a saturating solution $q \to 1$ cannot be excluded, particularly given the large discretisation effects affecting the spectrum at large ℓ [41].

A recent study considered the uncertainties in the simulations to extrapolate the axion number radiated by networks taking into account different extrapolation models [41]. If $q > 1$ at $\ell \sim 70$ is assumed, the axion yield is so large that $\langle|\dot{\theta}|^2\rangle$ is significant at t_1, in analogy to the kinetic misalignment in the pre-inflation scenario. Cosmic strings and walls tend to be subdominant at this stage. The delay in the oscillations covers a period where nonlinearities actually decrease the axion number, moderating the enhancement gained by the IR emission spectrum [38]. If $q = 1$ is assumed, these effects are not large. The combined theoretical uncertainty in the post-inflationary axion CDM scenario within a standard RD cosmology leads to the mass range [41],

$$50\ \mu\text{eV} \lesssim m_a \lesssim 0.5\ \text{meV}, \tag{3.3}$$

which encompasses the results of refs. [38, 42, 43], lying near the lower and upper ends of this range, respectively.[1]

The axion cold DM abundance from strings scales approximately as $f_a^{1.17}$, neglecting nonlinear effects. Using this scaling to extrapolate to the meV-mass regime suggests that post-inflationary axions contribute at the level of $1 - 50\%$ of the CDM, cf. figure 3.

[1]For a detailed overview and an in-depth discussion of the predictions and methodologies adopted by the different groups, we refer to section 4.2 of ref. [140].

JCAP07(2026)060

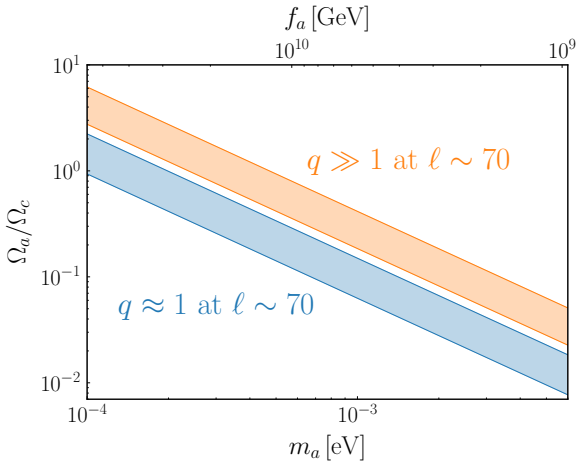


Figure 3. Abundance of $N_{\rm DW} = 1$ post-inflationary axions from strings as fraction of the observed CDM. Different colors correspond to different assumptions about the spectral index, $q \approx 1$ (blue) and $q \gg 1$ (orange) evaluated at the physical value of $\ell \sim 70$, and the latter includes the effect of nonlinearities discussed in ref. [38]. The colored regions also show the systematic uncertainties associated with the extrapolation of the simulation results estimated in ref. [41].

The above estimate of the axion CDM abundance in the post-inflationary scenario can be applied to the models with $N_{\rm DW} = 1$, where $N_{\rm DW}$, dubbed as a "domain wall number", is an integer representing the number of degenerate minima of the axion potential. For $N_{\rm DW} > 1$, the picture is very different, because in this case the axion field has $N_{\rm DW}$ CP-conserving, degenerate vacua, all of which get statistically equally populated in the Universe. After the QCD phase transition, the Universe would be a collection of domains separated by domain walls (DWs), sheet-like topological defects associated with the spontaneous breaking of a discrete $\mathbb{Z}_{N_{\rm DW}}$ subgroup of the $\mathrm{U}(1)_{\rm PQ}$ symmetry. The contribution of these walls can eventually dominate the energy density of the Universe, which is observationally excluded [46, 141], but small modifications of the standard scenario change this conclusion dramatically. As examples, we mention the effect of small PQ-breaking terms and models with more than one axion. The PQ-breaking terms, which may be completely natural from quantum gravity if PQ is a purely global symmetry, will lift these vacua by favouring the least energetic configuration [142]. This drives the collapse of the DWs and restores a Universe compatible with observations [46, 143, 144]. But these "biases" imply that the axion will not exactly cancel the CP violation of the SM in the vacuum and they are thus very strongly constrained by the upper limits on the neutron EDM [35, 145–147]. Limiting bias terms to moderate CP violation requires making them very small or very fine-tuned to zero in the true vacuum. If they are small, then the pressure difference between the domains is small, and DWs release their energy much later than the epoch of the QCD phase transition, leading to a huge boost in CDM such that it surpasses the observed CDM abundance. Therefore, if not excluded, meV axions tend to account for 100% of the CDM in this scenario. A small but non-vanishing CP violation induced by the bias terms for the collapse of DWs also leads to observable effects in the experimental searches for axion-mediated long-range forces [148], cf. ref. [149]. Furthermore, the late-time collapse of DWs could lead to the production of

JCAP07(2026)060

gravitational waves [146, 150] and the formation of primordial black holes [151], which could be a smoking gun for this scenario. Alternatively, if there are two PQ U(1) symmetries, and consequently two Nambu-Goldstone bosons, the string network will contain two types of strings and the domain walls may be eventually locked into cosmologically not-so-harmful string-bundles [152, 153], which might survive until today.

Despite several potentially interesting phenomenological consequences, the $N_{\rm DW} > 1$ scenario has not been studied numerically as intensively as the $N_{\rm DW} = 1$ case, see refs. [35, 146, 154]. More detailed studies are needed and much welcomed in view of the relevance and potential impact of the meV frontier detailed in this paper.

In summary, meV axions can account for a sizeable fraction, if not all, of the observed cold DM density and have very distinctive observational consequences. The misalignment mechanism requires a finely tuned initial condition with potential isocurvature fluctuations discoverable in the cosmic microwave background and other features [122]. The kinetic misalignment with large velocity implies also the presence of small and characteristic axion miniclusters [129, 130]. Even in the most constrained $N_{\rm DW} = 1$ post-inflationary scenario, meV axions contribute easily a few percent of the CDM abundance (and up to a 50%) and also imply axion miniclusters, although their size is typically larger and somehow uncertain [155]. Finally, in the $N_{\rm DW} > 1$ post-inflationary case, axions can naturally constitute all of the CDM, requiring new CP-violating physics with observable consequences and predicting primordial gravitational waves, black holes, and different (larger) axion miniclusters.

4 meV axions as dark radiation

Axions interact with SM particles via anomalous gauge couplings and derivative couplings to fermions, giving rise to cosmological signatures that extend beyond their role as DM. In the primordial thermal bath, which consists of a relativistic plasma of SM particles in thermal equilibrium at temperature T, axions can be efficiently produced through scatterings and decays [156–181]. If these interactions are sufficiently frequent, inverse processes drive axions into thermal equilibrium with the bath. If the couplings are instead too weak to ensure thermalization, axions can still be generated in appreciable abundances, potentially leaving observable cosmological imprints. In both scenarios, cosmic expansion eventually leads to a phase in which axions propagate freely along geodesics of the expanding Universe, described by the Friedmann–Lemaître–Robertson–Walker (FLRW) metric. In the former case, free propagation begins after *freeze-out*, while in the latter axions are produced through *freeze-in*.

The existence of a primordial thermal bath is firmly established at temperatures below the MeV scale, as evidenced by the successful prediction of light element abundances through Big Bang Nucleosynthesis (BBN). Extending this well-tested picture of the early Universe to higher temperatures is reasonable, although it must eventually break down during inflationary reheating. We only require that SM particles form a thermal bath during the epochs relevant for axion production, implying a reheat temperature just above the weak scale.

Once these two conditions are satisfied, namely the presence of an axion coupled to SM fields and a primordial thermal bath with temperatures reaching the weak scale, the subsequent cosmological evolution is fully determined. The resulting axion population is therefore *inevitable* and must be computed with care. In practice, the implications of this

JCAP07(2026)060

framework are explored by first calculating the axion abundance produced in the early Universe and then translating it into observable signatures.

4.1 Thermal production of axions

Thermal axions are produced at early times when the bath temperature is much larger than their mass, so their average kinetic energy greatly exceeds their mass. They arise in the ultrarelativistic regime, and we refer to this population as *hot axions*. As the Universe expands, axions follow FLRW geodesics and their momenta redshift, causing energies to decrease inversely with the scale factor. The thermal bath cools simultaneously, with its temperature decreasing according to entropy conservation. Up to order-one corrections from changes in the effective number of degrees of freedom, the axion "temperature" tracks that of the plasma. The quotation marks emphasize that this does not imply thermal equilibrium. Even after decoupling, or if equilibrium is never reached, the axion momentum distribution remains close to an equilibrium form, reflecting its thermal origin. For axions in the meV mass range, which remain relativistic at recombination, momentum and energy are effectively equivalent. Consequently, the average axion energy remains, up to order-one factors, comparable to the bath temperature, allowing it to be reliably tracked throughout cosmic evolution.

As long as they remain relativistic, axions contribute to the radiation energy density of the Universe. This contribution is constrained at two key epochs: during BBN, which probes the radiation content at temperatures around MeV, and at the time of CMB formation, when the temperature is approximately 0.3 eV. In both cases, axions with masses in the meV range remain relativistic and act as an additional radiation component. This extra contribution, commonly referred to as *dark radiation*, is parameterized in terms of an effective number of additional neutrino species,

$$\Delta N_{\rm eff} \equiv \frac{8}{7}\left(\frac{11}{4}\right)^{4/3}\frac{\rho_a}{\rho_\gamma}\,, \tag{4.1}$$

where ρ_a and ρ_γ denote the energy densities of relativistic axions and photons, respectively. The numerical prefactor accounts for the difference in quantum statistics between fermions and bosons, as well as for the temperature mismatch between the cosmic neutrino background and the CMB.

Once the axion couplings are specified, the problem reduces to determining the abundance of axions produced and their energy spectrum. This requires choosing a computational strategy. The central ingredient is the production rate, which for a given channel quantifies the number of axions produced per unit time and volume. When needed, the rate can be expressed differentially in momentum, a refinement useful below. In this section, we outline three common methods to evaluate the thermal axion contribution to $\Delta N_{\rm eff}$. A comprehensive overview is provided in ref. [176], where the methods are presented in increasing order of complexity and compared to assess their reliability. Fully general treatments are computationally demanding, so approximate methods are preferred whenever applicable.

- **Instantaneous decoupling.** The simplest method to estimate the axion abundance is the *instantaneous decoupling* approximation. It relies on two key assumptions: (i)

JCAP07(2026)060

axions thermalize with the plasma at early times; (ii) decoupling is sudden, occurring at a single temperature T_D for all momenta. The decoupling temperature is estimated by equating the production rate Γ to the Hubble rate H, $\Gamma(T_D) \simeq H(T_D)$. Consequently, the contribution to dark radiation can be expressed as $\Delta N_{\rm eff} \simeq 13.69\, g_{\star s}(T_D)^{-4/3}$, where $g_{\star s}(T)$ denotes the effective number of degrees of freedom contributing to the entropy density of the primordial thermal bath.

- **Tracking the number density.** The previous method is oversimplified for several reasons. It fails if axions never reach thermal equilibrium, missing freeze-in production, and the estimate $\Gamma(T_D) \simeq H(T_D)$ only captures the correct order of magnitude. Since $\Delta N_{\rm eff}$ is sensitive to T_D, particularly below the weak scale where the effective number of degrees of freedom changes rapidly, this approach can produce errors exceeding current experimental uncertainties. A more refined, still approximate, method follows the axion *number density* n_a via the Boltzmann equation

$$\frac{dn_a}{dt} + 3Hn_a = \gamma_a \left(1 - \frac{n_a}{n_a^{\rm eq}}\right) , \tag{4.2}$$

  where γ_a is the axion production rate per unit volume and $n_a^{\rm eq}$ the equilibrium density. This equation assumes Maxwell–Boltzmann statistics for all particles and kinetic equilibrium throughout production (see, e.g., the derivation in appendix C of ref. [176]). While the first assumption is generally valid due to small occupation numbers in the early Universe, the second can have a significant impact. The equation is conveniently solved using the comoving density $Y_a \equiv n_a/s$, which approaches a constant Y_a^∞ once production ceases, yielding $\Delta N_{\rm eff} \simeq 74.85\,(Y_a^\infty)^{4/3}$.

- **Full phase-space analysis.** The limitation of the approach described above can be overcome by performing a full phase-space analysis. Specifically, one can follow the time evolution of the *axion distribution* in momentum space, $f_a(k,t)$, by solving the integro-differential Boltzmann equation

$$\omega \frac{df_a(k,t)}{dt} = C_a[f_a(k,t)] . \tag{4.3}$$

  This approach allows one to track the evolution of each momentum mode individually. The collision operator C_a encodes all relevant production processes and consistently incorporates the quantum statistics of all participating particles. The Boltzmann equation can be coupled to the evolution equation for the thermal bath energy density, thereby accounting for energy exchange between the visible sector and dark radiation. Together with the Friedmann equation, these relations form a closed system that can be solved to follow the axion evolution in momentum space without assuming instantaneous or momentum-independent decoupling [176]. This framework naturally captures spectral distortions arising from non-instantaneous decoupling, which are missed by simpler methods. Compared to commonly used approximations, the resulting differences in the predicted $\Delta N_{\rm eff}$ can exceed the sensitivity of future CMB observations, emphasizing the need for this level of precision.

JCAP07(2026)060

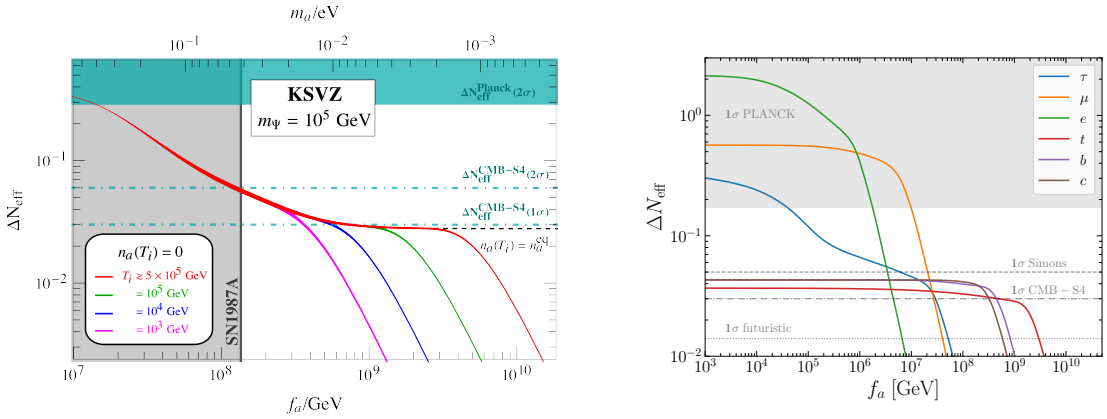


Figure 4. Predicted $\Delta N_{\rm eff}$ from thermal axion production as a function of f_a, compared with current and future CMB sensitivities. *Left.* KSVZ axion framework, with the corresponding m_a shown on the upper horizontal axis (reproduced from [170]. CC BY 4.0). *Right.* Axion couplings to SM fermions with unit Wilson coefficient, based on the full phase-space analysis of ref. [179] (reproduced from [179]. CC BY 4.0).

4.2 Dark radiation as a cosmological consequence

In the following, we discuss the predicted contribution to dark radiation from axion couplings to gluons and to SM fermions, respectively.

The left panel of figure 4 shows the predicted contribution to dark radiation from thermally produced axions, expressed as $\Delta N_{\rm eff}$, as a function of the axion decay constant f_a. The results are obtained within the KSVZ axion framework, where interactions with gluons dominate axion production; for this reason, the upper horizontal axis also indicates the corresponding axion mass m_a, which is in one-to-one correspondence with f_a. The axion abundance is computed by solving the Boltzmann equation for the number density, assuming a vanishing initial population. This conservative choice ensures that any axions produced during reheating or via other nonthermal mechanisms would only increase the final abundance, so the curves represent the minimal thermal contribution. Different curves correspond to different initial temperatures for the Boltzmann evolution; once this temperature exceeds the relevant fermion mass threshold, the resulting axion abundance becomes insensitive to this choice, reflecting the IR-dominated nature of production above this mass scale. The shaded region shows the current bounds set by Planck [182], which lie entirely within the parameter space already excluded by supernova bounds. Although these bounds are subject to astrophysical uncertainties, they underscore the value of complementary cosmological probes. In this context, measurements by the Simons Observatory and future CMB surveys [183, 184] will extend sensitivity to currently allowed regions, enabling the exploration of axion masses down to the meV scale.

The right panel of figure 4 shows predictions for $\Delta N_{\rm eff}$ as a function of the axion decay constant f_a, now arising from couplings to fermions. A derivative, flavor-conserving interaction is assumed with a Wilson coefficient set to unity, though other choices can be accommodated by rescaling f_a. In this case, the axion mass is unrelated to f_a, so the results are valid as long as m_a remains below the temperature at the last scattering surface, in particular down to the

JCAP07(2026)060

meV scale. The results are taken from ref. [179], where only couplings to charged leptons and heavy quarks are considered. Since charged leptons carry no color, their production rates can be reliably computed across the QCD confinement scale. For heavy quarks, only the top quark is sufficiently heavier than the GeV scale for robust predictions, while the bottom quark case is borderline and the charm quark case requires caution; these subtleties and their associated uncertainties are discussed in detail in ref. [179]. A key novelty of this study is the inclusion of a proper phase-space treatment of axion production. As advocated in ref. [176], a rigorous momentum-space framework is essential for accurate predictions of dark radiation in future data. Solving the full Boltzmann equation for the phase-space distribution goes beyond the instantaneous decoupling approximation and the assumption of kinetic equilibrium, while consistently incorporating quantum statistical effects. Non-instantaneous decoupling across different momentum modes leads to spectral distortions that affect $\Delta N_{\rm eff}$. Compared with conventional approximations, these corrections can exceed the projected sensitivity of upcoming CMB experiments, motivating this detailed analysis. Overall, the results update earlier approximate studies and quantify the ability of future CMB surveys to probe axion couplings to SM fermions; in particular, for heavier fermions, cosmological probes are expected to be more sensitive than terrestrial experiments.

4.3 Thermal axions: what's next?

Thermal axion production is an inevitable consequence of the early Universe once couplings to SM fields exist and the primordial plasma reaches at least electroweak-scale temperatures. Figure 4 quantifies this by showing the predicted $\Delta N_{\rm eff}$ as a function of the axion decay constant f_a. Further theoretical progress is desirable to sharpen these predictions and extend their validity. The results in the left panel of figure 4 are obtained within a framework combining different theoretical treatments of the axion production rate via the coupling to gluons: leading order in perturbative QCD above the confinement scale, leading order in chiral perturbation theory in the confined phase, and a smooth interpolation in the intermediate regime. The production rate itself is not directly observable and enters only as an input to the Boltzmann equation computing $\Delta N_{\rm eff}$; accordingly, sizeable modifications of the rate do not necessarily translate into equally large changes in the final observable (see appendix D of ref. [170]). Nevertheless, overcoming the current limitations in both QCD phases and treating the intermediate regime more quantitatively remain important goals. In particular, the convergence of the perturbative expansion at finite temperature may be less efficient than at zero temperature, both above [174, 177] and below [174, 185, 186] confinement. Fully momentum-resolved predictions currently exist for axion couplings to SM fermions [179–181] or pions [174, 175], but extending such analyses to gauge bosons, particularly gluons, remains a crucial challenge. The right panel of figure 4, obtained from a momentum-space treatment, highlights additional limitations: production via charm quarks occurs too close to the confinement scale to be fully reliable, while for light quarks a careful matching to a hadronic description is required in a delicate regime. While these challenges await resolution to achieve fully robust and precise predictions, axion dark radiation remains a key observable for testing early-Universe physics and constraining fundamental particle interactions in the era of precision cosmology.

JCAP07(2026)060

5 meV axions astrophysics

Light axions with feeble couplings can be plentifully produced in stellar interiors. Various direct and indirect searches have been devised to test this emission. As no evidence has emerged so far, astrophysical data result in some of the most stringent existing bounds on axions [107, 187]. Axions with masses $10^{-3}-10^{-2}$ eV are predicted in top-down model building approaches (section 2), can constitute dark matter in post-inflationary scenarios (section 3), and could also show up as thermal radiation at future CMB surveys (section 4). Coincidentally, such axions lie just at the edge of current stellar sensitivity.

The most suitable astrophysical probes depend on the axion coupling structure. In the KSVZ model — and in the DFSZ-I model for $\sin^2\beta \lesssim 0.2$ — the dominant constraints come from axion interactions with nucleons. Therefore, the most powerful "axion factories" are dense nuclear environments such as cooling neutron stars (NSs) [188] and the protoneutron stars (PNSs) formed in core-collapse supernovae (SNe) (for early work see e.g. [189–199]). These two systems probe similar physics, as the ratio of axion to neutrino luminosities is nearly temperature-independent, implying comparable relative effects of exotic cooling [200]. Observations of isolated NSs require that axion emission do not excessively accelerate cooling, which yields a bound $m_a \lesssim 16\,\mathrm{meV}$ for the KSVZ axion [201].

The classic SN constraints are also based on a cooling argument [189–199]. The PNS cools over $\sim$ 5-10 s mainly by neutrino emission, as confirmed by the SN 1987A neutrino burst. Excessive axion losses would shorten the burst by increasing the cooling rate, implying the condition $L_a \lesssim L_\nu$ at around 1 second post-bounce, when axion emission is peaking [106]. Numerical simulations including axion cooling reproduce this qualitative effect [195, 196], although they did not include PNS convection, which significantly impacts the neutrino burst [202]. Nevertheless, it is still a commonly adopted order-of-magnitude requirement that $L_a \lesssim L_\nu$ to avoid impacting the SN 1987A observations.

For large couplings, axions are not emitted volumetrically from the entire PNS, but rather from a decoupling surface inside of which they are in thermal equilibrium [196, 203]. The axion emission in this regime is diffusive, acting like an effective non-standard channel of thermal conduction [204]; as usual, the thermal conductivity is proportional to the axion mean free path, so that at large couplings the effiency of non-standard PNS cooling becomes negligible.

5.1 Axion production in dense nuclear media

Estimating the axion luminosity L_a remains challenging because of the poorly known properties of dense nuclear matter in SN cores; an incomplete list of works addressing this challenge includes refs. [189–194, 197, 198, 205–219]. Even the concept of well-defined nucleon quasiparticles becomes questionable: nuclear matter at these densities is only a marginal Fermi liquid. The typical nucleon–nucleon interaction rate [219] is $\Gamma \sim n_n v_{\rm rel}\sigma_{nn}F_{\rm deg}$, with $n_n \simeq 10^{38}\,\mathrm{cm}^{-3}$ the nuclear density, $v_{\rm rel} \sim 0.3c$ the relative velocity, $\sigma_{nn} \sim 40\,\mathrm{mb}$ the cross section at the relevant energies, and $F_{\rm deg} \sim 0.6$ a mild degeneracy factor. This gives $\Gamma \sim 30$–$40\,\mathrm{MeV}$, comparable to the nucleon kinetic energy $K \sim 50$–$100\,\mathrm{MeV}$. Consequently, individual nucleon excitations are short-lived, and treatments of axion production based on single-nucleon processes carry intrinsic uncertainties of order unity. While such approaches can yield reliable

JCAP07(2026)060

order-of-magnitude estimates of L_a, achieving precision better than a factor of ~ 2 is likely impossible within this framework.

Even assuming a single-particle picture, a detailed treatment of axion emission is far from trivial. The dominant emission process is nucleon-nucleon bremsstrahlung $NN \to NNa$, but a first-principle treatment requires a modeling of the nucleon-nucleon potential, and furthermore the potential itself is not guaranteed to be perturbative at the relevant center-of-mass energies. Light axions are sourced by the spin-isospin fluctuations of the nuclear medium, so the information on their emission is primarily encoded in the rate of spin fluctuations of a nucleon Γ_σ [106, 219]. If the coupling is predominantly to neutrons, then axion production can be triggered only by a fluctuation in the total spin of the pair of colliding neutrons $nn \to nna$; in turn, total spin fluctuations are predominantly caused by the tensor interaction dominated by one-pion-exchange [189–194], although at such large center-of-mass energies the amplitude for this exchange is substantially reduced, as phenomenologically modeled with heavier meson exchanges [213, 220]. However, for $np \to npa$ scattering, if the axion couples with different strengths to the nucleons (e.g. the KSVZ axion couples predominantly to protons), then it suffices that only the proton spin fluctuates. In this case, non-tensor interaction channels can contribute [219], which are dominated by contact interactions and therefore not well represented by one-pion-exchange. It goes without saying that the interaction amplitude for all these channels might itself suffer strong renormalization in the dense nuclear medium that are not fully controlled (e.g. refs. [221–223]).

In this uncertain setting, a very flexible way forward is to consider an energy-independent Γ_σ as a parametric measure of uncertainty [106]; in this approximation, the axion emission spectrum per unit stellar mass M and axion energy E_a is simply

$$\frac{d\dot{N}_a}{dE_a dM} = \frac{g_{ap}^2 Y_p}{8\pi^2 m_p^3} \frac{E_a}{e^{E_a/T}+1} \frac{\Gamma_\sigma}{1+(\Gamma_\sigma/2E_a)^2}, \tag{5.1}$$

where T is the medium temperature, Y_p is the proton mass fraction, and m_p is the proton mass. The properties of the internal core can vary within quite a wide range among different SNe [219], depending on the mass of the central PNS. Overall, a good measure of the range that different SNe can attain is in the total number of axions emitted; this can vary in the interval $N_a \sim 10^{56-57}\, g_9^2$, with $g_9 = g_{ap}/10^{-9}$, with heavier PNSs tending to the upper edge of this interval. The average energy of these axions is surprisingly stable $E_{\rm av} \sim 60 - 80\,{\rm MeV}$, much larger than the neutrino energy since these axions are emitted volumetrically over the entire core.

Axions may also be produced by pionic processes $\pi^- p \to na$ [198, 206, 207], a possibility recently revived in refs. [214, 224, 225]. A simple measure of how much this channel could contribute is the ratio between the number of axions emitted from pionic processes and from bremsstrahlung, which for a light PNS is roughly $\mathcal{R} \sim 33 Y_\pi$, where Y_π is the pion fraction in the core. According to the estimates in ref. [219], $Y_\pi \sim 0.03$ would lead to a correction $\mathcal{R} \sim 1$; the effects on the cooling rate of the PNS would be even larger, since pion-induced axion emission peaks above the pion mass, larger by a factor $2-3$ than the average energy of axions from bremsstrahlung. However, the authors of ref. [224] underestimated the upward energy shift of pions caused by their refraction in the dense nuclear medium; their later work [226]

JCAP07(2026)060

leads to a range $\Delta E_\pi \sim 100 - 150\,\mathrm{MeV}$. For comparison, parametric textbook estimates would lead to $\Delta E_\pi \sim 40 - 50\,\mathrm{MeV}$ [227]. Hence, the fraction Y_π would be suppressed by an additional factor $e^{-\Delta E_\pi/T} \sim 10^{-3} - 10^{-1}$, depending on how large ΔE_π ultimately is, and assuming a typical temperature $T \sim 30\,\mathrm{MeV}$. Hence, thermal pions remain an intriguing possibility for axion production, but uncertain by orders of magnitude.

Overall, excluding the pions, the cooling constraints from SN 1987A based on emission of axions with only bremsstrahlung shows a surprising stability among the many works in the literature [106, 212–214, 218, 219], with the most recent estimate setting it at $m_a \lesssim 12\,\mathrm{meV}$ [219]; a reasonable uncertainty on this constraint may span perhaps a factor 3 in mass, corresponding to roughly an order-of-magnitude uncertainty in the axion emission.

5.2 Axion conversion in astrophysical magnetic fields

An intriguing perspective to probe axions emitted from SNe is via their subsequent conversions to high-energy gamma-rays in astrophysical magnetic fields. This has long been considered in the literature in the context of conversions in the Galactic magnetic field [228–233], which could produce a 100-MeV-gamma-ray burst in correspondence of a SN. For SN 1987A, this would have been visible by the Solar Maximum Mission (SMM) [234] (see also refs. [235, 236]). However, SMM did not observe any such burst, leading to stringent bounds on axion-like particles coupling to photons or to photons and nucleons simultaneously. However, conversions in the Galactic magnetic field become inefficient for relatively light axions $m_a \gtrsim 10^{-6}\,\mathrm{eV}$. At such masses, the QCD axion has very feeble couplings, which cannot be reached by this method.

Recently, ref. [237] has proposed the intriguing idea that the magnetic field of the progenitor star of the SN might be a much more efficient axion-photon converter. The distances involved in the conversion are in this case much shorter, of the order of tens to hundreds of solar radii, compared with the kiloparsec scale of the Galactic magnetic field. This means that axions have much less space to convert into photons, so their overall conversion probability is smaller. However, it also implies that axions with much larger masses can convert efficiently.

For SN 1987A, the relatively weak sensitivity to the 100-MeV signal does not allow one to obtain any novel constraint, especially because of the largely unknown situation with regards to the surface magnetic field of its progenitor, Sanduleak −69 202. The latter was a blue supergiant (BSG), a class of supergiants whose measured magnetic fields is in the ballpark of $10 - 100\,\mathrm{G}$; ref. [237] obtained, with an optimistic value of 100 G, constraints on the ALP-photon coupling stronger than the level of the CAST exclusion. However, after removing the contribution of pionic emission as discussed above, as well as correcting for the adopted data sample from the SMM (since an artificially rescaled version from ref. [233] had been used) and accounting for the uncertainty in the progenitor radius, the overall constraints [219] turn out to be comparable with the CAST exclusion. One should stress, though, that without a direct observation of the magnetic field of Sanduleak −69 202, one cannot truly rely on these regions as excluded.

The next galactic SN might be observable with telescopes much more sensitive than the SMM satellite in the 100-MeV energy range. Our instrument of choice at present is the

JCAP07(2026)060

Fermi Large Area Telescope (LAT). With the typical effective area of Fermi-LAT, ref. [237] shows that a galactic SN at 10 kpc from Earth might lead to a detection of a gamma-ray burst from the QCD axion. On the other hand, this detection prospect includes a surface magnetic field of 1 kG, as well as the pionic contribution to axion production. As argued in ref. [219], such fields are actually not observed in BSGs, which seem to have fields at most as large as $\sim 100\,\mathrm{G}$. When accounting for typically lower magnetic fields, ref. [219] finds that a more realistic horizon of detection from a BSG progenitor is around 1 kpc. Moreover, BSG progenitors are quite rare, about 1% of core-collapse SNe [238, 239]; for the much more common RSG progenitors, the typical coherent fields are significantly lower, around $1 - 10\,\mathrm{G}$, although it is speculated that they may host turbulent small-scale fields reaching up to 100 G. In this case, the prospects for detection of RSGs might be quite close to those of BSGs at large axion masses [237].

On the other hand, as recently advocated in ref. [240], the best candidate for axion-photon conversion in a supernova progenitor would in fact be a Type Ibc SN, associated with more compact progenitors ($R \sim 0.1 - 1\,R_\odot$) [241] and correspondingly larger observed magnetic fields, ranging from hundreds of G [242–245] up to even 43 kG in an extreme case [246]. Their generally larger magnetic field and incidence rate (about 30% of all core-collapse SNe [238, 239, 247, 248]) make them an ideal target for gamma-ray burst detection from QCD axion conversion, reaching up even to SNe at a distance of 10 kpc, exploding in the Galactic Center [240].

Regardless of the nature of the next galactic SN, the 100-MeV-gamma-ray burst induced by axion conversion will only last a few seconds, the typical timescale over which the SN core cools down. Hence, Fermi-LAT, which at any moment only sees about a fifth of the sky, might easily miss it altogether. For this reason, the Berkeley group [237] has advocated for a constellation of satellites that might achieve Fermi-LAT sensitivity with a 4π field of view, ensuring coverage of the sky during the next galactic SN.

A final perspective for the future, mostly motivated by the recent case of GW170817 [249–252], is the production of axions in the merger of two neutron stars (NSMs), which produces a hot remnant very similar to the PNS formed within a core-collapse SN. Depending on the masses of the colliding neutron stars, this remnant is often expected to be unstable and collapse into a black hole over shorter timescales than in a SN, ranging from tens of milliseconds to a few seconds. More importantly, these events are much rarer than SNe, and therefore expected at extragalactic distances of tens of Mpc. In principle, they can be nearly as efficient as SNe in emitting axions, limited mainly by the shorter lifetime of the remnant. However, due to the larger distances, they are generally much less competitive when it comes to the observation of the gamma-ray burst from axion-photon conversion in the Galactic magnetic field [253]. Conversion within the magnetic field of the remnant, which can reach up to even $10^{14}\,\mathrm{G}$, might be significantly more efficient at large masses [237]. Despite such large magnetic fields, when realistic conditions for the merger remnant are considered, in particular by virtue of its shorter lifetime than SNe, its time-integrated axion emission and the larger expected distances conspire to make NSMs a much less sensitive probe of axion-photon conversion [254]. In fact, the situation is even worse, since the merger produces a sizable amount of dynamical ejecta which impede axion-photon conversion for

JCAP07(2026)060

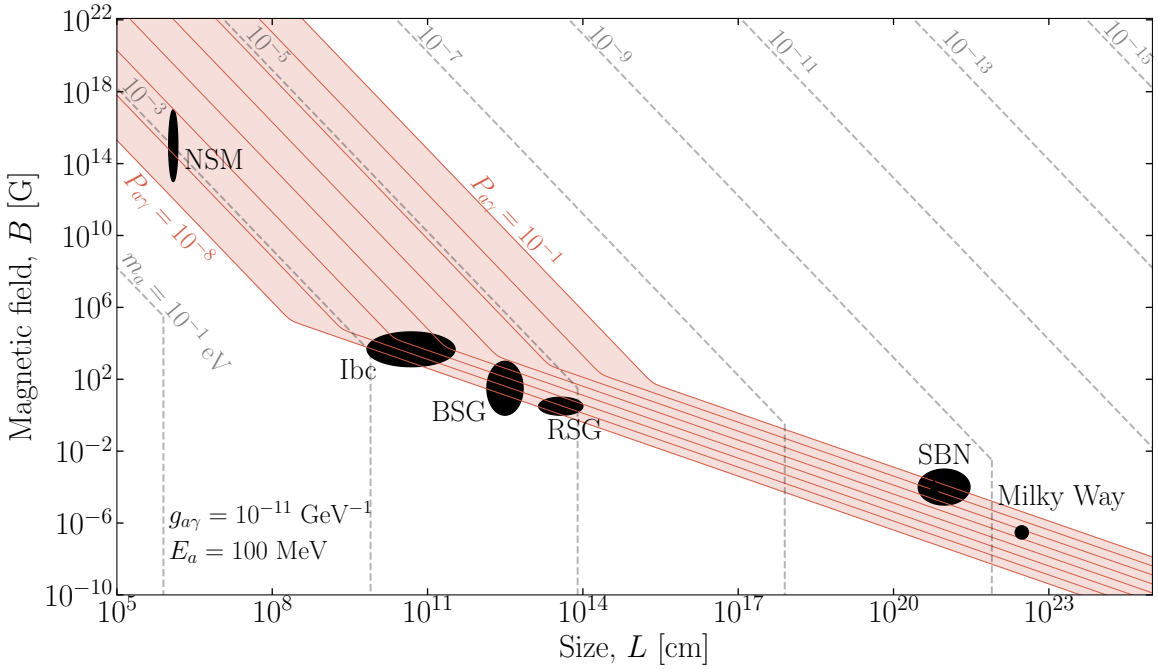


Figure 5. Hillas plot of the astrophysical sources as axion-photon converters. The colored lines identify the probability of axion-photon conversion for massless axions, while the gray lines identify the axion masses at which coherence in the axion-photon conversion is lost. Reproduced from [219]. The Author(s). CC BY 4.0.

a large fraction of the emitted axions [219], so that even for a future NSM one does not expect to probe any novel parameter space by this strategy.

Figure 5 summarizes succinctly the panorama of axion-photon conversion in astrophysical sources, using the format of the Hillas plot, widely known in cosmic-ray physics. The size and strength of the magnetic field is what determines both the maximum energy to which charged particles can be accelerated, and the axion-photon conversion probability. We see here that large sources with feeble magnetic fields, such as starburst nuclei [255] and the Milky Way, can efficiently interconvert axions and photons, due to their large coherence length. However, for the same reason, it takes a very small axion mass to disrupt the coherence and dramatically suppress the conversion efficiency. Compact sources, like the supernovae progenitors, have significantly lower conversion probabilities, but can maintain coherence up to significantly larger masses. Finally, neutron star mergers, with their very intense fields, are located in a region where the conversion probability is suppressed — visible from the change in slope of the red lines in figure 5 — so they are overall *less* efficient than stellar environments at converting axions to photons, even though their compact radii allows for an efficient conversion of slightly heavier axions.

5.3 Supernova axions in large-volume Cherenkov detectors

Large water Cherenkov detectors, such as Hyper-Kamiokande (HK) [256, 257], are primarily designed to observe neutrino fluxes from astrophysical sources, most notably core-collapse supernovae (SNe). In these environments, neutrinos dominate the cooling of the newly formed

JCAP07(2026)060

proto–neutron star. However, the extreme densities and temperatures reached during core collapse also make SNe efficient laboratories for the production of other light particles with feeble interactions with matter, and thus able to contribute to the cooling process.

Among such hypothetical particles, the QCD axion focus of this review is particularly well motivated. If axions couple to nucleons, they can be copiously produced in SN cores and escape the dense environment, carrying away energy. In the case of a sufficiently nearby SN, the resulting axion flux may be detectable on Earth through interactions in large-volume detectors.

Water Cherenkov experiments offer a natural detection strategy for such axion fluxes. In addition to neutrino-induced events, axions can be absorbed in water via inelastic scattering on nucleons, producing energetic secondary particles that initiate Cherenkov cascades. The goal of this section is to review the theoretical framework and detection prospects for axions in water Cherenkov detectors, with particular emphasis on axion–nucleon interactions and on spectral features that allow axion-induced signals to be distinguished from the neutrino background. The discussion closely follows the effective-field-theory treatment developed in ref. [258].

Axion detection in water Cherenkov experiments has also been discussed in the context of axion couplings that arise independently of the derivative axion–nucleon interaction. In particular, the axion–gluon coupling generically induces an effective interaction between the axion field and the nucleon electric dipole moment (EDM). This so-called nucleon EDM portal represents a model-independent feature of the QCD axion and leads to axion–photon–nucleon interactions even in scenarios where the standard axion couplings to photons and fermions are suppressed.

The phenomenology of SN axions produced through the nucleon EDM portal, as well as their detection via axion-induced photon signals in large water Cherenkov detectors, has been investigated in detail in ref. [259], which provides a benchmark study of this detection strategy. In that framework, axion emission is dominated by Compton-like processes involving photons in the SN medium, while detection proceeds primarily through the inverse process $a + p \to p + \gamma$. The resulting Cherenkov signatures were shown to exhibit distinctive spectral features at energies well above the bulk of the neutrino signal.

The present discussion adopts a complementary perspective, following the approach developed in ref. [258]. Rather than focusing on the EDM-induced axion–photon–nucleon interaction, attention is restricted to the most general derivative axion–nucleon couplings encoded in the low-energy chiral effective theory. This framework enables a unified treatment of axion emission and absorption driven by axion–nucleon interactions, and highlights the role of hadronic final states — notably neutral pions — as efficient initiators of Cherenkov cascades in water.

From the perspective of the broader experimental landscape reviewed in this work, searches for SN axions in large-volume Cherenkov detectors occupy a distinct and complementary role. Helioscopes target axions thermally produced in the solar interior, haloscopes search for axions comprising the local dark matter halo, and light-shining-through-walls experiments rely on controlled laboratory sources — all three primarily probing axion–photon interactions. By contrast, Cherenkov detectors probe axions produced in the extreme environments of core-

JCAP07(2026)060

collapse supernovae and are directly sensitive to axion–nucleon couplings through absorption processes. As such, they provide access to regions of parameter space that are largely orthogonal to those explored by photon-based experiments.

At the same time, the relevant axion mass range is set by the typical energies of axions thermally produced in SN cores, which naturally extends into the meV regime [107, 260]. In this sense, SN axion searches at Cherenkov detectors complement ongoing efforts to extend experimental sensitivity to meV-scale axions using helioscopes, haloscopes, and condensed-matter systems. Although the reliance on rare astrophysical transients limits the achievable event rate, the use of existing large-scale detectors and the direct sensitivity to hadronic couplings make Cherenkov-based searches a valuable component of the experimental program for meV axions.

5.3.1 Detection framework and theoretical setup

The detection framework considered here consists of three main components: axion production in a core-collapse SN, propagation of the axion flux to Earth, and axion absorption in a water Cherenkov detector.

Axions are assumed to be produced in the SN core through their couplings to nucleons. The resulting flux depends on the axion–nucleon couplings, the core temperature, and the nuclear equation of state. Once produced, axions stream freely out of the SN and propagate essentially without attenuation to Earth.

At the detector, axions can be absorbed through processes of the form

$$a + N \to N + \gamma, \qquad a + N \to N + \pi^0, \tag{5.2}$$

where N denotes a nucleon. The photon or neutral pion in the final state initiates an electromagnetic cascade in water, producing Cherenkov light. These processes are analogous, at the level of detector response, to neutrino-induced interactions, but lead to distinct spectral signatures.

Both axion emission and absorption are computed within a unified effective field theory framework, namely chiral perturbation theory (ChPT) extended to include the axion field [261]. This ensures a consistent treatment of hadronic physics at the source and in the detector.

At energies well below the QCD confinement scale $\Lambda_{\rm QCD} \approx 1$ GeV, the relevant degrees of freedom are hadrons rather than quarks and gluons. The interactions of the light pseudoscalar meson octet are governed by the approximate chiral symmetries of QCD, which form the basis of ChPT.

The QCD axion carries the same quantum numbers as neutral pseudoscalar mesons such as the π^0 and the η. As a result, it can be incorporated naturally into ChPT as an additional pseudoscalar field [261]. In this framework, the interactions of the axion with mesons and baryons are fixed by chiral symmetry and by the underlying axion–quark couplings. At the quark level, the axion interaction takes the schematic form

$$\mathcal{L}_{aqq} = \frac{\partial_\mu a}{f_a} \left(\bar{q}\, \gamma_L^\mu k_L\, q_L + \bar{q}\, \gamma_R^\mu k_R\, q_R \right), \tag{5.3}$$

where f_a is the axion decay constant and $k_{L,R}$ are coupling matrices acting on the light-quark triplet $q = (u, d, s)^T$.

JCAP07(2026)060

Matching onto the hadronic theory yields, among other terms, derivative axion–nucleon interactions of the form (e.g. [156])

$$\mathcal{L}_{aNN} = \frac{\partial_\mu a}{2f_a} \sum_{N=p,n} C_{aNN}\, \bar{N}\gamma^\mu\gamma_5 N\,,$$

where the coefficients C_{aNN} are calculable functions of the underlying axion–quark couplings.

The effective axion–nucleon couplings C_{aNN} can be specified in several ways. Representative scenarios include:

1. **Benchmark UV-complete models.** In the KSVZ model [14, 15], the axion–nucleon couplings are determined by running effects alone, giving

$$C_{ann}|_{\rm KSVZ} = 0.012\,, \qquad C_{app}|_{\rm KSVZ} = -0.452\,. \tag{5.4}$$

   In the DFSZ model [16, 17], the couplings depend on the ratio $\tan\beta$ of the two Higgs vacuum expectation values,

$$C_{ann}|_{\rm DFSZ} = -0.123 + 0.406\,\sin^2\beta\,, \tag{5.5}$$
$$C_{app}|_{\rm DFSZ} = -0.169 - 0.430\,\sin^2\beta\,, \tag{5.6}$$

   with $\tan\beta \in [0.25, 170]$. The couplings' maximum magnitudes are $|C_{app}| \simeq 0.60$ and $|C_{ann}| \simeq 0.28$.

2. **Agnostic effective scenario.** In this approach, C_{app} and C_{ann} are treated as independent parameters subject only to observational constraints. The most relevant constraints arise from:

   - neutron-star cooling [201], which requires $C_{ann}\, m_N/f_a \lesssim 1.15\times10^{-9}$ and $C_{app}\, m_N/f_a \lesssim 1.09\times10^{-9}$;
   - supernova cooling, implemented through the Raffelt bound [195, 260], requiring the axion luminosity to satisfy $L_a \lesssim L_\nu$, as inferred from SN1987A [262–267].

   In each case, the stronger of the two bounds is applied. For the benchmark SN parameters used in figure 6 (see below), the SN bound is more constraining and yields $|C_{app}| < 2.1$ and $|C_{ann}| < 2.0$ [258, 268].

5.3.2 Axion detection in water Cherenkov detectors

In a core-collapse SN, the emission of axions may accompany the neutrino burst. Both species can be detected on Earth through interactions with nucleons in a water Cherenkov detector, leading to processes of the general form

$$\alpha + N \to N' + X\,, \tag{5.7}$$

where $\alpha = \nu, a$ and X is a "Cherenkov parton", a particle, such as $e^\pm$, γ, or π^0, capable of initiating a cascade leading to Cherenkov light. For axions, the dominant Cherenkov-producing channels are

$$a + p \to p + \gamma, \qquad a + N \to N + \pi^0. \tag{5.8}$$

JCAP07(2026)060

The associated differential cross sections $\sigma_{\alpha X}$ are computed within the same chiral EFT framework used for axion production. From them, the differential number spectrum of a Cherenkov-emitting particle X induced by a flux of coolers α is given by

$$\frac{dN_X^{(\alpha)}}{dE_X} = \frac{N_t}{4\pi d^2} \int dE_\alpha \, \frac{d\sigma_{\alpha X}(E_\alpha, E_X)}{dE_X} \, \frac{dN_\alpha}{dE_\alpha} \,, \tag{5.9}$$

where N_t is the number of target nucleons in the detector and d is the SN distance. The expected event yield scales linearly with detector size and as $1/d^2$ with distance.

5.3.3 Spectral features and detectability

A defining advantage of large-volume water Cherenkov detectors in the context of SN axions lies in the markedly different spectral imprints left by axion-induced and neutrino-induced interactions. These differences arise both from the underlying particle physics governing axion absorption on nucleons and from the kinematics of the resulting final states that initiate Cherenkov cascades in water.

At a qualitative level, axion absorption through inelastic nucleon scattering,

$$a + N \to N + X \,,$$

with $X = \gamma, \pi^0$, produces secondary particles with characteristic energies of order $\mathcal{O}(100)$ MeV or higher. By contrast, the dominant neutrino signal in water Cherenkov detectors is generated by inverse beta decay, $\bar{\nu}p \to ne^+$, whose positron spectrum peaks at significantly lower energies, typically $\mathcal{O}(10)$ MeV. This kinematic separation is a robust consequence of the much larger axion energies expected from thermal emission in the SN core, combined with the non-negligible hadronic mass scales entering the axion–nucleon absorption processes.

The results shown in figure 6 are obtained for a representative set of SN and detector parameters. Specifically, axion emission is computed using the DD2 nuclear equation of state [269], with core temperature $T = 30$ MeV, baryon number density $n_B = n_{\rm sat}$, proton fraction $Y_p = 0.3$, and a SN-to-Earth distance of $d = 0.2$ kpc. The three line styles in the left panel correspond to the KSVZ, DFSZ, and agnostic coupling scenarios described above. For an extensive discussion of the microphysics and SN parameters, see refs. [258, 268]. The left panel of figure 6 illustrates this separation by comparing the Cherenkov-parton spectra induced by neutrino absorption with those arising from axion absorption for a representative core-collapse SN model. The neutrino-induced positron spectrum peaks at low energies and rapidly falls off above $\sim$ 50–60 MeV. In contrast, the axion-induced spectra populate a much harder energy range. Among the latter, the π^0 production channel,

$$a + N \to N + \pi^0 \,,$$

is particularly prominent. Its spectrum peaks at energies of order 100–200 MeV, well beyond the bulk of the neutrino background. The single-photon channel $ap \to p\gamma$ is also present but is subdominant both in rate and in characteristic energy.

This hierarchy between the π^0 and γ channels has a clear physical origin. In ChPT, the axion couples derivatively to the nucleon axial current, which naturally enhances pion emission relative to radiative processes. As a result, once the kinematic threshold for π^0 production

JCAP07(2026)060

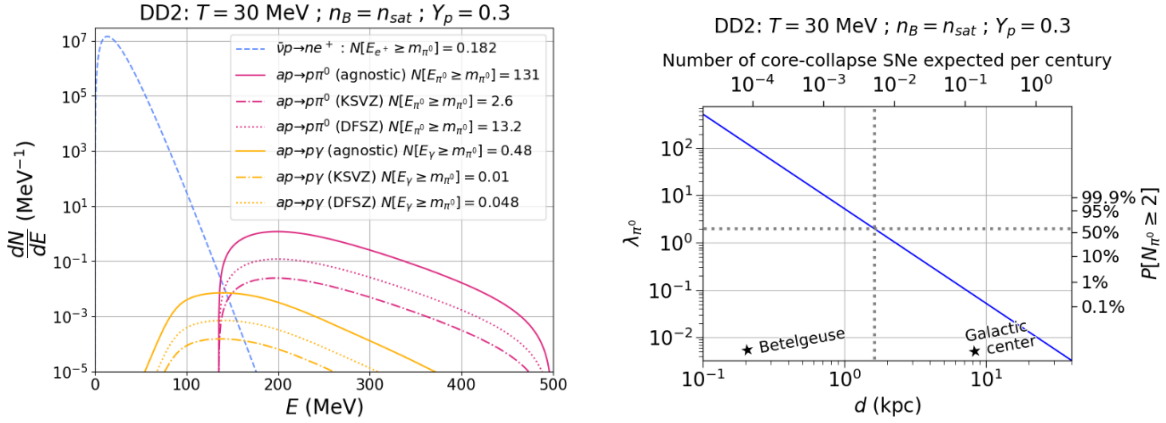


Figure 6. *Left.* Comparison between neutrino-induced and axion-induced Cherenkov spectra for a representative core-collapse SN, illustrating the separation in characteristic energies. Different line styles correspond to the KSVZ, DFSZ, and agnostic coupling scenarios (see text). The axion signal is dominated by the π^0 production channel and peaks well above the neutrino background. *Right.* Expected number of axion-induced π^0 events as a function of the SN distance. The horizontal line indicates a nominal detectability threshold of two events. For details on the microphysics and SN parameters used, see text. Reproduced from ref. [258]. CC BY 4.0..

is crossed, the π^0 channel becomes the dominant source of axion-induced Cherenkov light. For energies above the pion mass, the axion-induced π^0 spectrum typically overwhelms both the photon channel and the residual neutrino background.

From the experimental point of view, this spectral separation is crucial. Energies above $\sim$ 140–150 MeV lie beyond the regime where neutrino-induced events are abundant, and detector simulations [258] indicate that the background in this range is expected to be negligible on the timescale of a SN burst. Moreover, neutral pions' prompt decay into two energetic photons produces distinctive multi-ring topologies that can be efficiently reconstructed. For Hyper-Kamiokande the π^0 reconstruction efficiency in this energy range can reach the level of $\mathcal{O}(80\%)$, with the majority of events classified as two-ring π^0-like. These features make the π^0 channel a particularly clean experimental handle on axion absorption.

While the spectral properties determine the intrinsic discriminating power of Cherenkov detectors, the ultimate detectability of a SN axion signal is governed by the expected event rate. For a given axion model and SN realization, the number of axion-induced π^0 events in an energy range R can be expressed as

$$\lambda(C_{app}, C_{ann}; R) = \int_R dE_{\pi^0} \, \frac{dN^{(a)}_{\pi^0}}{dE_{\pi^0}} \,,$$

and depends sensitively on the axion–nucleon couplings, the core temperature, and the distance of the SN. Cooling constraints from neutron stars and from SN 1987A typically limit λ to at most a few hundred events even for very nearby explosions (0.2 kpc).

The dependence on the SN core temperature is particularly pronounced. Increasing the temperature from 30 to 40 MeV enhances the axion emissivity by nearly an order of magnitude, reflecting its steep scaling with temperature. As a consequence, predicted event rates can

JCAP07(2026)060

vary by almost a factor of ten across this temperature range. This sensitivity motivates adopting conservative benchmark temperatures when assessing detectability prospects.

A further, and unavoidable, limitation arises from the geometric dilution of the axion flux. Since the event rate scales as $1/d^2$ with the SN distance d, only explosions within a few kiloparsecs can yield an observable axion signal. This behavior is illustrated in the right panel of figure 6, which shows the expected number of axion-induced π^0 events as a function of distance for representative SN models and axion couplings. Requiring a minimal detectability threshold of two events typically restricts the observable range to $d \lesssim 2$ kpc.

Such nearby core-collapse SNe are rare. While neutrino bursts are expected from the Milky Way at a rate of $\mathcal{O}(1)$ per century, only a small fraction of these events occur within the distance required for axion detection via Cherenkov light. Crude estimates suggest that the rate of SNe capable of producing a detectable axion burst is at the level of $\mathcal{O}(10^{-2})$ per century. This rarity underscores the importance of *maximizing the axion signal yield per event*.

In this context, the enhancement provided by the π^0 channel relative to single-photon emission should be regarded as a necessary but not sufficient step toward realistic detection prospects. While the hard π^0-initiated spectrum provides a clean experimental handle with negligible neutrino background above ~ 150 MeV, the overall sensitivity remains limited by the steep $1/d^2$ suppression of the event rate with supernova distance, and calls for further spectrum-enhancement mechanisms.

In summary, water Cherenkov detectors provide a conceptually clean and experimentally mature avenue for probing axion–nucleon interactions through axion absorption from nearby core-collapse supernovae. While neutrino bursts are detectable from much larger distances, axion detection requires a fortuitously *close* event.

Among the available absorption channels, axion-induced π^0 production offers the most promising signal, owing to its higher rate and higher characteristic energy. The estimates presented here are intentionally conservative, as they include only axion absorption on free protons in water.

A central challenge for the future is therefore to identify and quantify additional sources of signal enhancement beyond this baseline treatment. Natural candidates include axion absorption on neutrons; alternative absorption processes, such as $a + N \to Y + X$, where Y is a baryon other than a nucleon and X produces Cherenkov light (these processes exploit in reverse order the interactions considered in ref. [270]); a dedicated treatment of axion–oxygen scattering, which remains largely unexplored and could substantially increase the effective target mass. Establishing the size and robustness of such effects is essential given the rarity of sufficiently nearby SNe.

In this respect, SN axion searches at Cherenkov detectors should be viewed not as competitors to laboratory-based experiments, but as a complementary probe of meV-scale axions that is uniquely sensitive to axion–nucleon interactions in dense nuclear environments.

6 meV axions experiments

Experimentally probing the meV axion frontier is particularly challenging. In this section, we focus in detail on a representative subset of experimental directions, which were discussed as part of the "meV Mass Axion Frontier" workshop, including helioscope searches such

JCAP07(2026)060

as CAST [271] and BabyIAXO [125, 272]; and proposed meV haloscope searches such as CADEx [273, 274], and experimental proposals based on antiferromagnets [275], highly excited electron cycltotron [276], fifth force searches [277].

However, we emphasise that a broad variety of complementary strategies is currently being developed. For example, the QUAX experiment searches for the axion-electron coupling using a ferromagnetic haloscope as well as the axion-photon coupling using a standard resonant cavity for masses around 36 μeV [278–280]. ALPHA is a plasma haloscope which uses tunable metamaterials to target masses up to 186 μeV [281, 282]. There are also several broadband concepts targeting this mass range, including BREAD [283], which is a dish-antenna haloscope using a parabolic reflector to focus the resulting signal; and LAMPOST [284], which uses a multi-layer dielectric haloscope, read out using a superconducting nanowire single-photon detector, to target the meV-eV mass range. In addition, ARIADNE aims to probe axion-mediated 'magnetic' forces in the mass range 0.1–10 meV [148, 285]. A number of recent proposals have further expanded the experimental landscape by exploring novel resonant, interferometric, and condensed-matter-based techniques adapted to meV-scale axions [286–288].

6.1 Extending axion mass sensitivity in CAST

The CERN Axion Solar Telescope (CAST) was a ground-based experiment located in Geneva (Switzerland) that searched for axions originating from the Sun. To look for axions, CAST pointed a decommissioned LHC prototype dipole magnet toward the Sun, with various X-ray detectors installed at both ends of the magnet. To date, CAST has been the most sensitive existing helioscope, making use of a prototype superconducting LHC dipole magnet that provided a magnetic field of 9 T. CAST was able to follow the Sun twice a day during sunset and sunrise for a total of 3 h. At both ends of the 10 m long magnet, X-ray detectors [289–292] were mounted to search for photons from Primakoff conversion. The analysis of the data acquired during the first phase of the experiment yielded the most restrictive experimental upper limit on the axion–photon coupling constant for axion masses up to about 0.02 eV/c^2. During the second phase, CAST extended its mass sensitivity by tuning the electron density in the magnetic conversion region. Hence, providing the photons with an effective mass m_γ [293]:

$$\left(\frac{m_a^2}{\mathrm{eV}^2}\right) \ll \left(\frac{m_\gamma^2}{\mathrm{eV}^2}\right) + 2 \cdot \left(\frac{E_a/\mathrm{eV}}{L \cdot \mathrm{eV}}\right) \tag{6.1}$$

so that for m_a values in the neighborhood of the chosen m_γ the maximum sensitivity is restored.

During the operation of ^{4}He as a buffer gas in the magnet bores CAST established an upper limit on the axion–photon coupling of $g_{a\gamma} < 1.47 \times 10^{-10}\,\mathrm{GeV}^{-1}$ at 95% CL. for axion masses $0.02 \lesssim m_a \lesssim 0.39$ eV [294] and after the upgrade to operate with ^{3}He CAST established an upper limit on the axion–photon coupling of $g_{a\gamma} < 2.3 \times 10^{-10}\,\mathrm{GeV}^{-1}$ at 95% CL. for axion masses $0.39 \lesssim m_a \lesssim 0.64$ eV [295] and $g_{a\gamma} < 3.3 \times 10^{-10}\,\mathrm{GeV}^{-1}$ at 95% CL. for axion masses $0.64 \lesssim m_a \lesssim 1.19$ eV [296].

JCAP07(2026)060

6.1.1 Effective photon masses at CAST

The electron density (n_e) of the gas filling the cold bore drives the physics of the axion Primakoff conversion at CAST. The effective mass of the photon arising can be obtained as:

$$m_\gamma^2 = \omega_p^2 = 4\pi n_e \frac{e^2}{m_e} = 4\pi n_e r_e \tag{6.2}$$

being ω_p the plasma frequency and r_e the electron radius. At CAST, Helium-3 and helium-4 were chosen due the experimental constraints such as temperature of magnet operation.

CAST data taking stepped over different densities of gas to allow the search of different axion masses. Achieving the target gas density presented a demanding challenge, requiring not only computational fluid dynamics simulations of the full system, including effects such as hydrostatics, convection, and buoyancy, but also a highly precise gas-injection system capable of controlling the density to an accuracy of a few tenths of parts per million. A detailed examination of the experimental data and simulations revealed clear deviations from the ideal gas law. At extremely low temperatures, gas molecules move much more slowly, making intermolecular forces no longer negligible. Under these conditions, equations of state such as the Peng–Robinson model provide a more accurate description by accounting not only for molecular interactions and compressibility but also for the non-spherical nature of real molecules (see right panel of figure 7).

At experiments like CAST, the Primakoff conversion of axions depends on the density of electrons present in the system as well as parameters such as the intensity of the magnetic field, and the length of the path that axions travel through the media,

$$P_{a\to\gamma} = \frac{1}{4} g_{a\gamma}^2 \exp(-\Gamma L) \left| \int_L \exp(\Gamma l/2 + iql) B_\perp(l) dl \right|^2. \tag{6.3}$$

Here, we would like to bring the attention to the reader that convection currents of the gas between the X-ray windows and the inner regions of the cold bore translated to a magnetic field profiles dependent on the electron density and tilt of the experiment (see left panel of figure 7).

Although the superfluid that cools down CAST magnet assures stable temperatures in the inner regions of the cold bore, the temperature of the X-ray windows and the density of the gas present in the system influence the impact of the convection currents to the effective magnet length. For instance, if we let the temperature of the X-ray windows to drift together with the cold bore gas while increasing the density of the system, the effective length of the magnet follows a linear dependence with the pressure achieved in the system.

Moreover, as previously discussed, gravitational forces can introduce a density gradient along the gas column in the magnet region. In its second-phase analysis, CAST accounted for this effect by reproducing the various data-taking conditions using computational fluid dynamics, with the measured temperatures and pressures along the coldbore serving as boundary conditions.

This procedure yields an effective photon mass that depends not only on the system pressure but also on the polar angle at which that pressure is measured. Using this effective density, together with CAST's exposure to the Sun CAST was able to determine precisely the effective photon mass during every single solar tracking (see figure 9 for an example).

JCAP07(2026)060

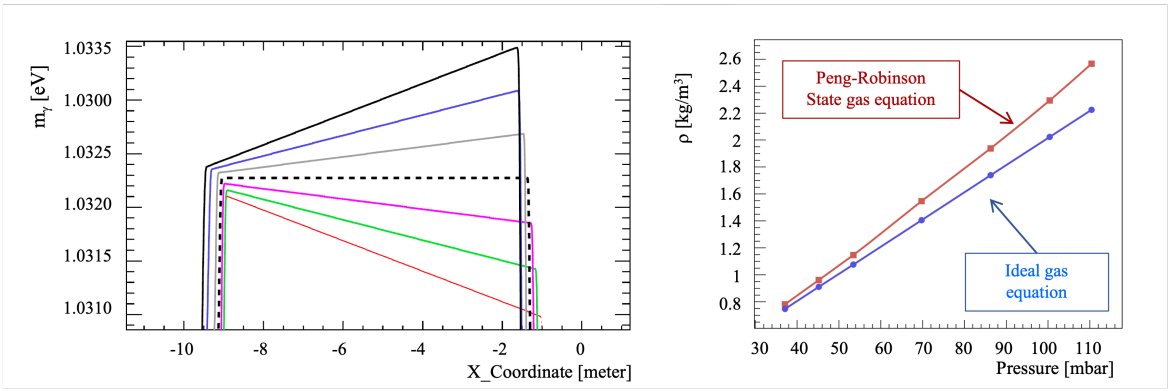


Figure 7. *Left.* Effective photon mass in the CAST cold bore as a function of the magnet tilt during solar tracking, shown together with the corresponding gas density in the bore. *Right.* Evolution of the cold-bore gas density at rest, calculated using the Ideal Gas equation of state (blue) and the Peng–Robinson equation of state (red), both consistent with CAST measurements. © (2011) IEEE. Reprinted, with permission, from [297].

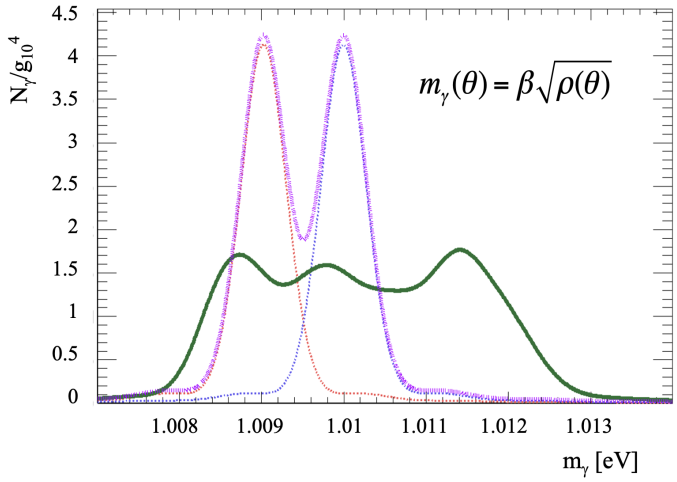


Figure 8. Theoretical recovery of the coherence condition at selected axion masses (dashed blue and red curves) and their combined contribution (dashed purple), compared with the effective response of the experiment (green curve) once all experimental boundary conditions are included. © (2011) IEEE. Reprinted, with permission, from [297].

6.2 Axion mass-scanning strategy of BabyIAXO

Following the operational strategy established by CAST, the BabyIAXO physics program is organized into two data-taking phases, each corresponding to approximately 1.5 years of exposure with an effective 12 hours of solar tracking per day [125, 272]. During the first phase, the magnetic field region will be operated under vacuum, providing sensitivity to the axion–photon coupling $g_{a\gamma}$ for axion masses up to several tens of meV, where axion–photon conversion remains coherent. At higher masses the coherence condition is lost and a low-Z buffer gas will be introduced to extend the mass sensitivity to larger values. Building upon CAST experience, BabyIAXO will operate the magnet bores near room temperature to

JCAP07(2026)060

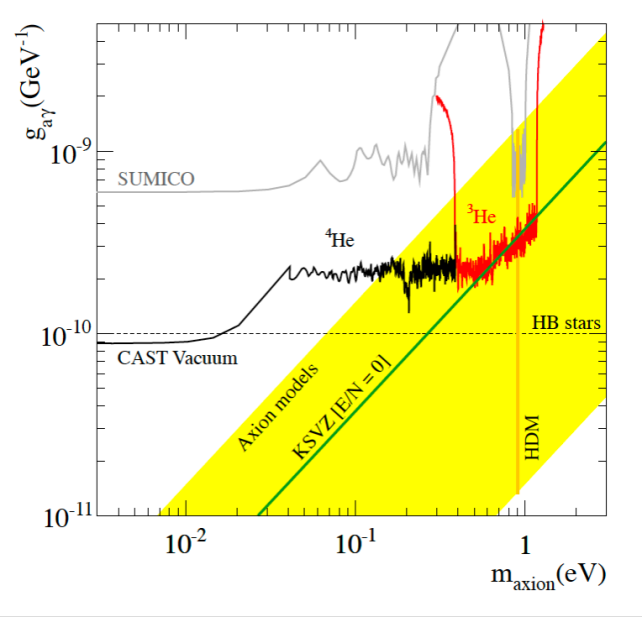


Figure 9. CAST exclusion limits on the axion–photon coupling at 95% CL using all data from Phase I and Phase II [296]. The CAST sensitivity is shown alongside the Horizontal Branch (HB) star bound [298]. The yellow band denotes the range of predicted QCD axion models, and the green curve represents the KSVZ model with E/N = 0. Reproduced from [296]. CC BY 3.0.

maintain the validity of the ideal-gas approximation and minimize convection effects that could otherwise arise. Helium-4 is the chosen gas, and axion masses up to $m_a = 0.25\,\mathrm{eV}$ are planned to be scanned, requiring at least 73 discrete gas-density nodes.

Continuous coverage in axion mass is obtained by choosing the gas-density steps such that adjacent resonances overlap at their full width at half maximum (FWHM). Figure 10 illustrates the planned mass-scan structure, where the relative modulation amplitudes of the expected photon counts N_γ from Primakoff and ABC axion components indicate that the Primakoff flux is particularly sensitive to the exact resonance spacing.

The exposure time assigned to each density setting is chosen to scale as $t_{\mathrm{exp}} \propto m_a^{-4}$ in order to reproduce the expected KSVZ-like mass dependence of the sensitivity curve. However, for the lowest-mass density settings this requirement is relaxed, as it would exceed the total 1.5 yr allocated to the gas phase. The exposure of the first five density settings is reduced and redistributed uniformly among them. This strategy is chosen because for the lowest-density settings the resonance width spans a comparatively large mass range, leading to non-negligible contributions across several mass nodes.

6.3 Post-discovery strategies for axion mass determination

Helioscope searches such as BabyIAXO offer an additional method for determining the axion mass. When an axion signal is detected during the gaseous phase, the coherence condition creates a direct correlation between the effective photon mass in the medium and the incident axion mass, enabling a precise inference of the latter. In addition, the spectral distribution of the detected axions also provides information relevant to characterizing the particle. Both

JCAP07(2026)060

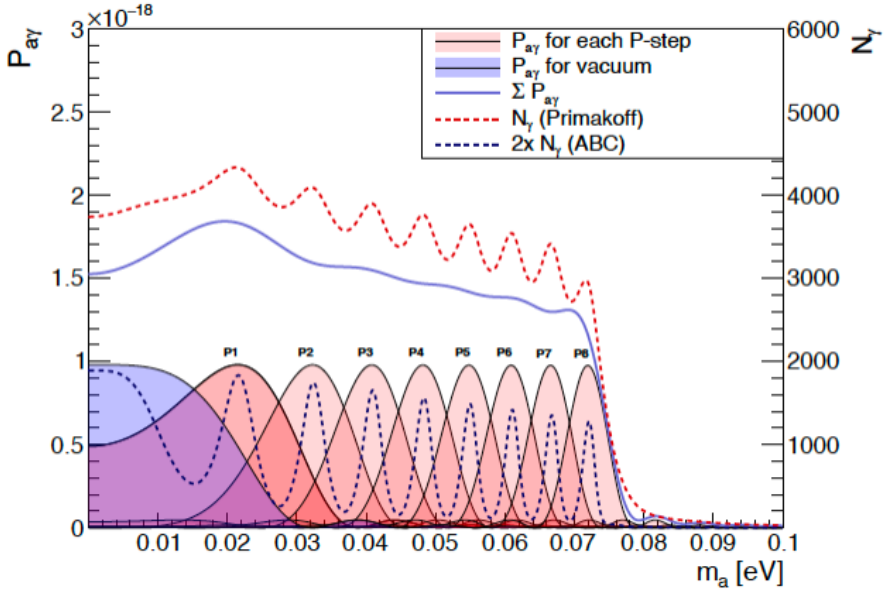


Figure 10. Axion–photon conversion probability for $g_{a\gamma} = 10^{-10}\,\mathrm{GeV}^{-1}$ in a 2 T magnetic field of 10 m length for a photon energy of 4.2 keV. The probability is shown for the vacuum configuration (blue shading) and for the first eight gas-density settings (red shading) that enable a continuous axion-mass scan. The figure also displays the probability integrated at 4.2 keV, as well as the corresponding expected photon yield after convolution with the axion flux (including both Primakoff and ABC components). The flux is integrated over a 70 cm diameter magnet and an exposure time of 540 hours per setting, with the ABC flux evaluated assuming $g_{ae} = 10^{-12}$. Reproduced from [299]. CC BY 4.0.

the Primakoff and axion–electron spectra change depending on whether the axion is detected under resonant or non-resonant conditions.

Figure 11 shows the expected spectra for axions with masses above 0.02 eV when the IAXO magnet is operated under vacuum. Axions out of resonance, but that lie close to satisfying the coherence condition produce spectra with a distinct shape, including a shift of the average detected energy toward higher values. As the axion mass moves further away from the resonance condition defined by the experimental setup, the spectrum develops a more pronounced ripple structure. These spectral features provide key information for determining the axion mass and allow for further tuning of the experiment.

Additional strategies can be implemented to determine the mass of a discovered axion in the sub-0.02 eV regime. One viable approach involves reducing the effective length of the magnetic field within the helioscope. Shortening the magnetic region relaxes the coherence requirement and modifies the interference pattern of axion–photon conversion, making the signal more sensitive to small deviations between the axion mass and the effective photon mass. By performing measurements at multiple, deliberately varied magnetic lengths, the experiment can extract the characteristic modulation in conversion probability that encodes the axion mass. This method provides a complementary mass-determination channel in parameter regions where the standard gaseous phase operation is less effective.

JCAP07(2026)060

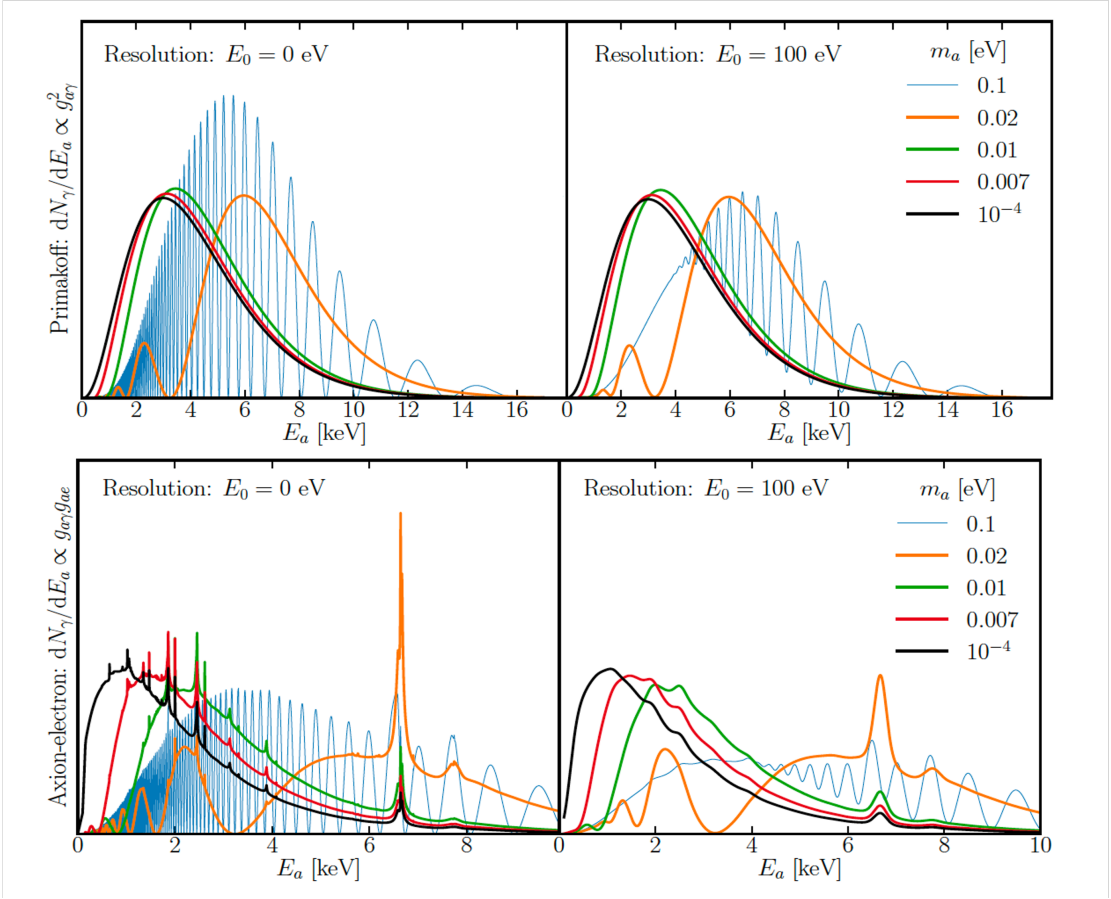


Figure 11. Differential X-ray spectra as a function of energy from solar axion conversion inside a 20 m long, 2.5 T magnet. Spectra are shown for several axion masses m_a for both the solar Primakoff (*upper panels*) and axion–electron (*lower panels*) flux components. The left panels present the raw spectra, while the right panels show the spectra after convolution with a Gaussian energy resolution of width $E_0 = 100$ eV. All spectra are normalized to unity for comparison; the inset shows the total integrated number of events N_γ as a function of the five masses, assuming $g_{a\gamma} = 10^{-11}\,\mathrm{GeV}^{-1}$. Reproduced from [300]. CC BY 4.0.

6.4 Pushing the haloscope searches towards the meV range: The CADEx experiment

Haloscope experiments aim to detect DM axions from the halo of the Milky Way, through their conversion into photons in a strong magnetic field. The probability of axion-photon conversion is small, given the small expected value of the axion-photon coupling $g_{a\gamma}$ [12]. This probability is typically enhanced in haloscope experiments using resonant cavities: when the axion mass matches the resonant frequency of the cavity $f = m_a c^2/(2\pi\hbar)$, the conversion probability is enhanced by the quality factor Q of the cavity. By tuning the resonant frequency of the cavity, haloscopes can probe a range of axion masses. With typical (unloaded) quality factors of $Q_0 \sim 10^5$, a range of haloscope searches have begun probing the QCD axion parameter space in the range $m_a \in [2, 50]\,\mu$eV, including ADMX [301–303], CAPP [304, 305], HAYSTAC [306–309] and QUAX [279, 280]. A number of searches have

JCAP07(2026)060

also provided constraints below the CAST limit [271], up to masses of $\sim 0.1\,\mathrm{meV}$, including GigaBREAD [310], GrAHal [311], MADMAX [312], ORGAN [313–316], RADES [317, 318], TASEH [319], UF/RBF [320–322].

However, pushing haloscope searches to higher masses presents a number of challenges. The resonant frequency of a cavity is typically set by its physical size L, such that it matches the photon wavelength $L \sim \lambda = c/f$. As the target axion mass (and therefore the desired resonant frequency) is increased, the size of the cavity must be decreased. This means that the sensitive volume of the cavity, $V \sim L^3 \sim \lambda^3$ drops rapidly with increasing axion mass. In addition, the cavity power in the haloscope is typically picked up by an antenna and amplified. This coherent amplification adds an irreducible noise contribution, meaning that the noise level cannot be suppressed below the so-called Standard Quantum Limit, SQL, (at least using standard amplification techniques). This irreducible noise contribution becomes more significant with increasing frequency, further limiting the sensitivity of high-mass axion searches using coherent readouts.

The Canfranc Axion Detection Experiment (CADEx) is a proposed search for axions in the mass range $330 - 460\,\mu\mathrm{eV}$ (corresponding to W-band frequencies, in the range $80 - 110\,\mathrm{GHz}$) [273, 274]. CADEx is a resonant-cavity-based search which aims to address the challenges described above in a number of ways. First, the reduction in sensitive volume at high frequencies will be mitigated through the coherent combination of seven flat rectangular cavities. The smallest dimension of each cavity, which sets the resonant frequency, is approximately $a \sim 1.7\,\mathrm{mm}$, while the other two dimensions are much larger ($40 - 60\,a$), thereby maximizing the sensitive volume of each cavity while fitting in a 10 T superconducting magnet bore. In the CADEx experiment, the frequency sweep is performed by tuning the thin dimension of the cavity using a sliding-wall mechanism [273], subsequently demonstrated at frequencies around 26 GHz [323, 324]. The output from each of the seven cavities will be extracted using horn antennas and coherently combined and routed to the detecting system using a quasi-optical free-space setup, ensuring phase coherence among cavities.

Second, the detection system is based on an array of superconducting Kinetic Inductance Detectors (KIDs) [325]. KIDs are superconducting resonators whose resonance properties, i.e. kinetic inductance, change in response to absorbed radiation. They are not limited by the SQL and their sensitivity surpasses that achieved by traditionally employed heterodyne receivers in this frequency range. An array of multiple KIDs based on Ti/Al bilayers will be used to sense the output signal for the haloscope [326]. On-chip polarization discrimination will be implemented to perform correlation analysis between the polarized axion-photon conversion signal and the unpolarized background.

The CADEx experiment, planned to be installed at the Laboratorio Subterráneo de Canfranc (LSC), is currently in the design and technological demonstration stage. Typical parameters for the baseline setup of CADEx include a cavity quality factor of $Q_0 = 10^5$, a total cavity volume of $V = 0.08\,\mathrm{L}$ and a noise equivalent power (NEP) of $3 \times 10^{-20}\,\mathrm{W}\sqrt{\mathrm{Hz}}$ for the KIDs sensors. With these, CADEx expects to be sensitive to axions in the QCD band, probing couplings of $g_{a\gamma} \lesssim 1.5 \times 10^{-13}\,\mathrm{GeV}^{-1}$ for an axion mass of $370\,\mu\mathrm{eV}$ over a 3 month exposure. Owing to the broadband nature of KIDs, CADEx serves both as a technological pathfinder for high-frequency axion searches and as a complementary technological platform to

JCAP07(2026)060

proposed broadband haloscope experiments targeting high axion masses, such as BREAD [283], BRASS [327], DALI [328].

6.5 meV axion quasiparticles

6.5.1 Discovery of meV axion quasiparticles

Wilczek first proposed in 1987 [330] the possibility that condensed matter systems may exhibit axion-like physics, in particular realising the axion-photon interaction term with some effective degree of freedom, i.e. axion quasiparticles (AQs). The AQ action is:

$$S = \int d^4x \left\{ \frac{f_\Theta^2}{2} \left[(\partial_t \delta\Theta)^2 - (v_i^2 \partial_i \delta\Theta)^2 - m_\Theta^2 \delta\Theta^2 \right] + \frac{\alpha}{\pi} (\delta\Theta + \Theta_0) \vec{E} \cdot \vec{B} \right\} , \tag{6.4}$$

where Θ_0 is the constant background field (fixed by the material), $\delta\Theta$ is the dynamical AQ, and m_Θ, f_Θ, v_i are the AQ mass, decay constant, and speed respectively.

A significant development in this field occurred in 2009 when Li et al. [331] proposed that topological magnetic insulators were suitable candidate materials. In such materials, the AQ arises from fluctuations in antiferromagnetic order. The original proposal supposed that this requires fluctuations directly in the order parameter, S_z, the "longitudinal magnon", which only occurs when the unit cell breaks P and T symmetries. Such a scenario is proposed to be realised in iron-doped Bismuth Selenide, $(Bi_{1-x}Fe_x)_2Se_3$ [331], or in Manganese Bismuth Telluride 2-2-5, $Mn_2Bi_2Te_5$ [332]. These materials, and the AQ phase in them, proved difficult to realise in the laboratory, in part because excitation of longitudinal magnons is difficult to achieve.

There is also a class of so-called "axion insulator" materials that are more well studied and realised in the lab (e.g. refs. [333–336]). Axion insulators are characterised by the presence of a constant electromagnetic Θ_0 term with $\Theta_0 \neq 0, \pi$, but where symmetries forbid dynamics for $\delta\Theta$. The axion insulator Manganese Bismuth Telluride 1-2-4, $MnBi_2Te_4$, is well studied and is known to possess antiferromagnetism below its Néel temperature [337]. Recently, Qiu et al. [329] demonstrated that the application of an in-plane magnetic field to even-layer $MnBi_2Te_4$ has the effect to tilt the spins in the model, leading to an effective change in the order parameter projected out of the plane caused by a transverse magnon, which is much easier to excite. Furthermore, Qiu et al. were able to demonstrate that in such a setting the out-of-phase magnon couples to the Θ (Chern-Simons) term of electromagnetism, inducing rotation in polarisation of an incident laser beam onto the sample, i.e. birefringence. By measuring the frequency of this rotation with ultrafast pump-probe optics, Qiu et al. demonstrate the existence of the AQ in this material, and measure its mass (frequency) to be $m_\Theta = 0.18$ meV (44 GHz).

An illustration of the physics behind AQs and their recent discovery is shown in figure 12, while figure 13 shows the headline result of the discovery of the AQ and measurement of its mass.

The basic physics that places the AQ in the meV range is the role of the antiferromagnetic anisotropy field, H_A, in setting the mass of the transverse magnons (see e.g. refs. [338, 339]),

JCAP07(2026)060

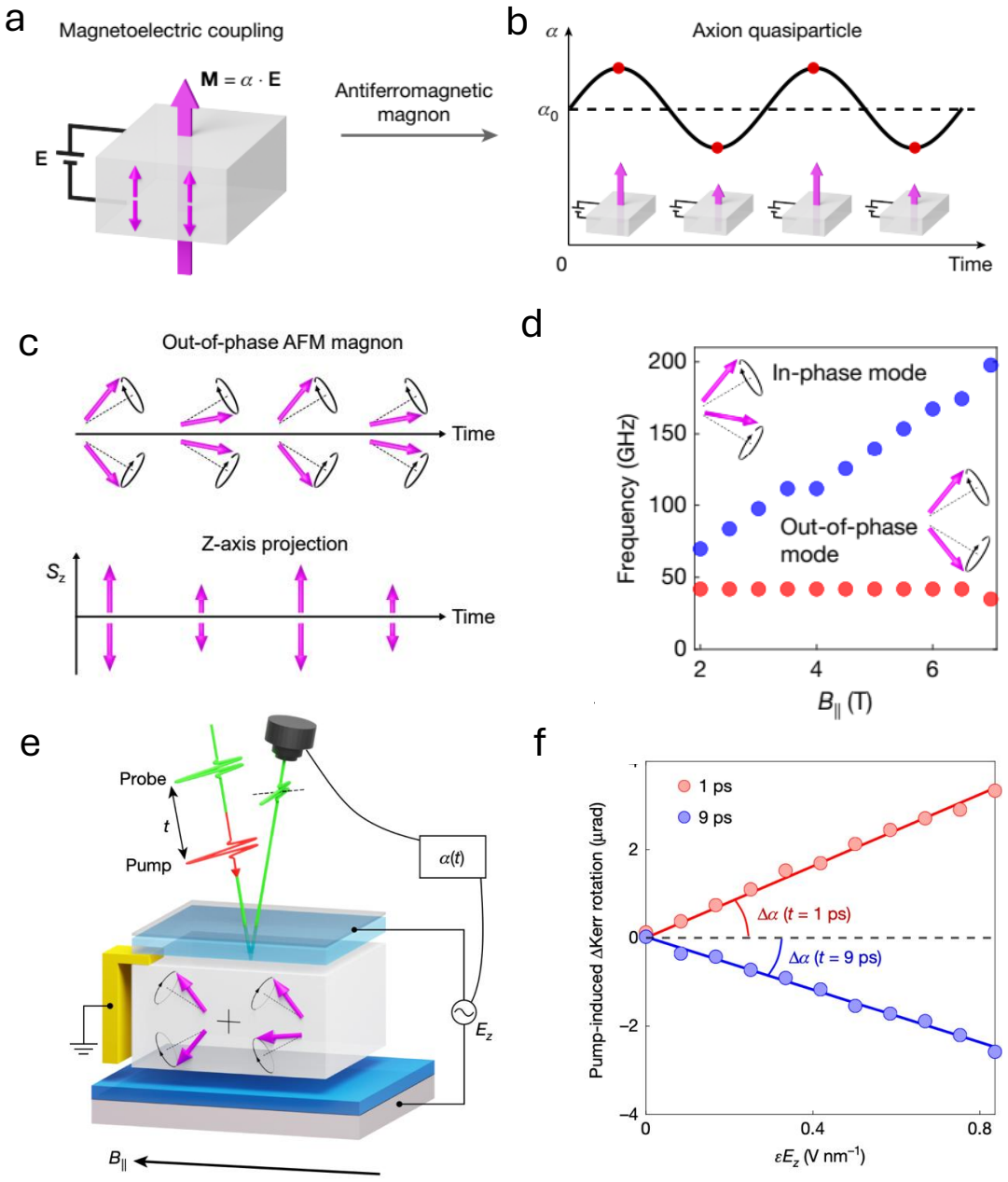


Figure 12. Axion quasiparticle in $MnBi_2Te_4$. **a, b:** In condensed matter, the θ angle is directly proportional to the trace of the magnetoelectric coupling, $\Theta = \pi \frac{2h}{3e^2} \sum_{i=x,y,z} \alpha_{ii}$). Thus, a time varioation in α induced by an antiferromagnetic magnon corresponds to the axion quasiparticle. **c:** Time evolution of out-of-phase magnon and $\hat{z}$ projection of the out-of-phase magnon, S_z, which resembles the antiferromagnetic amplitude mode. The axion quasiparticle is the coherent oscillation of the magnetoelectric coupling. **d:** Experimentally measured frequencies for the in-phase magnon and out-of-phase magnon modes as a function of the in-plane magnetic field $B_\parallel$ of 6-layer $MnBi_2Te_4$. **e:** Schematic experimental setup to probe the time-dependent magnetoelectric coupling. The pump laser launches coherent magnons; The probe laser, combined with the dual gate E_z, measures $\frac{d\text{Kerr rotation}}{dE_z}$; By varying the delay time t, we can measure pump-induced $\Delta\alpha(t)$ with femtosecond resolution. **f:** Measured pump-induced Kerr rotation $\Delta\text{Kerr}(t)$ as a function of E_z and t. Reproduced from [329], with permission from Springer Nature.

JCAP07(2026)060

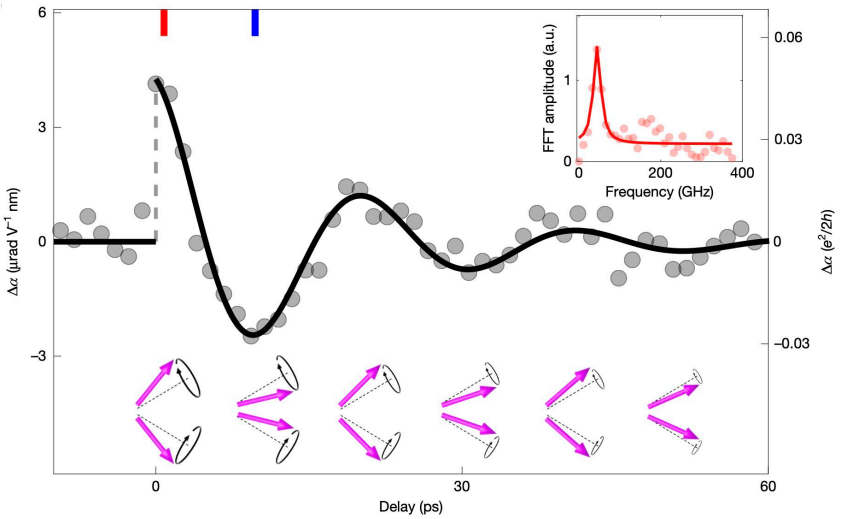


Figure 13. Experimental measurements of the theta angle oscillation for the axion quasiparticle in $MnBi_2Te_4$. Measured magnetoelectric coupling α oscillation as a function of time. The theta angle (axion quasiparticle) is directly proportional to the magnetoelectric coupling by $\Theta = \frac{2\pi h}{e^2}\alpha$. Arrows indicate spins of the tilted magnon such that the projection leads to an oscillation in S_z (see figure 12) Inset: fourier transform of the signal, indicating the axion quasiparticle frequency is 44 GHz, i.e. $m_\Theta = 0.18$ meV. Reproduced from [329], with permission from Springer Nature.

with typical values of $\mu_B H_A \sim \mathcal{O}(\text{meV})$. Thus we expect that should other AQ materials be discovered that exploit antiferromagnetism then they too will have AQs in the meV range.[2]

AQ-photon mixing is thought to be strong enough that in the presence of a background magnetic field the AQ hyridizes with the electric field, forming states known as *polaritons*. The polariton dispersion relation has two branches, $\omega_\pm$. In a material with refractive index n and AQ velocity $v \approx 0$, the dispersion relation is:

$$\omega_\pm(k)^2 = \frac{1}{2}\left[\omega_{\text{LO}}^2 + \frac{k^2}{n^2}\right] \pm \frac{1}{2}\sqrt{\left(\omega_{\text{LO}}^2 - \frac{k^2}{n^2}\right)^2 - 4b^2\frac{k^2}{n^2}}\,, \tag{6.5}$$

where ω_{LO} is the "longitudinal optical" frequency:

$$\omega_{\text{LO}}^2 = m_\Theta^2 + b^2\,, \quad b^2 = \frac{\alpha}{2\pi n^2}\frac{B_0^2}{f_\Theta^2}\,. \tag{6.6}$$

The techniques employed in ref. [329], which excite the AQ off resonance with an optical probe, have not measured the AQ-polariton. The presence of the polariton can be inferred from the gap in the dispersion relation between m_Θ and ω_{LO} [331]. By performing transmission measurements in this range of frequencies, it would be possible to measure f_Θ, as well as the losses in the material (discussed further below) [339]. Density functional theory calculations performed in ref. [329] predict $f_\Theta = 82$ eV, close to cruder estimates made in ref. [339]: this prediction remains to be confirmed experimentally.

[2]The natural meV range of AFMR implies that an AFMR QUAX-like haloscope following refs. [278, 340] may be a candidate experiment for follow up to measure the axion-electron coupling at meV.

JCAP07(2026)060

6.5.2 Axion quasiparticles for meV axion dark matter

The AQ-polariton can be exploited for axion DM detection, as first proposed in ref. [341], where it is referred to as "TOORAD" (TOpolOgical Resonant Axion Detection). The "+" polariton branch with dispersion relation ω_+ is the same as that of a massive particle with mass $\omega_{\rm LO}$. Axion DM sources an electric field in the material as usual, but now the electric field hybridizes with the AQ, and the polariton modes are driven. Resonance is achieved when $\omega_{\rm LO} \approx m_a$ (see also ref. [342]).

It can be shown that the AQ-polariton driven by axion DM can be modelled using an effective refractive index [339]:

$$n_\Theta = n^2 \left(1 - \frac{b^2}{\omega^2 - m_\Theta^2}\right) . \tag{6.7}$$

Resonance occurs when n_Θ approaches zero. Having $n_\Theta < 1$ causes internal reflections and a piece of AQ material starts to behave as a resonant cavity [339]. Techniques developed to study dielectric haloscopes [343] can then be employed to compute the boost factor, β, to the axion DM induced power emitted at frequency $\omega_{\rm LO}$ from the material surface. In previous works, the correct physics giving rise to the AQ (in plane B-field to tilt the transverse magnon) was not known, but it turns out that this difference has only a minor effect on the range of B-induced tuning predicted for the AQ-polariton.

Ref. [339] estimated the relevant contributions to the material losses, Γ, and the dominant losses are thought to be due to magnetic impurities, Γ_m, and finite resistivity, Γ_ρ (i.e. conductive losses). Ref. [329] computed the complex refractive index in $MnBi_2Te_4$ using density functional theory, which gives $n = 6.4$, $\Gamma_\rho/\omega = 0.2 \times 10^{-3}$, again largely confirming cruder estimates [339]. Magnetic impurity losses can be estimated to be $\Gamma_m/\omega = 0.7 \times 10^{-3}$ following ref. [344].

In the absence of losses, the AQ-polariton resonance allows for axion DM detection at high frequency in a totally volume-independent way, which is already a significant feature. The presence of losses, however, leads to a maximum in the boost factor β set by when the total optical path (accounting for finesse) reaches the skin depth. For the estimated parameters of $MnBi_2Te_4$ the maximum thickness is of order 0.4 mm, which is already extremely thick in material terms: a realistic method to reach such thickness would be to deposit layers sandwiched with dielectric [329].

A significant feature of the AQ-polariton approach to axion DM detection is in resonance tuning: the resonant frequency is controlled by the externally applied B-field. In the set-up of ref. [329] the bending of spins caused by the in-plane magnetic field $B_{||}$ is precisely what is being exploited to generate the AQ in the first place, and the AQ was shown to be present and stable in the range 2 to 7 T. The same in-plane B-field will cause axion DM to drive the AQ-polariton. Thus, in ref. [329] the range of resonant frequencies was chosen by varying $B_{||}$ in the range 1 to 10 T, which corresponds to:

$$0.7 \text{ meV} \lesssim m_a \lesssim 7 \text{ meV} \quad \text{(scanning range of } MnBi_2Te_4 \text{ for } B = 1 - 10 \text{ T)} . \tag{6.8}$$

Refs. [329, 339] showed that (under some assumptions about future detectors in this range) it will be possible to search for QCD axion DM above 1 meV inside its model band [12]

JCAP07(2026)060

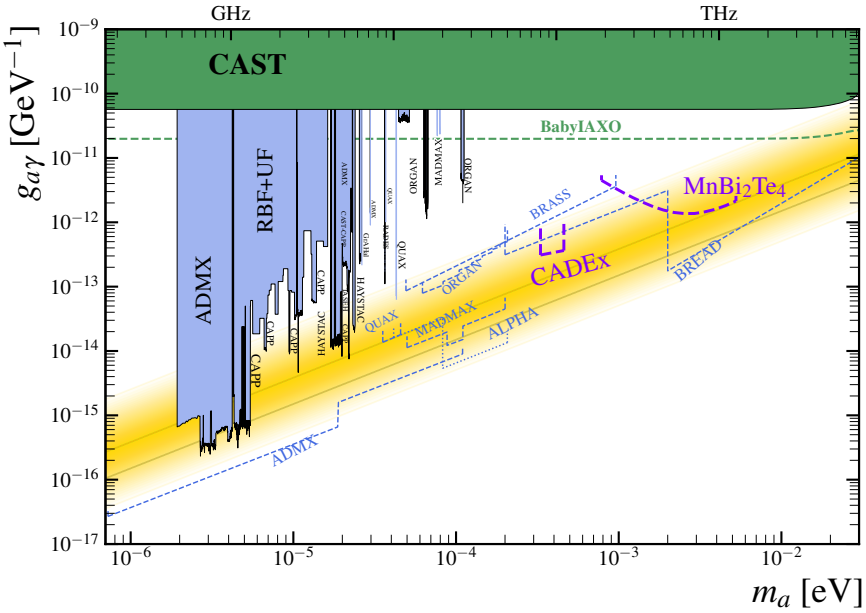


Figure 14. Existing (solid) and projected (dashed) constraints on the axion photon coupling, $g_{a\gamma}$. Highlighted in purple are the proposed DM haloscopes discussed in this paper: CADEx (section 6.4) and the AQ material $MnBi_2Te_4$ (section 6.5). The yellow band indicates QCD axion models. CADEx is sensitive to the QCD axion for $m_a \approx 0.4$ meV. The AQ material is sensitive to the QCD axion for $m_a \approx 1 - 7$ meV. Figure produced using AxionLimits [345] (where references for the other shown limits can be found). Reproduced with permission from [345].

using these techniques. Figure 14 shows the projected sensitivity of an AQ-based haloscope using $MnBi_2Te_4$, with measured and calculated parameters and experimental assumptions as outlined in ref. [329].

7 Discussion and conclusions

The meV mass range has emerged as a focal point in axion physics, where advances across theory, cosmology, astrophysics, and experiment converge with remarkable coherence. In this review, we have surveyed the current status of meV axion research, highlighting both the theoretical motivations that single out this mass window and the diverse experimental strategies poised to probe it in the coming years.

From the theoretical perspective, field-theoretic approaches to the PQ quality problem generically favour decay constants around $f_a \sim 5 \times 10^9$ GeV, corresponding to axion masses in the meV range. This regime can also be the outcome of large classes of well-motivated ultraviolet completions of the axion framework. In fact, the low-energy limit of string compactifications on CY manifolds can realise an meV-scale QCD axion either as a closed string mode arising from the dimensional reduction of higher dimensional forms, or as the phase of an open string mode charged under an anomalous U(1) on branes. The two different model building options can lead to a pre- as well as to a post-inflationary scenario. Experimental programmes targeting the meV axion regime can therefore be exploited as probes of the structure of the string landscape. Moreover, since axions come with saxion

JCAP07(2026)060

partners tied to the same moduli dynamics, sensitivity to meV axions can also inform us about saxion masses and couplings.

The cosmological phenomenology of meV axions is rich and multifaceted. While the standard misalignment mechanism with $\mathcal{O}(1)$ initial angles yields a subdominant dark matter contribution at these masses, alternative production scenarios — including large-misalignment tuning, kinetic misalignment, and post-inflationary dynamics with topological defects — can accommodate meV axions as viable cold dark matter candidates. The precise predictions for the latter scenario remain subject to ongoing theoretical investigation, particularly regarding the spectral properties of axion emission from cosmic strings. Independently of their role as dark matter, thermal production of axions in the early Universe represents an inevitable cosmological consequence that will be probed by next-generation CMB experiments. The projected sensitivity to $\Delta N_{\rm eff}$ will test thermal axion populations precisely in the meV mass range, offering a powerful and complementary discovery channel.

Astrophysical observations currently provide the most stringent constraints on meV axions. Observations of neutron-star cooling and the SN 1987A neutrino burst independently limit the axion mass to $m_a \lesssim 10$–20 meV for KSVZ-type couplings, with residual uncertainties stemming from the challenging physics of dense nuclear matter. These bounds place the meV frontier tantalisingly close to current sensitivity thresholds. Looking forward, the next Galactic core-collapse supernova offers a unique opportunity: axion-to-photon conversion in the magnetic field of the progenitor star could produce a detectable gamma-ray burst, providing a direct probe of QCD axion couplings at meV masses. The detection prospects depend sensitively on the progenitor type, with compact Type Ibc supernovae (representing 30% of the total core-collapse SN rate) emerging as particularly promising targets, due to their stronger magnetic fields than both red and blue supergiants. Ensuring full-sky gamma-ray coverage during the next Galactic supernova constitutes a compelling science case for future satellite missions. Additionally, large-volume Cherenkov detectors provide a complementary probe of axion-nucleon couplings through absorption of supernova axions, with the π^0 production channel yielding distinctive spectral signatures above the neutrino background.

On the experimental front, the landscape has been transformed by a convergence of mature and emerging technologies. The helioscope programme, building on the pioneering results of CAST, is advancing through BabyIAXO toward the full IAXO experiment, which will systematically scan the meV mass range with sensitivity reaching the QCD axion band. Buffer-gas techniques enable coherent axion-photon conversion at elevated masses, while improved X-ray optics and low-background detectors enhance the signal-to-noise ratio. High-frequency haloscope concepts, exemplified by CADEx, are pushing resonant-cavity searches toward the 100 μeV–meV regime, complementing the helioscope approach with sensitivity to the local dark matter density rather than the solar axion flux.

Finally, a particularly exciting recent development is the experimental discovery of axion quasiparticles in topological antiferromagnets. The observation of an axion quasiparticle with mass $m_\Theta \simeq 0.18$ meV in $MnBi_2Te_4$ not only validates the underlying axion electrodynamics in a controlled laboratory setting but also opens new avenues for dark matter detection. The axion-polariton hybridisation in these materials creates volume-independent resonant

JCAP07(2026)060

enhancement that can be tuned across the meV range by varying an external magnetic field, offering a qualitatively new approach to high-frequency axion searches.

Several open questions and challenges remain. On the theoretical side, a complete understanding of axion production from cosmic string networks — and its implications for post-inflationary cosmology — awaits further progress in numerical simulations and analytical modelling. The physics of axion emission from dense nuclear matter, while qualitatively understood, carries irreducible uncertainties at the factor-of-few level that propagate into astrophysical bounds. Experimentally, the primary challenge lies in extending sensitivity to the QCD axion coupling strength across the full meV mass range, a goal that will require sustained investment in detector technology and infrastructure.

Despite these challenges, the overall picture is one of remarkable convergence and opportunity. The meV axion hypothesis is now subject to a coordinated assault from multiple independent directions: helioscopes probing solar axion production, haloscopes and quasiparticle detectors searching for dark matter signals, precision cosmology constraining thermal relics, and astrophysical observations setting limits from stellar and supernova environments. This multiplicity of approaches offers not only redundancy but also the prospect of cross-validation in the event of a positive signal, enabling robust characterisation of axion properties including mass, couplings, and cosmological abundance.

The coming decade will be decisive for meV axion physics. The commissioning of BabyIAXO and the continued development of IAXO will bring helioscope sensitivity into the QCD axion band. Future CMB experiments will probe thermal axion contributions to dark radiation with unprecedented precision. The maturation of axion quasiparticle techniques may enable tunable resonant searches across the meV range. And the next Galactic supernova, whenever it occurs, will provide a singular opportunity to detect or constrain axion emission from the most extreme astrophysical environments. Together, these developments position the meV mass range as one of the most compelling and experimentally accessible frontiers in the search for physics beyond the Standard Model.

Acknowledgments

This article is based upon work from COST Action COSMIC WISPers (CA21106). We warmly thank Federico Mescia for the kind hospitality at the Laboratori Nazionali di Frascati during the workshop "The meV Mass Axion Frontier: Challenges and Opportunities" (https://agenda.infn.it/event/48801/) and for providing us with good food and wine that helped to keep our spirits up.

Maurizio Giannotti acknowledges support from the Spanish Agencia Estatal de Investigación under grant PID2019-108122GB-C31, funded by MCIN/AEI/10.13039/501100011033, and from the "European Union NextGenerationEU/PRTR" (Planes complementarios, Programa de Astrofísica y Física de Altas Energías). Additionally, Maurizio Giannotti acknowledges funding from the European Union's Horizon 2020 research and innovation programme under the European Research Council (ERC) grant agreement ERC-2017-AdG788781 (IAXO+).

The work of Mathieu Kaltschmidt, Maurizio Giannotti and Javier Redondo is supported by the grants PGC2022-126078NB-C21 and PID2024-160228NB-I00 funded by MCIN/AEI/-10.13039501100011033 and ERDF – A way of making Europe, and DGA-FSE 2023-E21-23R by

JCAP07(2026)060

the Government of Aragón, Spain, and the European Union NextGenerationEU Recovery and Resilience Program on Astrofísica y Física de Altas Energías CEFCA-CAPA-ITAINNOVA. Additionally, Mathieu Kaltschmidt is supported by the Government of Aragón, Spain, with a PhD fellowship as specified in DGA-ORDEN-CUS/702/2022.

The work of Ken'ichi Saikawa is supported by JSPS KAKENHI Grant Number JP24K07015.

Edoardo Vitagliano and Alessandro Lella are supported by the Italian MUR through the FIS 2 project FIS-2023-01577 (DD n. 23314 10-12-2024, CUP C53C24001460001).

Giuseppe Lucente (SLAC) acknowledges support from the U.S. Department of Energy under contract number DE-AC02-76SF00515.

David J.E. Marsh is supported by an Ernest Rutherford Fellowship (Grant No. ST/T004037/1) and a consolidator grant (Grant No. ST/X000753/1) from the Science and Technologies Facilities Council, United Kingdom.

The work of Alessandro Mirizzi is partially supported by the research grant number 2022E2J4RK "PANTHEON: Perspectives in Astroparticle and Neutrino THEory with Old and New messengers" under the program PRIN 2022 (Mission 4, Component 1, CUP I53D23001110006) funded by the Italian Ministero dell'Università e della Ricerca (MUR) and by the European Union – Next Generation EU.

The work of Francesco D'Eramo and Edoardo Vitagliano is supported in part by the Italian MUR Departments of Excellence grant 2023–2027 "Quantum Frontiers".

The work of Luca Di Luzio and Federico Mescia is partially supported by the European Union – Next Generation EU and by the Italian Ministry of University and Research (MUR) via the PRIN 2022 project n. 2022K4B58X – AxionOrigins

The work of Francesco D'Eramo, Alessandro Lella, Federico Mescia, Alessandro Mirizzi and Edoardo Vitagliano is supported by Istituto Nazionale di Fisica Nucleare (INFN) through the Theoretical Astroparticle Physics (TAsP) project.

Alicia Gomez thanks the Spanish Agencia Estatal de Investigación (AEI, MICIU) for their support under the Project PID2022-137779OB-C41 financed by MCIN /AEI/10.13039 /501100011033/FEDER, EU and from "Tecnologías avanzadas para la exploración del Universo y sus componentes" (PR47/21 TAU-CM) project funded by Comunidad de Madrid and "NextGenerationEU"/PRTR.

The work of Diego Guadagnoli has received funding from the French ANR, under contract ANR-23-CE31-0018 ('InvISYble'), that is gratefully acknowledged.

Bradley J. Kavanagh thanks the Spanish Agencia Estatal de Investigación (AEI, MICIU) for their support under the Project DMpheno2lab (PID2022-139494NB-I00) financed by MCIN /AEI /10.13039/501100011033 / FEDER, EU.

Elisa Todarello has received funding from the European Union's Horizon 2020 research and innovation programme under the Marie Skłodowska-Curie grant agreement No. 101204903, and from the STFC Consolidated Grant [Grant No. ST/T000732/1].

Nicole Righi is supported by the ERC NOTIMEFORCOSMO, 101126304.

The work in Su-Yang Xu group was supported by CATS, an Energy Frontier Research Center (EFRC) funded by the US Department of Energy (DOE) Office of Science, through the Ames National Laboratory under contract DE-AC0207CH11358, the Office of Naval

JCAP07(2026)060

Research (ONR) grant the N000142512285, and the National Science Foundation (NSF) Career Grant No. DMR-2143177, the Air Force Office of Scientific Research (AFOSR) grant FA9550-23-1-0040.

Damiano F.G. Fiorillo was supported by the Alexander von Humboldt Foundation (Germany) for most of the completion of the project.

JCAP07(2026)060

A List of acronyms

ABC	Atomic, Bremsstrahlung and Compton processes
ALP	Axion-Like Particle
AMR	Adaptive Mesh Refinement
AQ	Axion Quasiparticle
BBN	Big-Bang Nucleosynthesis
BSG	Blue Supergiant
CADEx	Canfranc Axion Detection Experiment
CAST	CERN Axion Solar Telescope
CDM	Cold Dark Matter
ChPT	Chiral Perturbation Theory
CL	Confidence Level
CMB	Cosmic Microwave Background
CP	Charge-Parity (symmetry/violation)
DFSZ	Dine–Fischler–Srednicki–Zhitnitsky (benchmark axion model)
DIGA	Dilute Instanton Gas Approximation
DM	Dark Matter
DW	Domain Wall
EDM	Electric Dipole Moment
EFT	Effective Field Theory
Fermi-LAT	Fermi Large Area Telescope
FLRW	Friedmann-Lemaître-Robertson Walker (metric)
FRST	Fine, Regular, and Star (triangulations in string theory)
FWHM	Full Width at Half Maximum
GLSM	Gauged Linear Sigma Model
HB	Horizontal Branch (star)
HK	Hyper-Kamiokande
HPC	High-Performance Computing
IAXO	International Axion Observatory
IIB	Type IIB (string theory)
KIDs	Kinetic Inductance Detectors
KM	Kinetic Misalignment
KSVZ	Kim–Shifman–Vainshtein–Zakharov (benchmark axion model)
LHC	Large Hadron Collider
LMA	Large Misalignment Angle
LSC	Laboratorio Subterráneo de Canfranc
nEDM	neutron Electric Dipole Moment
NEP	Noise Equivalent Power
NG	Nambu–Goto
NS	Neutron Star

JCAP07(2026)060

NSM	Neutron Star Merger
PNS	Proto-Neutron Star
PQ	Peccei–Quinn
QCD	Quantum Chromodynamics
RD	Radiation Domination
RSG	Red Supergiant
SM	Standard Model
SMM	Solar Maximum Mission
SN	Supernova
SQL	Standard Quantum Limit
SUSY	Supersymmetry
UV	Ultraviolet
VEV	Vacuum Expectation Value
WD	White Dwarf

References

[1] G.G. Raffelt, J. Redondo and N. Viaux Maira, *The meV mass frontier of axion physics*, *Phys. Rev. D* **84** (2011) 103008 [arXiv:1110.6397] [INSPIRE].

[2] J.P. Conlon, *The QCD axion and moduli stabilisation*, *JHEP* **05** (2006) 078 [hep-th/0602233] [INSPIRE].

[3] M. Cicoli, M. Goodsell and A. Ringwald, *The type IIB string axiverse and its low-energy phenomenology*, *JHEP* **10** (2012) 146 [arXiv:1206.0819] [INSPIRE].

[4] I. Broeckel et al., *Moduli stabilisation and the statistics of axion physics in the landscape*, *JHEP* **08** (2021) 059 [*Addendum ibid.* **01** (2022) 191] [arXiv:2105.02889] [INSPIRE].

[5] M. Cicoli, A. Hebecker, J. Jaeckel and M. Wittner, *Axions in string theory — slaying the Hydra of dark radiation*, *JHEP* **09** (2022) 198 [arXiv:2203.08833] [INSPIRE].

[6] M. Cicoli et al., *Explicit de Sitter Flux Vacua for Global String Models with Chiral Matter*, *JHEP* **05** (2014) 001 [arXiv:1312.0014] [INSPIRE].

[7] M. Cicoli, V.A. Diaz, V. Guidetti and M. Rummel, *The 3.5 keV Line from Stringy Axions*, *JHEP* **10** (2017) 192 [arXiv:1707.02987] [INSPIRE].

[8] R. Petrossian-Byrne and G. Villadoro, *Open string axiverse*, *JHEP* **07** (2025) 049 [arXiv:2503.16387] [INSPIRE].

[9] V. Loladze, A. Platschorre and M. Reig, *Higher axion strings*, *JHEP* **08** (2025) 182 [arXiv:2503.18707] [INSPIRE].

[10] V.M. Mehta et al., *Superradiance Exclusions in the Landscape of Type IIB String Theory*, arXiv:2011.08693 [INSPIRE].

[11] V.M. Mehta et al., *Superradiance in string theory*, *JCAP* **07** (2021) 033 [arXiv:2103.06812] [INSPIRE].

[12] L. Di Luzio, M. Giannotti, E. Nardi and L. Visinelli, *The landscape of QCD axion models*, *Phys. Rept.* **870** (2020) 1 [arXiv:2003.01100] [INSPIRE].

JCAP07(2026)060

[13] M. Gorghetto and G. Villadoro, *Topological Susceptibility and QCD Axion Mass: QED and NNLO corrections*, *JHEP* **03** (2019) 033 [arXiv:1812.01008] [INSPIRE].

[14] J.E. Kim, *Weak Interaction Singlet and Strong CP Invariance*, *Phys. Rev. Lett.* **43** (1979) 103 [INSPIRE].

[15] M.A. Shifman, A.I. Vainshtein and V.I. Zakharov, *Can Confinement Ensure Natural CP Invariance of Strong Interactions?*, *Nucl. Phys. B* **166** (1980) 493 [INSPIRE].

[16] A.R. Zhitnitsky, *On Possible Suppression of the Axion Hadron Interactions* (in Russian), *Sov. J. Nucl. Phys.* **31** (1980) 260 [INSPIRE].

[17] M. Dine, W. Fischler and M. Srednicki, *A Simple Solution to the Strong CP Problem with a Harmless Axion*, *Phys. Lett. B* **104** (1981) 199 [INSPIRE].

[18] M. Srednicki, *Axion Couplings to Matter. 1. CP Conserving Parts*, *Nucl. Phys. B* **260** (1985) 689 [INSPIRE].

[19] G. Grilli di Cortona, E. Hardy, J. Pardo Vega and G. Villadoro, *The QCD axion, precisely*, *JHEP* **01** (2016) 034 [arXiv:1511.02867] [INSPIRE].

[20] L. Di Luzio, F. Mescia and E. Nardi, *Redefining the Axion Window*, *Phys. Rev. Lett.* **118** (2017) 031801 [arXiv:1610.07593] [INSPIRE].

[21] L. Di Luzio, F. Mescia and E. Nardi, *Window for preferred axion models*, *Phys. Rev. D* **96** (2017) 075003 [arXiv:1705.05370] [INSPIRE].

[22] V. Plakkot and S. Hoof, *Anomaly ratio distributions of hadronic axion models with multiple heavy quarks*, *Phys. Rev. D* **104** (2021) 075017 [arXiv:2107.12378] [INSPIRE].

[23] L. Di Luzio, S. Hoof, C. Marinissen and V. Plakkot, *Catalogues of cosmologically self-consistent hadronic QCD axion models*, *JCAP* **04** (2025) 072 [arXiv:2412.17896] [INSPIRE].

[24] K. Choi, S.H. Im, C.B. Park and S. Yun, *Minimal Flavor Violation with Axion-like Particles*, *JHEP* **11** (2017) 070 [arXiv:1708.00021] [INSPIRE].

[25] M. Chala, G. Guedes, M. Ramos and J. Santiago, *Running in the ALPs*, *Eur. Phys. J. C* **81** (2021) 181 [arXiv:2012.09017] [INSPIRE].

[26] M. Bauer et al., *The Low-Energy Effective Theory of Axions and ALPs*, *JHEP* **04** (2021) 063 [arXiv:2012.12272] [INSPIRE].

[27] K. Choi, S.H. Im, H.J. Kim and H. Seong, *Precision axion physics with running axion couplings*, *JHEP* **08** (2021) 058 [arXiv:2106.05816] [INSPIRE].

[28] L. Di Luzio et al., *Running effects on QCD axion phenomenology*, *Phys. Rev. D* **108** (2023) 115004 [arXiv:2305.11958] [INSPIRE].

[29] L. Di Luzio, F. Mescia, E. Nardi and S. Okawa, *Renormalization group effects in astrophobic axion models*, *Phys. Rev. D* **106** (2022) 055016 [arXiv:2205.15326] [INSPIRE].

[30] J. Preskill, M.B. Wise and F. Wilczek, *Cosmology of the Invisible Axion*, *Phys. Lett. B* **120** (1983) 127 [INSPIRE].

[31] L.F. Abbott and P. Sikivie, *A Cosmological Bound on the Invisible Axion*, *Phys. Lett. B* **120** (1983) 133 [INSPIRE].

[32] M. Dine and W. Fischler, *The Not So Harmless Axion*, *Phys. Lett. B* **120** (1983) 137 [INSPIRE].

[33] R.L. Davis, *Cosmic Axions from Cosmic Strings*, *Phys. Lett. B* **180** (1986) 225 [INSPIRE].

JCAP07(2026)060

[34] T. Hiramatsu, M. Kawasaki, K. Saikawa and T. Sekiguchi, *Production of dark matter axions from collapse of string-wall systems*, *Phys. Rev. D* **85** (2012) 105020 [*Erratum ibid.* **86** (2012) 089902] [arXiv:1202.5851] [INSPIRE].

[35] M. Kawasaki, K. Saikawa and T. Sekiguchi, *Axion dark matter from topological defects*, *Phys. Rev. D* **91** (2015) 065014 [arXiv:1412.0789] [INSPIRE].

[36] M. Gorghetto, E. Hardy and G. Villadoro, *Axions from Strings: the Attractive Solution*, *JHEP* **07** (2018) 151 [arXiv:1806.04677] [INSPIRE].

[37] M. Buschmann, J.W. Foster and B.R. Safdi, *Early-Universe Simulations of the Cosmological Axion*, *Phys. Rev. Lett.* **124** (2020) 161103 [arXiv:1906.00967] [INSPIRE].

[38] M. Gorghetto, E. Hardy and G. Villadoro, *More axions from strings*, *SciPost Phys.* **10** (2021) 050 [arXiv:2007.04990] [INSPIRE].

[39] M. Hindmarsh, J. Lizarraga, A. Lopez-Eiguren and J. Urrestilla, *Comment on "More Axions from Strings"*, arXiv:2109.09679 [INSPIRE].

[40] M. Buschmann et al., *Dark matter from axion strings with adaptive mesh refinement*, *Nature Commun.* **13** (2022) 1049 [arXiv:2108.05368] [INSPIRE].

[41] K. Saikawa, J. Redondo, A. Vaquero and M. Kaltschmidt, *Spectrum of global string networks and the axion dark matter mass*, *JCAP* **10** (2024) 043 [arXiv:2401.17253] [INSPIRE].

[42] H. Kim, J. Park and M. Son, *Axion dark matter from cosmic string network*, *JHEP* **07** (2024) 150 [arXiv:2402.00741] [INSPIRE].

[43] J.N. Benabou, M. Buschmann, J.W. Foster and B.R. Safdi, *Axion Mass Prediction from Adaptive Mesh Refinement Cosmological Lattice Simulations*, *Phys. Rev. Lett.* **134** (2025) 241003 [arXiv:2412.08699] [INSPIRE].

[44] J. Correia et al., *Scaling density of axion strings in terasite simulations*, *Phys. Rev. D* **111** (2025) 063532 [arXiv:2410.18064] [INSPIRE].

[45] J. Correia et al., *The spectrum of axions in a scaling string network*, arXiv:2512.13653 [INSPIRE].

[46] P. Sikivie, *Of Axions, Domain Walls and the Early Universe*, *Phys. Rev. Lett.* **48** (1982) 1156 [INSPIRE].

[47] M. Farina, D. Pappadopulo, F. Rompineve and A. Tesi, *The photo-philic QCD axion*, *JHEP* **01** (2017) 095 [arXiv:1611.09855] [INSPIRE].

[48] P. Agrawal, J.J. Fan, M. Reece and L.-T. Wang, *Experimental Targets for Photon Couplings of the QCD Axion*, *JHEP* **02** (2018) 006 [arXiv:1709.06085] [INSPIRE].

[49] L. Di Luzio et al., *Astrophobic Axions*, *Phys. Rev. Lett.* **120** (2018) 261803 [arXiv:1712.04940] [INSPIRE].

[50] F. Björkeroth et al., *Axion-electron decoupling in nucleophobic axion models*, *Phys. Rev. D* **101** (2020) 035027 [arXiv:1907.06575] [INSPIRE].

[51] L. Darmé, L. Di Luzio, M. Giannotti and E. Nardi, *Selective enhancement of the QCD axion couplings*, *Phys. Rev. D* **103** (2021) 015034 [arXiv:2010.15846] [INSPIRE].

[52] A. Hook, *Solving the Hierarchy Problem Discretely*, *Phys. Rev. Lett.* **120** (2018) 261802 [arXiv:1802.10093] [INSPIRE].

[53] L. Di Luzio, B. Gavela, P. Quilez and A. Ringwald, *An even lighter QCD axion*, *JHEP* **05** (2021) 184 [arXiv:2102.00012] [INSPIRE].

JCAP07(2026)060

[54] L. Di Luzio, B. Gavela, P. Quilez and A. Ringwald, *Dark matter from an even lighter QCD axion: trapped misalignment*, *JCAP* **10** (2021) 001 [arXiv:2102.01082] [INSPIRE].

[55] R.D. Peccei and H.R. Quinn, *CP Conservation in the Presence of Instantons*, *Phys. Rev. Lett.* **38** (1977) 1440 [INSPIRE].

[56] R.D. Peccei and H.R. Quinn, *Constraints Imposed by CP Conservation in the Presence of Instantons*, *Phys. Rev. D* **16** (1977) 1791 [INSPIRE].

[57] S. Weinberg, *A New Light Boson?*, *Phys. Rev. Lett.* **40** (1978) 223 [INSPIRE].

[58] F. Wilczek, *Problem of Strong P and T Invariance in the Presence of Instantons*, *Phys. Rev. Lett.* **40** (1978) 279 [INSPIRE].

[59] H.M. Georgi, L.J. Hall and M.B. Wise, *Grand Unified Models With an Automatic Peccei-Quinn Symmetry*, *Nucl. Phys. B* **192** (1981) 409 [INSPIRE].

[60] M. Dine and N. Seiberg, *String Theory and the Strong CP Problem*, *Nucl. Phys. B* **273** (1986) 109 [INSPIRE].

[61] S.M. Barr and D. Seckel, *Planck scale corrections to axion models*, *Phys. Rev. D* **46** (1992) 539 [INSPIRE].

[62] M. Kamionkowski and J. March-Russell, *Planck scale physics and the Peccei-Quinn mechanism*, *Phys. Lett. B* **282** (1992) 137 [hep-th/9202003] [INSPIRE].

[63] R. Holman et al., *Solutions to the strong CP problem in a world with gravity*, *Phys. Lett. B* **282** (1992) 132 [hep-ph/9203206] [INSPIRE].

[64] S. Ghigna, M. Lusignoli and M. Roncadelli, *Instability of the invisible axion*, *Phys. Lett. B* **283** (1992) 278 [INSPIRE].

[65] V.A. Rubakov, *Grand unification and heavy axion*, *JETP Lett.* **65** (1997) 621 [hep-ph/9703409] [INSPIRE].

[66] Z. Berezhiani, L. Gianfagna and M. Giannotti, *Strong CP problem and mirror world: The Weinberg-Wilczek axion revisited*, *Phys. Lett. B* **500** (2001) 286 [hep-ph/0009290] [INSPIRE].

[67] L. Randall, *Composite axion models and Planck scale physics*, *Phys. Lett. B* **284** (1992) 77 [INSPIRE].

[68] B.A. Dobrescu, *The strong CP problem versus Planck scale physics*, *Phys. Rev. D* **55** (1997) 5826 [hep-ph/9609221] [INSPIRE].

[69] K.S. Babu, I. Gogoladze and K. Wang, *Stabilizing the axion by discrete gauge symmetries*, *Phys. Lett. B* **560** (2003) 214 [hep-ph/0212339] [INSPIRE].

[70] M. Redi and R. Sato, *Composite Accidental Axions*, *JHEP* **05** (2016) 104 [arXiv:1602.05427] [INSPIRE].

[71] H. Fukuda, M. Ibe, M. Suzuki and T.T. Yanagida, *A "gauged" U(1) Peccei–Quinn symmetry*, *Phys. Lett. B* **771** (2017) 327 [arXiv:1703.01112] [INSPIRE].

[72] L. Di Luzio, E. Nardi and L. Ubaldi, *Accidental Peccei-Quinn symmetry protected to arbitrary order*, *Phys. Rev. Lett.* **119** (2017) 011801 [arXiv:1704.01122] [INSPIRE].

[73] Q. Bonnefoy, E. Dudas and S. Pokorski, *Axions in a highly protected gauge symmetry model*, *Eur. Phys. J. C* **79** (2019) 31 [arXiv:1804.01112] [INSPIRE].

[74] B. Lillard and T.M.P. Tait, *A High Quality Composite Axion*, *JHEP* **11** (2018) 199 [arXiv:1811.03089] [INSPIRE].

JCAP07(2026)060

[75] M.B. Gavela, M. Ibe, P. Quilez and T.T. Yanagida, *Automatic Peccei–Quinn symmetry*, *Eur. Phys. J. C* **79** (2019) 542 [arXiv:1812.08174] [INSPIRE].

[76] H.-S. Lee and W. Yin, *Peccei-Quinn symmetry from a hidden gauge group structure*, *Phys. Rev. D* **99** (2019) 015041 [arXiv:1811.04039] [INSPIRE].

[77] M. Ardu et al., *Axion quality from the (anti)symmetric of SU($\mathcal{N}$)*, *JHEP* **11** (2020) 090 [arXiv:2007.12663] [INSPIRE].

[78] L. Di Luzio, *Accidental SO(10) axion from gauged flavour*, *JHEP* **11** (2020) 074 [arXiv:2008.09119] [INSPIRE].

[79] W. Yin, *Scale and quality of Peccei-Quinn symmetry and weak gravity conjectures*, *JHEP* **10** (2020) 032 [arXiv:2007.13320] [INSPIRE].

[80] R. Contino, A. Podo and F. Revello, *Chiral models of composite axions and accidental Peccei-Quinn symmetry*, *JHEP* **04** (2022) 180 [arXiv:2112.09635] [INSPIRE].

[81] L. Di Luzio, G. Landini, F. Mescia and V. Susič, *High-quality Peccei-Quinn symmetry from the interplay of vertical and horizontal gauge symmetries*, *Eur. Phys. J. C* **86** (2026) 5 [arXiv:2503.16648] [INSPIRE].

[82] E. Witten, *Some Properties of O(32) Superstrings*, *Phys. Lett. B* **149** (1984) 351 [INSPIRE].

[83] N. Arkani-Hamed, H.-C. Cheng, P. Creminelli and L. Randall, *Extra natural inflation*, *Phys. Rev. Lett.* **90** (2003) 221302 [hep-th/0301218] [INSPIRE].

[84] K.-W. Choi, *A QCD axion from higher dimensional gauge field*, *Phys. Rev. Lett.* **92** (2004) 101602 [hep-ph/0308024] [INSPIRE].

[85] N. Craig and M. Kongsore, *High-quality axions from higher-form symmetries in extra dimensions*, *Phys. Rev. D* **111** (2025) 015047 [arXiv:2408.10295] [INSPIRE].

[86] M. Cicoli, C. Mayrhofer and R. Valandro, *Moduli Stabilisation for Chiral Global Models*, *JHEP* **02** (2012) 062 [arXiv:1110.3333] [INSPIRE].

[87] M. Cicoli, F. Muia and P. Shukla, *Global Embedding of Fibre Inflation Models*, *JHEP* **11** (2016) 182 [arXiv:1611.04612] [INSPIRE].

[88] M. Cicoli et al., *Chiral Global Embedding of Fibre Inflation Models*, *JHEP* **11** (2017) 207 [arXiv:1709.01518] [INSPIRE].

[89] M. Cicoli, A. Grassi, O. Lacombe and F.G. Pedro, *Chiral global embedding of Fibre Inflation with $\overline{D3}$ uplift*, *JHEP* **06** (2025) 090 [arXiv:2412.08723] [INSPIRE].

[90] M. Cicoli, M. Goodsell, J. Jaeckel and A. Ringwald, *Testing String Vacua in the Lab: From a Hidden CMB to Dark Forces in Flux Compactifications*, *JHEP* **07** (2011) 114 [arXiv:1103.3705] [INSPIRE].

[91] R. Allahverdi, M. Cicoli, B. Dutta and K. Sinha, *Correlation between Dark Matter and Dark Radiation in String Compactifications*, *JCAP* **10** (2014) 002 [arXiv:1401.4364] [INSPIRE].

[92] A. Hees et al., *Violation of the equivalence principle from light scalar dark matter*, *Phys. Rev. D* **98** (2018) 064051 [arXiv:1807.04512] [INSPIRE].

[93] G.D. Coughlan et al., *Cosmological Problems for the Polonyi Potential*, *Phys. Lett. B* **131** (1983) 59 [INSPIRE].

[94] T. Banks, D.B. Kaplan and A.E. Nelson, *Cosmological implications of dynamical supersymmetry breaking*, *Phys. Rev. D* **49** (1994) 779 [hep-ph/9308292] [INSPIRE].

JCAP07(2026)060

[95] B. de Carlos, J.A. Casas, F. Quevedo and E. Roulet, *Model independent properties and cosmological implications of the dilaton and moduli sectors of 4-d strings*, *Phys. Lett. B* **318** (1993) 447 [hep-ph/9308325] [INSPIRE].

[96] J.P. Conlon and F.G. Pedro, *Moduli Redefinitions and Moduli Stabilisation*, *JHEP* **06** (2010) 082 [arXiv:1003.0388] [INSPIRE].

[97] V. Balasubramanian, P. Berglund, J.P. Conlon and F. Quevedo, *Systematics of moduli stabilisation in Calabi-Yau flux compactifications*, *JHEP* **03** (2005) 007 [hep-th/0502058] [INSPIRE].

[98] M. Cicoli, J.P. Conlon and F. Quevedo, *General Analysis of LARGE Volume Scenarios with String Loop Moduli Stabilisation*, *JHEP* **10** (2008) 105 [arXiv:0805.1029] [INSPIRE].

[99] M. Cicoli, J.P. Conlon and F. Quevedo, *Systematics of String Loop Corrections in Type IIB Calabi-Yau Flux Compactifications*, *JHEP* **01** (2008) 052 [arXiv:0708.1873] [INSPIRE].

[100] R. Blumenhagen, S. Moster and E. Plauschinn, *Moduli Stabilisation versus Chirality for MSSM like Type IIB Orientifolds*, *JHEP* **01** (2008) 058 [arXiv:0711.3389] [INSPIRE].

[101] A. Chauhan et al., *Deep observations of the Type IIB flux landscape*, *JHEP* **07** (2025) 271 [arXiv:2501.03984] [INSPIRE].

[102] M. Kreuzer and H. Skarke, *Complete classification of reflexive polyhedra in four-dimensions*, *Adv. Theor. Math. Phys.* **4** (2000) 1209 [hep-th/0002240] [INSPIRE].

[103] M. Demirtas, A. Rios-Tascon and L. McAllister, *CYTools: A Software Package for Analyzing Calabi-Yau Manifolds*, arXiv:2211.03823 [INSPIRE].

[104] S.V.P. Fallon, J. Halverson, L. McAllister and Y. Zhu, *F-theory Axiverse*, arXiv:2511.20458 [INSPIRE].

[105] M. Demirtas, C. Long, L. McAllister and M. Stillman, *The Kreuzer-Skarke Axiverse*, *JHEP* **04** (2020) 138 [arXiv:1808.01282] [INSPIRE].

[106] G.G. Raffelt, *Astrophysical axion bounds*, *Lect. Notes Phys.* **741** (2008) 51 [hep-ph/0611350] [INSPIRE].

[107] A. Caputo and G. Raffelt, *Astrophysical Axion Bounds: The 2024 Edition*, *PoS* **COSMICWISPers** (2024) 041 [arXiv:2401.13728] [INSPIRE].

[108] N. Gendler and D.J.E. Marsh, *Possible Implications of QCD Axion Dark Matter Constraints from Helioscopes and Haloscopes for the String Theory Landscape*, *Phys. Rev. Lett.* **134** (2025) 081602 [arXiv:2407.07143] [INSPIRE].

[109] N. Gendler, D.J.E. Marsh, L. McAllister and J. Moritz, *Glimmers from the axiverse*, *JCAP* **09** (2024) 071 [arXiv:2309.13145] [INSPIRE].

[110] M. Cicoli, D. Ciupke, S. de Alwis and F. Muia, α' *Inflation: moduli stabilisation and observable tensors from higher derivatives*, *JHEP* **09** (2016) 026 [arXiv:1607.01395] [INSPIRE].

[111] M. Demirtas et al., *PQ axiverse*, *JHEP* **06** (2023) 092 [arXiv:2112.04503] [INSPIRE].

[112] J.N. Benabou, K. Fraser, M. Reig and B.R. Safdi, *String theory and grand unification suggest a submicroelectronvolt QCD axion*, *Phys. Rev. D* **112** (2025) 066003 [arXiv:2505.15884] [INSPIRE].

[113] E. Sheridan et al., *Fuzzy axions and associated relics*, *JHEP* **09** (2025) 016 [arXiv:2412.12012] [INSPIRE].

JCAP07(2026)060

[114] M. Cicoli et al., *D-Branes at del Pezzo Singularities: Global Embedding and Moduli Stabilisation*, *JHEP* **09** (2012) 019 [arXiv:1206.5237] [INSPIRE].

[115] M. Cicoli et al., *D3/D7 Branes at Singularities: Constraints from Global Embedding and Moduli Stabilisation*, *JHEP* **07** (2013) 150 [arXiv:1304.0022] [INSPIRE].

[116] M. Cicoli et al., *Global Orientifolded Quivers with Inflation*, *JHEP* **11** (2017) 134 [arXiv:1706.06128] [INSPIRE].

[117] M. Cicoli et al., *The Standard Model quiver in de Sitter string compactifications*, *JHEP* **08** (2021) 109 [arXiv:2106.11964] [INSPIRE].

[118] K. Choi, H.P. Nilles, C.S. Shin and M. Trapletti, *Sparticle Spectrum of Large Volume Compactification*, *JHEP* **02** (2011) 047 [arXiv:1011.0999] [INSPIRE].

[119] R. Blumenhagen et al., *SUSY Breaking in Local String/F-Theory Models*, *JHEP* **09** (2009) 007 [arXiv:0906.3297] [INSPIRE].

[120] L. Aparicio et al., *Sequestered de Sitter String Scenarios: Soft-terms*, *JHEP* **11** (2014) 071 [arXiv:1409.1931] [INSPIRE].

[121] G. Ballesteros, J. Redondo, A. Ringwald and C. Tamarit, *Standard Model–axion–seesaw–Higgs portal inflation. Five problems of particle physics and cosmology solved in one stroke*, *JCAP* **08** (2017) 001 [arXiv:1610.01639] [INSPIRE].

[122] A. Arvanitaki et al., *Large-misalignment mechanism for the formation of compact axion structures: Signatures from the QCD axion to fuzzy dark matter*, *Phys. Rev. D* **101** (2020) 083014 [arXiv:1909.11665] [INSPIRE].

[123] S. Borsanyi et al., *Calculation of the axion mass based on high-temperature lattice quantum chromodynamics*, *Nature* **539** (2016) 69 [arXiv:1606.07494] [INSPIRE].

[124] T. Kobayashi, R. Kurematsu and F. Takahashi, *Isocurvature Constraints and Anharmonic Effects on QCD Axion Dark Matter*, *JCAP* **09** (2013) 032 [arXiv:1304.0922] [INSPIRE].

[125] IAXO collaboration, *Physics potential of the International Axion Observatory (IAXO)*, *JCAP* **06** (2019) 047 [arXiv:1904.09155] [INSPIRE].

[126] R.T. Co, L.J. Hall and K. Harigaya, *Axion Kinetic Misalignment Mechanism*, *Phys. Rev. Lett.* **124** (2020) 251802 [arXiv:1910.14152] [INSPIRE].

[127] C. Eröncel, R. Sato, G. Servant and P. Sørensen, *ALP dark matter from kinetic fragmentation: opening up the parameter window*, *JCAP* **10** (2022) 053 [arXiv:2206.14259] [INSPIRE].

[128] M. Fasiello, J. Lizarraga, A. Papageorgiou and A. Urio, *Kinetic fragmentation of the QCD axion on the lattice*, *JCAP* **09** (2025) 019 [arXiv:2507.01822] [INSPIRE].

[129] C. Eröncel and G. Servant, *ALP dark matter mini-clusters from kinetic fragmentation*, *JCAP* **01** (2023) 009 [arXiv:2207.10111] [INSPIRE].

[130] K. Chathirathas, C. Eröncel, M. Kaltschmidt, J. Redondo and K. Saikawa, *Axion Miniclusters in the Pre-Inflationary Scenario*, in preparation (2026).

[131] V.B. Klaer and G.D. Moore, *The dark-matter axion mass*, *JCAP* **11** (2017) 049 [arXiv:1708.07521] [INSPIRE].

[132] V.B. Klaer and G.D. Moore, *How to simulate global cosmic strings with large string tension*, *JCAP* **10** (2017) 043 [arXiv:1707.05566] [INSPIRE].

[133] V.B. Klaer and G.D. Moore, *Global cosmic string networks as a function of tension*, *JCAP* **06** (2020) 021 [arXiv:1912.08058] [INSPIRE].

JCAP07(2026)060

[134] L. Fleury and G.D. Moore, *Axion dark matter: strings and their cores*, *JCAP* **01** (2016) 004 [arXiv:1509.00026] [INSPIRE].

[135] A. Vaquero, J. Redondo and J. Stadler, *Early seeds of axion miniclusters*, *JCAP* **04** (2019) 012 [arXiv:1809.09241] [INSPIRE].

[136] D.P. Bennett and F.R. Bouchet, *High resolution simulations of cosmic string evolution. 1. Network evolution*, *Phys. Rev. D* **41** (1990) 2408 [INSPIRE].

[137] D. Daverio et al., *Energy-momentum correlations for Abelian Higgs cosmic strings*, *Phys. Rev. D* **93** (2016) 085014 [*Erratum ibid.* **95** (2017) 049903] [arXiv:1510.05006] [INSPIRE].

[138] A. Vilenkin and T. Vachaspati, *Radiation of Goldstone Bosons From Cosmic Strings*, *Phys. Rev. D* **35** (1987) 1138 [INSPIRE].

[139] R.L. Davis and E.P.S. Shellard, *Antisymmetric Tensors and Spontaneous Symmetry Breaking*, *Phys. Lett. B* **214** (1988) 219 [INSPIRE].

[140] A. Arza et al., *The COSMIC WISPers White Paper: The physics case for Weakly Interacting Slim Particles*, arXiv:2603.03433 [INSPIRE].

[141] Y.B. Zeldovich, I.Y. Kobzarev and L.B. Okun, *Cosmological Consequences of the Spontaneous Breakdown of Discrete Symmetry*, *Zh. Eksp. Teor. Fiz.* **67** (1974) 3 [INSPIRE].

[142] R. Kallosh, A.D. Linde, D.A. Linde and L. Susskind, *Gravity and global symmetries*, *Phys. Rev. D* **52** (1995) 912 [hep-th/9502069] [INSPIRE].

[143] G.B. Gelmini, M. Gleiser and E.W. Kolb, *Cosmology of Biased Discrete Symmetry Breaking*, *Phys. Rev. D* **39** (1989) 1558 [INSPIRE].

[144] S.E. Larsson, S. Sarkar and P.L. White, *Evading the cosmological domain wall problem*, *Phys. Rev. D* **55** (1997) 5129 [hep-ph/9608319] [INSPIRE].

[145] S. Chang, C. Hagmann and P. Sikivie, *Studies of the motion and decay of axion walls bounded by strings*, *Phys. Rev. D* **59** (1999) 023505 [hep-ph/9807374] [INSPIRE].

[146] T. Hiramatsu, M. Kawasaki, K. Saikawa and T. Sekiguchi, *Axion cosmology with long-lived domain walls*, *JCAP* **01** (2013) 001 [arXiv:1207.3166] [INSPIRE].

[147] A. Ringwald and K. Saikawa, *Axion dark matter in the post-inflationary Peccei-Quinn symmetry breaking scenario*, *Phys. Rev. D* **93** (2016) 085031 [*Addendum ibid.* **94** (2016) 049908] [arXiv:1512.06436] [INSPIRE].

[148] A. Arvanitaki and A.A. Geraci, *Resonantly Detecting Axion-Mediated Forces with Nuclear Magnetic Resonance*, *Phys. Rev. Lett.* **113** (2014) 161801 [arXiv:1403.1290] [INSPIRE].

[149] M. Giannotti et al., *Stellar Recipes for Axion Hunters*, *JCAP* **10** (2017) 010 [arXiv:1708.02111] [INSPIRE].

[150] K. Saikawa, *A review of gravitational waves from cosmic domain walls*, *Universe* **3** (2017) 40 [arXiv:1703.02576] [INSPIRE].

[151] F. Ferrer et al., *Primordial Black Holes from the QCD axion*, *Phys. Rev. Lett.* **122** (2019) 101301 [arXiv:1807.01707] [INSPIRE].

[152] J. Lee, K. Murai, F. Takahashi and W. Yin, *More is different: multi-axion dynamics changes topological defect evolution*, *JCAP* **04** (2025) 002 [arXiv:2409.09749] [INSPIRE].

[153] J. Lee, K. Murai, F. Takahashi and W. Yin, *Resolving the QCD axion domain wall problem with a light axion*, *JHEP* **01** (2026) 124 [arXiv:2507.07075] [INSPIRE].

JCAP07(2026)060

[154] M. Gorghetto and E. Hardy, *Post-inflationary axions: a minimal target for axion haloscopes*, *JHEP* **05** (2023) 030 [arXiv:2212.13263] [INSPIRE].

[155] G. Pierobon et al., *Miniclusters from axion string simulations*, *JCAP* **05** (2026) 060 [arXiv:2307.09941] [INSPIRE].

[156] S. Chang and K. Choi, *Hadronic axion window and the big bang nucleosynthesis*, *Phys. Lett. B* **316** (1993) 51 [hep-ph/9306216] [INSPIRE].

[157] E. Masso, F. Rota and G. Zsembinszki, *On axion thermalization in the early universe*, *Phys. Rev. D* **66** (2002) 023004 [hep-ph/0203221] [INSPIRE].

[158] P. Graf and F.D. Steffen, *Thermal axion production in the primordial quark-gluon plasma*, *Phys. Rev. D* **83** (2011) 075011 [arXiv:1008.4528] [INSPIRE].

[159] C. Brust, D.E. Kaplan and M.T. Walters, *New Light Species and the CMB*, *JHEP* **12** (2013) 058 [arXiv:1303.5379] [INSPIRE].

[160] A. Salvio, A. Strumia and W. Xue, *Thermal axion production*, *JCAP* **01** (2014) 011 [arXiv:1310.6982] [INSPIRE].

[161] F. D'Eramo, L.J. Hall and D. Pappadopulo, *Multiverse Dark Matter: SUSY or Axions*, *JHEP* **11** (2014) 108 [arXiv:1409.5123] [INSPIRE].

[162] D. Baumann, D. Green and B. Wallisch, *New Target for Cosmic Axion Searches*, *Phys. Rev. Lett.* **117** (2016) 171301 [arXiv:1604.08614] [INSPIRE].

[163] R.Z. Ferreira and A. Notari, *Observable Windows for the QCD Axion Through the Number of Relativistic Species*, *Phys. Rev. Lett.* **120** (2018) 191301 [arXiv:1801.06090] [INSPIRE].

[164] F. D'Eramo, R.Z. Ferreira, A. Notari and J.L. Bernal, *Hot Axions and the H_0 tension*, *JCAP* **11** (2018) 014 [arXiv:1808.07430] [INSPIRE].

[165] F. Arias-Aragón et al., *Cosmic Imprints of XENON1T Axions*, *JCAP* **11** (2020) 025 [arXiv:2007.06579] [INSPIRE].

[166] F. Arias-Aragón et al., *Production of Thermal Axions across the ElectroWeak Phase Transition*, *JCAP* **03** (2021) 090 [arXiv:2012.04736] [INSPIRE].

[167] R.Z. Ferreira, A. Notari and F. Rompineve, *Dine-Fischler-Srednicki-Zhitnitsky axion in the CMB*, *Phys. Rev. D* **103** (2021) 063524 [arXiv:2012.06566] [INSPIRE].

[168] D. Green, Y. Guo and B. Wallisch, *Cosmological implications of axion-matter couplings*, *JCAP* **02** (2022) 019 [arXiv:2109.12088] [INSPIRE].

[169] F. D'Eramo, F. Hajkarim and S. Yun, *Thermal Axion Production at Low Temperatures: A Smooth Treatment of the QCD Phase Transition*, *Phys. Rev. Lett.* **128** (2022) 152001 [arXiv:2108.04259] [INSPIRE].

[170] F. D'Eramo, F. Hajkarim and S. Yun, *Thermal QCD Axions across Thresholds*, *JHEP* **10** (2021) 224 [arXiv:2108.05371] [INSPIRE].

[171] F. D'Eramo and S. Yun, *Flavor violating axions in the early Universe*, *Phys. Rev. D* **105** (2022) 075002 [arXiv:2111.12108] [INSPIRE].

[172] F. D'Eramo et al., *Cosmological bound on the QCD axion mass, redux*, *JCAP* **09** (2022) 022 [arXiv:2205.07849] [INSPIRE].

[173] L. Caloni, M. Gerbino, M. Lattanzi and L. Visinelli, *Novel cosmological bounds on thermally-produced axion-like particles*, *JCAP* **09** (2022) 021 [arXiv:2205.01637] [INSPIRE].

JCAP07(2026)060

[174] A. Notari, F. Rompineve and G. Villadoro, *Improved Hot Dark Matter Bound on the QCD Axion*, *Phys. Rev. Lett.* **131** (2023) 011004 [arXiv:2211.03799] [INSPIRE].

[175] F. Bianchini, G.G. di Cortona and M. Valli, *QCD axion: Some like it hot*, *Phys. Rev. D* **110** (2024) 123527 [arXiv:2310.08169] [INSPIRE].

[176] F. D'Eramo, F. Hajkarim and A. Lenoci, *Dark radiation from the primordial thermal bath in momentum space*, *JCAP* **03** (2024) 009 [arXiv:2311.04974] [INSPIRE].

[177] K. Bouzoud and J. Ghiglieri, *Thermal axion production at hard and soft momenta*, *JHEP* **01** (2025) 163 [arXiv:2404.06113] [INSPIRE].

[178] L. Caloni, P. Stengel, M. Lattanzi and M. Gerbino, *Constraining UV freeze-in of light relics with current and next-generation CMB observations*, *JCAP* **10** (2024) 106 [arXiv:2405.09449] [INSPIRE].

[179] F. D'Eramo and A. Lenoci, *Back to the phase space: Thermal axion dark radiation via couplings to standard model fermions*, *Phys. Rev. D* **110** (2024) 116028 [arXiv:2410.21253] [INSPIRE].

[180] M. Badziak and M. Laletin, *Precise predictions for the QCD axion contribution to dark radiation with full phase-space evolution*, *JHEP* **02** (2025) 108 [arXiv:2410.18186] [INSPIRE].

[181] M. Badziak, A. Gomułka, M. Laletin and K. Szafrański, *Improved cosmological constraints on axion-lepton interactions*, *Phys. Dark Univ.* **52** (2026) 102335 [arXiv:2511.14864] [INSPIRE].

[182] PLANCK collaboration, *Planck 2018 results. VI. Cosmological parameters*, *Astron. Astrophys.* **641** (2020) A6 [*Erratum ibid.* **652** (2021) C4] [arXiv:1807.06209] [INSPIRE].

[183] SIMONS OBSERVATORY collaboration, *The Simons Observatory: Science goals and forecasts*, *JCAP* **02** (2019) 056 [arXiv:1808.07445] [INSPIRE].

[184] CMB-S4 collaboration, *Snowmass 2021 CMB-S4 White Paper*, arXiv:2203.08024 [DOI:10.2172/1872087] [INSPIRE].

[185] L. Di Luzio, G. Martinelli and G. Piazza, *Breakdown of chiral perturbation theory for the axion hot dark matter bound*, *Phys. Rev. Lett.* **126** (2021) 241801 [arXiv:2101.10330] [INSPIRE].

[186] L. Di Luzio et al., *Axion-pion thermalization rate in unitarized NLO chiral perturbation theory*, *Phys. Rev. D* **108** (2023) 035025 [arXiv:2211.05073] [INSPIRE].

[187] P. Carenza et al., *Axion astrophysics*, *Phys. Rept.* **1117** (2025) 1 [arXiv:2411.02492] [INSPIRE].

[188] N. Iwamoto, *Axion Emission from Neutron Stars*, *Phys. Rev. Lett.* **53** (1984) 1198 [INSPIRE].

[189] G. Raffelt and D. Seckel, *Bounds on Exotic Particle Interactions from SN 1987a*, *Phys. Rev. Lett.* **60** (1988) 1793 [INSPIRE].

[190] J.R. Ellis and K.A. Olive, *Constraints on Light Particles From Supernova Sn1987a*, *Phys. Lett. B* **193** (1987) 525 [INSPIRE].

[191] M.S. Turner, *Axions from SN 1987a*, *Phys. Rev. Lett.* **60** (1988) 1797 [INSPIRE].

[192] R. Mayle et al., *Constraints on Axions from SN 1987A*, *Phys. Lett. B* **203** (1988) 188 [INSPIRE].

[193] R. Mayle et al., *Updated Constraints on Axions from SN 1987a*, *Phys. Lett. B* **219** (1989) 515 [INSPIRE].

[194] R.P. Brinkmann and M.S. Turner, *Numerical Rates for Nucleon-Nucleon Axion Bremsstrahlung*, *Phys. Rev. D* **38** (1988) 2338 [INSPIRE].

JCAP07(2026)060

[195] A. Burrows, M.S. Turner and R.P. Brinkmann, *Axions and SN 1987a*, *Phys. Rev. D* **39** (1989) 1020 [INSPIRE].

[196] A. Burrows, M.T. Ressell and M.S. Turner, *Axions and SN1987A: Axion Trapping*, *Phys. Rev. D* **42** (1990) 3297 [INSPIRE].

[197] H.-T. Janka, W. Keil, G. Raffelt and D. Seckel, *Nucleon spin fluctuations and the supernova emission of neutrinos and axions*, *Phys. Rev. Lett.* **76** (1996) 2621 [astro-ph/9507023] [INSPIRE].

[198] W. Keil et al., *A fresh look at axions and SN-1987A*, *Phys. Rev. D* **56** (1997) 2419 [astro-ph/9612222] [INSPIRE].

[199] C. Hanhart, D.R. Phillips and S. Reddy, *Neutrino and axion emissivities of neutron stars from nucleon-nucleon scattering data*, *Phys. Lett. B* **499** (2001) 9 [astro-ph/0003445] [INSPIRE].

[200] D.F.G. Fiorillo, A. Lella, C.A.J. O'Hare and E. Vitagliano, *Leading Bounds on Micrometer to Picometer Fifth Forces from Neutron Star Cooling*, *Phys. Rev. Lett.* **135** (2025) 211003 [arXiv:2506.19906] [INSPIRE].

[201] M. Buschmann et al., *Upper Limit on the QCD Axion Mass from Isolated Neutron Star Cooling*, *Phys. Rev. Lett.* **128** (2022) 091102 [arXiv:2111.09892] [INSPIRE].

[202] D.F.G. Fiorillo et al., *Supernova simulations confront SN 1987A neutrinos*, *Phys. Rev. D* **108** (2023) 083040 [arXiv:2308.01403] [INSPIRE].

[203] A. Caputo, G. Raffelt and E. Vitagliano, *Radiative transfer in stars by feebly interacting bosons*, *JCAP* **08** (2022) 045 [arXiv:2204.11862] [INSPIRE].

[204] D.F.G. Fiorillo, T. Pitik and E. Vitagliano, *Energy Transfer by Feebly Interacting Particles in Supernovae: The Trapping Regime*, *Phys. Rev. Lett.* **135** (2025) 071005 [arXiv:2503.13653] [INSPIRE].

[205] G. Raffelt and D. Seckel, *Multiple scattering suppression of the bremsstrahlung emission of neutrinos and axions in supernovae*, *Phys. Rev. Lett.* **67** (1991) 2605 [INSPIRE].

[206] M.S. Turner, *Dirac neutrinos and SN1987A*, *Phys. Rev. D* **45** (1992) 1066 [INSPIRE].

[207] G. Raffelt and D. Seckel, *A selfconsistent approach to neutral current processes in supernova cores*, *Phys. Rev. D* **52** (1995) 1780 [astro-ph/9312019] [INSPIRE].

[208] G. Raffelt and G. Sigl, *Numerical toy model calculation of the nucleon spin autocorrelation function in a supernova core*, *Phys. Rev. D* **60** (1999) 023001 [hep-ph/9808476] [INSPIRE].

[209] A. Sedrakian and A.E.L. Dieperink, *Coherent neutrino radiation in supernovae at two loops*, *Phys. Rev. D* **62** (2000) 083002 [astro-ph/0002228] [INSPIRE].

[210] E.N.E. van Dalen, A.E.L. Dieperink and J.A. Tjon, *Neutrino emission in neutron stars*, *Phys. Rev. C* **67** (2003) 065807 [nucl-th/0303037] [INSPIRE].

[211] G.I. Lykasov, C.J. Pethick and A. Schwenk, *A unified approach to structure factors and neutrino processes in nucleon matter*, *Phys. Rev. C* **78** (2008) 045803 [arXiv:0808.0330] [INSPIRE].

[212] J.H. Chang, R. Essig and S.D. McDermott, *Supernova 1987A Constraints on Sub-GeV Dark Sectors, Millicharged Particles, the QCD Axion, and an Axion-like Particle*, *JHEP* **09** (2018) 051 [arXiv:1803.00993] [INSPIRE].

[213] P. Carenza et al., *Improved axion emissivity from a supernova via nucleon-nucleon bremsstrahlung*, *JCAP* **10** (2019) 016 [*Erratum ibid.* **05** (2020) E01] [arXiv:1906.11844] [INSPIRE].

JCAP07(2026)060

[214] P. Carenza et al., *Enhanced Supernova Axion Emission and its Implications*, *Phys. Rev. Lett.* **126** (2021) 071102 [arXiv:2010.02943] [INSPIRE].

[215] K. Choi, H.J. Kim, H. Seong and C.S. Shin, *Axion emission from supernova with axion-pion-nucleon contact interaction*, *JHEP* **02** (2022) 143 [arXiv:2110.01972] [INSPIRE].

[216] S.-Y. Ho, J. Kim, P. Ko and J.-H. Park, *Supernova axion emissivity with $\Delta(1232)$ resonance in heavy baryon chiral perturbation theory*, *Phys. Rev. D* **107** (2023) 075002 [arXiv:2212.01155] [INSPIRE].

[217] A. Lella et al., *Protoneutron stars as cosmic factories for massive axionlike particles*, *Phys. Rev. D* **107** (2023) 103017 [arXiv:2211.13760] [INSPIRE].

[218] A. Lella et al., *Getting the most on supernova axions*, *Phys. Rev. D* **109** (2024) 023001 [arXiv:2306.01048] [INSPIRE].

[219] D.F.G. Fiorillo et al., *Axion-photon conversion in transient compact stars: Systematics, constraints, and opportunities*, *JCAP* **03** (2026) 053 [arXiv:2509.13322] [INSPIRE].

[220] T.E.O. Ericson and J.F. Mathiot, *Axion Emission from SN 1987a: Nuclear Physics Constraints*, *Phys. Lett. B* **219** (1989) 507 [INSPIRE].

[221] A. Schwenk, P. Jaikumar and C. Gale, *Neutrino bremsstrahlung in neutron matter from effective nuclear interactions*, *Phys. Lett. B* **584** (2004) 241 [nucl-th/0309072] [INSPIRE].

[222] A. Schwenk and B. Friman, *Polarization contributions to the spin dependence of the effective interaction in neutron matter*, *Phys. Rev. Lett.* **92** (2004) 082501 [nucl-th/0307089] [INSPIRE].

[223] P.S. Shternin, M. Baldo and P. Haensel, *In-medium enhancement of the modified Urca neutrino reaction rates*, *Phys. Lett. B* **786** (2018) 28 [arXiv:1807.06569] [INSPIRE].

[224] B. Fore and S. Reddy, *Pions in hot dense matter and their astrophysical implications*, *Phys. Rev. C* **101** (2020) 035809 [arXiv:1911.02632] [INSPIRE].

[225] T. Fischer et al., *Observable signatures of enhanced axion emission from protoneutron stars*, *Phys. Rev. D* **104** (2021) 103012 [arXiv:2108.13726] [INSPIRE].

[226] B. Fore, N. Kaiser, S. Reddy and N.C. Warrington, *Mass of charged pions in neutron-star matter*, *Phys. Rev. C* **110** (2024) 025803 [arXiv:2301.07226] [INSPIRE].

[227] T. Ericson and W. Weise, *Pions and nuclei*, Clarendon Press (1988).

[228] J.W. Brockway, E.D. Carlson and G.G. Raffelt, *SN1987A gamma-ray limits on the conversion of pseudoscalars*, *Phys. Lett. B* **383** (1996) 439 [astro-ph/9605197] [INSPIRE].

[229] J.A. Grifols, E. Massó and R. Toldrà, *Gamma-rays from SN1987A due to pseudoscalar conversion*, *Phys. Rev. Lett.* **77** (1996) 2372 [astro-ph/9606028] [INSPIRE].

[230] A. Payez et al., *Revisiting the SN1987A gamma-ray limit on ultralight axion-like particles*, *JCAP* **02** (2015) 006 [arXiv:1410.3747] [INSPIRE].

[231] F. Calore et al., *Bounds on axionlike particles from the diffuse supernova flux*, *Phys. Rev. D* **102** (2020) 123005 [arXiv:2008.11741] [INSPIRE].

[232] F. Calore et al., *3D template-based Fermi-LAT constraints on the diffuse supernova axion-like particle background*, *Phys. Rev. D* **105** (2022) 063028 [arXiv:2110.03679] [INSPIRE].

[233] S. Hoof and L. Schulz, *Updated constraints on axion-like particles from temporal information in supernova SN1987A gamma-ray data*, *JCAP* **03** (2023) 054 [arXiv:2212.09764] [INSPIRE].

[234] D.J. Forrest et al., *The gamma ray spectrometer for the Solar Maximum Mission*, *Solar Phys.* **65** (1980) 15.

JCAP07(2026)060

[235] E.L. Chupp, W.T. Vestrand and C. Reppin, *Experimental Limits on the Radiative Decay of SN1987A Neutrinos*, *Phys. Rev. Lett.* **62** (1989) 505 [INSPIRE].

[236] L. Oberauer, C. Hagner, G. Raffelt and E. Rieger, *Supernova bounds on neutrino radiative decays*, *Astropart. Phys.* **1** (1993) 377 [INSPIRE].

[237] C.A. Manzari, Y. Park, B.R. Safdi and I. Savoray, *Supernova Axions Convert to Gamma Rays in Magnetic Fields of Progenitor Stars*, *Phys. Rev. Lett.* **133** (2024) 211002 [arXiv:2405.19393] [INSPIRE].

[238] O. Graur et al., *LOSS Revisited. II. The Relative Rates of Different Types of Supernovae Vary between Low- and High-mass Galaxies*, *Astrophys. J.* **837** (2017) 121 [arXiv:1609.02923] [INSPIRE].

[239] X. Ma et al., *Supernovae at distances < 40 Mpc: I. Catalogues and fractions of supernovae in a complete sample*, *Astron. Astrophys.* **698** (2025) A305 [arXiv:2504.04393] [INSPIRE].

[240] F.R. Candón et al., *Stripped-Envelope Supernovae for QCD Axion Detection*, *Phys. Rev. Lett.* **136** (2026) 171001 [arXiv:2511.13815] [INSPIRE].

[241] T.M. Tauris, N. Langer and P. Podsiadlowski, *Ultra-stripped supernovae: progenitors and fate*, *Mon. Not. Roy. Astron. Soc.* **451** (2015) 2123 [arXiv:1505.00270] [INSPIRE].

[242] A. de la Chevrotière et al., *Searching for Magnetic Fields in 11 Wolf-Rayet Stars: Analysis of Circular Polarization Measurements from ESPaDOnS*, *Astrophys. J.* **781** (2014) 73.

[243] S. Hubrig et al., *Searching for a magnetic field in Wolf-Rayet stars using FORS 2 spectropolarimetry*, *Mon. Not. Roy. Astron. Soc.* **458** (2016) 3381 [arXiv:1603.01441].

[244] S. Hubrig, M. Schöller, A. Cikota and S.P. Järvinen, *The search for magnetic fields in two Wolf-Rayet stars and the discovery of a variable magnetic field in WR 55*, *Mon. Not. Roy. Astron. Soc. Lett.* **499** (2020) L116 [arXiv:2010.00983].

[245] S.P. Järvinen et al., *The magnetic, spectroscopic, and photometric variability of the Wolf–Rayet star WR 55*, *Mon. Not. Roy. Astron. Soc. Lett.* **524** (2023) L21 [arXiv:2306.05038].

[246] T. Shenar et al., *A massive helium star with a sufficiently strong magnetic field to form a magnetar*, *Science* **381** (2023) 761 [arXiv:2308.08591] [INSPIRE].

[247] I.K.W. Kleiser et al., *Peculiar Type II Supernovae from Blue Supergiants*, *Mon. Not. Roy. Astron. Soc.* **415** (2011) 372 [arXiv:1101.1298] [INSPIRE].

[248] T. Pessi et al., *Supernova rates and luminosity functions from ASAS-SN II: 2014–2017 core-collapse supernovae and their subtypes*, *Astron. Astrophys.* **703** (2025) A34 [arXiv:2508.10985] [INSPIRE].

[249] LIGO Scientific and Virgo collaborations, *GW170817: Observation of Gravitational Waves from a Binary Neutron Star Inspiral*, *Phys. Rev. Lett.* **119** (2017) 161101 [arXiv:1710.05832] [INSPIRE].

[250] LIGO Scientific et al. collaborations, *Multi-messenger Observations of a Binary Neutron Star Merger*, *Astrophys. J. Lett.* **848** (2017) L12 [arXiv:1710.05833] [INSPIRE].

[251] LIGO Scientific et al. collaborations, *Gravitational Waves and Gamma-rays from a Binary Neutron Star Merger: GW170817 and GRB 170817A*, *Astrophys. J. Lett.* **848** (2017) L13 [arXiv:1710.05834] [INSPIRE].

[252] LIGO Scientific and Virgo collaborations, *Properties of the binary neutron star merger GW170817*, *Phys. Rev. X* **9** (2019) 011001 [arXiv:1805.11579] [INSPIRE].

JCAP07(2026)060

[253] D.F.G. Fiorillo and F. Iocco, *Axions from neutron star mergers*, *Phys. Rev. D* **105** (2022) 123007 [INSPIRE].

[254] F. Lecce et al., *Probing axionlike particles with multimessenger observations of neutron star mergers*, *Phys. Rev. D* **112** (2025) 023001 [arXiv:2504.02032] [INSPIRE].

[255] F. Lecce et al., *Detecting light axions from supernovae in nearby galaxies*, arXiv:2512.04185 [INSPIRE].

[256] K. Abe et al., *Letter of Intent: The Hyper-Kamiokande Experiment — Detector Design and Physics Potential —*, arXiv:1109.3262 [INSPIRE].

[257] HYPER-KAMIOKANDE collaboration, *Hyper-Kamiokande Design Report*, arXiv:1805.04163 [INSPIRE].

[258] M. Cavan-Piton et al., *Probing the general axion-nucleon interaction in water Cherenkov experiments*, *JHEP* **07** (2025) 070 [arXiv:2503.17490] [INSPIRE].

[259] G. Lucente et al., *Axion signatures from supernova explosions through the nucleon electric-dipole portal*, *Phys. Rev. D* **105** (2022) 123020 [arXiv:2203.15812] [INSPIRE].

[260] G.G. Raffelt, *Astrophysical methods to constrain axions and other novel particle phenomena*, *Phys. Rept.* **198** (1990) 1 [INSPIRE].

[261] H. Georgi, D.B. Kaplan and L. Randall, *Manifesting the Invisible Axion at Low-energies*, *Phys. Lett. B* **169** (1986) 73 [INSPIRE].

[262] R.M. Bionta et al., *Observation of a Neutrino Burst in Coincidence with Supernova SN 1987a in the Large Magellanic Cloud*, *Phys. Rev. Lett.* **58** (1987) 1494 [INSPIRE].

[263] IMB collaboration, *Angular Distribution of Events From Sn1987a*, *Phys. Rev. D* **37** (1988) 3361 [INSPIRE].

[264] KAMIOKANDE-II collaboration, *Observation of a Neutrino Burst from the Supernova SN 1987a*, *Phys. Rev. Lett.* **58** (1987) 1490 [INSPIRE].

[265] K.S. Hirata et al., *Observation in the Kamiokande-II Detector of the Neutrino Burst from Supernova SN 1987a*, *Phys. Rev. D* **38** (1988) 448 [INSPIRE].

[266] E.N. Alekseev, L.N. Alekseeva, V.I. Volchenko and I.V. Krivosheina, *Possible Detection of a Neutrino Signal on 23 February 1987 at the Baksan Underground Scintillation Telescope of the Institute of Nuclear Research*, *JETP Lett.* **45** (1987) 589 [INSPIRE].

[267] E.N. Alekseev, L.N. Alekseeva, I.V. Krivosheina and V.I. Volchenko, *Detection of the Neutrino Signal From SN1987A in the LMC Using the Inr Baksan Underground Scintillation Telescope*, *Phys. Lett. B* **205** (1988) 209 [INSPIRE].

[268] M. Cavan-Piton, *Novel strategies for new low-mass particles searches at Colliders and from Stellar Objects*, Ph.D. thesis, Université Savoie Mont Blanc, France (2025).

[269] M. Hempel and J. Schaffner-Bielich, *Statistical Model for a Complete Supernova Equation of State*, *Nucl. Phys. A* **837** (2010) 210 [arXiv:0911.4073] [INSPIRE].

[270] M. Cavan-Piton et al., *Axion Emission from Strange Matter in Core-Collapse SNe*, *Phys. Rev. Lett.* **133** (2024) 121002 [arXiv:2401.10979] [INSPIRE].

[271] CAST collaboration, *New Upper Limit on the Axion-Photon Coupling with an Extended CAST Run with a Xe-Based Micromegas Detector*, *Phys. Rev. Lett.* **133** (2024) 221005 [arXiv:2406.16840] [INSPIRE].

JCAP07(2026)060

[272] IAXO collaboration, *Conceptual design of BabyIAXO, the intermediate stage towards the International Axion Observatory*, *JHEP* **05** (2021) 137 [arXiv:2010.12076] [INSPIRE].

[273] B. Aja et al., *The Canfranc Axion Detection Experiment (CADEx): search for axions at 90 GHz with Kinetic Inductance Detectors*, *JCAP* **11** (2022) 044 [arXiv:2206.02980] [INSPIRE].

[274] B. Aja et al., *The CADEx Experiment: A new haloscope axion search in the 330–460 micro-eV mass range at the Canfranc Underground Laboratory (LSC)*, *PoS* **COSMICWISPers2024** (2025) 039 [INSPIRE].

[275] P.G. Catinari, A. Esposito and S. Pavaskar, *Hunting axion dark matter with antiferromagnets: A case study with nickel oxide*, *Phys. Rev. D* **112** (2025) 035007 [arXiv:2411.11971] [INSPIRE].

[276] X. Fan et al., *Highly excited electron cyclotron for QCD axion and dark-photon detection*, *Phys. Rev. D* **111** (2025) 075022 [arXiv:2410.05549] [INSPIRE].

[277] Y. Grossman, B. Yu and S. Zhou, *Axion forces in axion backgrounds*, *JHEP* **01** (2026) 145 [arXiv:2504.00104] [INSPIRE].

[278] R. Barbieri et al., *Searching for galactic axions through magnetized media: the QUAX proposal*, *Phys. Dark Univ.* **15** (2017) 135 [arXiv:1606.02201] [INSPIRE].

[279] QUAX collaboration, *Search for galactic axions with a traveling wave parametric amplifier*, *Phys. Rev. D* **108** (2023) 062005 [arXiv:2304.07505] [INSPIRE].

[280] QUAX collaboration, *Search for axion dark matter with the QUAX–LNF tunable haloscope*, *Phys. Rev. D* **110** (2024) 022008 [arXiv:2402.19063] [INSPIRE].

[281] M. Lawson et al., *Tunable axion plasma haloscopes*, *Phys. Rev. Lett.* **123** (2019) 141802 [arXiv:1904.11872] [INSPIRE].

[282] ALPHA collaboration, *Searching for dark matter with plasma haloscopes*, *Phys. Rev. D* **107** (2023) 055013 [arXiv:2210.00017] [INSPIRE].

[283] BREAD collaboration, *Broadband Solenoidal Haloscope for Terahertz Axion Detection*, *Phys. Rev. Lett.* **128** (2022) 131801 [arXiv:2111.12103] [INSPIRE].

[284] J. Chiles et al., *New Constraints on Dark Photon Dark Matter with Superconducting Nanowire Detectors in an Optical Haloscope*, *Phys. Rev. Lett.* **128** (2022) 231802 [arXiv:2110.01582] [INSPIRE].

[285] ARIADNE collaboration, *Progress on the ARIADNE axion experiment*, *Springer Proc. Phys.* **211** (2018) 151 [arXiv:1710.05413] [INSPIRE].

[286] A. Mitridate, T. Trickle, Z. Zhang and K.M. Zurek, *Detectability of Axion Dark Matter with Phonon Polaritons and Magnons*, *Phys. Rev. D* **102** (2020) 095005 [arXiv:2005.10256] [INSPIRE].

[287] A. Berlin, A.J. Millar, T. Trickle and K. Zhou, *Physical signatures of fermion-coupled axion dark matter*, *JHEP* **05** (2024) 314 [arXiv:2312.11601] [INSPIRE].

[288] A. Arvanitaki et al., *Detecting the QCD Axion via the Ferroaxionic Force with Piezoelectric Materials*, *Phys. Rev. Lett.* **136** (2026) 081803 [arXiv:2411.10516] [INSPIRE].

[289] D. Autiero et al., *The CAST Time Projection Chamber*, *New J. Phys.* **9** (2007) 171 [physics/0702189] [INSPIRE].

[290] P. Abbon et al., *The micromegas detector of the CAST experiment*, *New J. Phys.* **9** (2007) 170 [physics/0702190] [INSPIRE].

JCAP07(2026)060

[291] M. Kuster et al., *The X-ray Telescope of CAST*, *New J. Phys.* **9** (2007) 169 [physics/0702188] [INSPIRE].

[292] C. Krieger, J. Kaminski, M. Lupberger and K. Desch, *A GridPix-based X-ray detector for the CAST experiment*, *Nucl. Instrum. Meth. A* **867** (2017) 101 [INSPIRE].

[293] K. van Bibber, P.M. McIntyre, D.E. Morris and G.G. Raffelt, *A Practical Laboratory Detector for Solar Axions*, *Phys. Rev. D* **39** (1989) 2089 [INSPIRE].

[294] CAST collaboration, *New solar axion search using the CERN Axion Solar Telescope with ^{4}He filling*, *Phys. Rev. D* **92** (2015) 021101 [arXiv:1503.00610] [INSPIRE].

[295] CAST collaboration, *Search for Sub-eV Mass Solar Axions by the CERN Axion Solar Telescope with ^{3}He Buffer Gas*, *Phys. Rev. Lett.* **107** (2011) 261302 [arXiv:1106.3919] [INSPIRE].

[296] CAST collaboration, *Search for Solar Axions by the CERN Axion Solar Telescope with ^{3}He Buffer Gas: Closing the Hot Dark Matter Gap*, *Phys. Rev. Lett.* **112** (2014) 091302 [arXiv:1307.1985] [INSPIRE].

[297] CAST collaboration, *Determination of effective axion masses in the helium-3 buffer of CAST*, in the proceedings of the *2011 IEEE Nuclear Science Symposium and Medical Imaging Conference*, Valencia, Spain, October 23–29 (2011) [DOI:10.1109/NSSMIC.2011.6154466] [INSPIRE].

[298] G.G. Raffelt, *Stars as laboratories for fundamental physics: The astrophysics of neutrinos, axions, and other weakly interacting particles*, University of Chicago Press (1996), [ISBN 978-0-226-70272-8].

[299] IAXO collaboration, *An accurate solar axions ray-tracing response of BabyIAXO*, *JHEP* **02** (2025) 159 [arXiv:2411.13915] [INSPIRE].

[300] T. Dafni et al., *Weighing the solar axion*, *Phys. Rev. D* **99** (2019) 035037 [arXiv:1811.09290] [INSPIRE].

[301] ADMX collaboration, *A Search for Invisible Axion Dark Matter with the Axion Dark Matter Experiment*, *Phys. Rev. Lett.* **120** (2018) 151301 [arXiv:1804.05750] [INSPIRE].

[302] ADMX collaboration, *Extended Search for the Invisible Axion with the Axion Dark Matter Experiment*, *Phys. Rev. Lett.* **124** (2020) 101303 [arXiv:1910.08638] [INSPIRE].

[303] ADMX collaboration, *Search for Invisible Axion Dark Matter in the 3.3–4.2 μeV Mass Range*, *Phys. Rev. Lett.* **127** (2021) 261803 [arXiv:2110.06096] [INSPIRE].

[304] J. Kim et al., *Near-Quantum-Noise Axion Dark Matter Search at CAPP around 9.5 μeV*, *Phys. Rev. Lett.* **130** (2023) 091602 [arXiv:2207.13597] [INSPIRE].

[305] CAPP collaboration, *Extensive Search for Axion Dark Matter over 1 GHz with CAPP'S Main Axion Experiment*, *Phys. Rev. X* **14** (2024) 031023 [arXiv:2402.12892] [INSPIRE].

[306] HAYSTAC collaboration, *Results from phase 1 of the HAYSTAC microwave cavity axion experiment*, *Phys. Rev. D* **97** (2018) 092001 [arXiv:1803.03690] [INSPIRE].

[307] HAYSTAC collaboration, *A quantum-enhanced search for dark matter axions*, *Nature* **590** (2021) 238 [arXiv:2008.01853] [INSPIRE].

[308] HAYSTAC collaboration, *New results from HAYSTAC's phase II operation with a squeezed state receiver*, *Phys. Rev. D* **107** (2023) 072007 [arXiv:2301.09721] [INSPIRE].

[309] HAYSTAC collaboration, *Dark Matter Axion Search with HAYSTAC Phase II*, *Phys. Rev. Lett.* **134** (2025) 151006 [arXiv:2409.08998] [INSPIRE].

JCAP07(2026)060

[310] GigaBREAD collaboration, *First Axionlike Particle Results from a Broadband Search for Wavelike Dark Matter in the 44 to 52 μeV Range with a Coaxial Dish Antenna*, *Phys. Rev. Lett.* **134** (2025) 171002 [arXiv:2501.17119] [INSPIRE].

[311] T. Grenet et al., *The Grenoble Axion Haloscope platform (GrAHal): development plan and first results*, arXiv:2110.14406 [INSPIRE].

[312] MADMAX collaboration, *First Search for Axion Dark Matter with a MADMAX Prototype*, *Phys. Rev. Lett.* **135** (2025) 041001 [arXiv:2409.11777] [INSPIRE].

[313] ORGAN collaboration, *The ORGAN Experiment: An axion haloscope above 15 GHz*, *Phys. Dark Univ.* **18** (2017) 67 [arXiv:1706.00209] [INSPIRE].

[314] ORGAN collaboration, *Limits on Dark Photons, Scalars, and Axion-Electromagnetodynamics with the ORGAN Experiment*, *Annalen Phys.* **536** (2024) 2200622 [arXiv:2212.01971] [INSPIRE].

[315] ORGAN collaboration, *Direct search for dark matter axions excluding ALP cogenesis in the 63- to 67-μeV range with the ORGAN experiment*, *Sci. Adv.* **8** (2022) abq3765 [arXiv:2203.12152] [INSPIRE].

[316] ORGAN collaboration, *Near-quantum-limited axion dark matter search with the ORGAN experiment around 26 μeV*, *Phys. Rev. D* **111** (2025) 095007 [arXiv:2407.18586] [INSPIRE].

[317] CAST collaboration, *First results of the CAST-RADES haloscope search for axions at 34.67 μeV*, *JHEP* **10** (2020) 075 [arXiv:2104.13798] [INSPIRE].

[318] S. Ahyoune et al., *RADES axion search results with a high-temperature superconducting cavity in an 11.7 T magnet*, *JHEP* **04** (2025) 113 [arXiv:2403.07790] [INSPIRE].

[319] TASEH collaboration, *First Results from the Taiwan Axion Search Experiment with a Haloscope at 19.6 μeV*, *Phys. Rev. Lett.* **129** (2022) 111802 [arXiv:2205.05574] [INSPIRE].

[320] S. De Panfilis et al., *Limits on the Abundance and Coupling of Cosmic Axions at* $4.5 < m_a < 5.0\,\mu eV$, *Phys. Rev. Lett.* **59** (1987) 839 [INSPIRE].

[321] W. Wuensch et al., *Results of a Laboratory Search for Cosmic Axions and Other Weakly Coupled Light Particles*, *Phys. Rev. D* **40** (1989) 3153 [INSPIRE].

[322] C. Hagmann et al., *First results from a second generation galactic axion experiment*, *Nucl. Phys. B Proc. Suppl.* **51** (1996) 209 [astro-ph/9607022] [INSPIRE].

[323] B.T. McAllister, A.P. Quiskamp and M.E. Tobar, *Tunable rectangular resonant cavities for axion haloscopes*, *Phys. Rev. D* **109** (2024) 015013 [arXiv:2309.12098] [INSPIRE].

[324] A. Quiskamp et al., *Exclusion of Axionlike-Particle Cogenesis Dark Matter in a Mass Window above 100 μeV*, *Phys. Rev. Lett.* **132** (2024) 031601 [arXiv:2310.00904] [INSPIRE].

[325] P.K. Day et al., *A broadband superconducting detector suitable for use in large arrays*, *Nature* **425** (2003) 817 [INSPIRE].

[326] V. Rollano et al., *Dark characterization of Ti/Al LEKIDs for the search of axions in the W-band*, arXiv:2510.01913 [INSPIRE].

[327] F. Bajjali et al., *First results from BRASS-p broadband searches for hidden photon dark matter*, *JCAP* **08** (2023) 077 [arXiv:2306.05934] [INSPIRE].

[328] J. De Miguel, *A dark matter telescope probing the 6 to 60 GHz band*, *JCAP* **04** (2021) 075 [arXiv:2003.06874] [INSPIRE].

JCAP07(2026)060

[329] J.-X. Qiu et al., *Observation of the axion quasiparticle in 2D $MnBi_2Te_4$*, *Nature* **641** (2025) 62 [arXiv:2504.12572] [INSPIRE].

[330] F. Wilczek, *Two Applications of Axion Electrodynamics*, *Phys. Rev. Lett.* **58** (1987) 1799 [INSPIRE].

[331] R. Li, J. Wang, X. Qi and S.-C. Zhang, *Dynamical Axion Field in Topological Magnetic Insulators*, *Nature Phys.* **6** (2010) 284 [arXiv:0908.1537] [INSPIRE].

[332] J. Zhang et al., *Large Dynamical Axion Field in Topological Antiferromagnetic Insulator $Mn_2Bi_2Te_5$*, *Chin. Phys. Lett.* **37** (2020) 077304 [arXiv:1906.07891] [INSPIRE].

[333] X.-L. Qi, T. Hughes and S.-C. Zhang, *Topological Field Theory of Time-Reversal Invariant Insulators*, *Phys. Rev. B* **78** (2008) 195424 [arXiv:0802.3537] [INSPIRE].

[334] A.M. Essin, J.E. Moore and D. Vanderbilt, *Magnetoelectric polarizability and axion electrodynamics in crystalline insulators*, *Phys. Rev. Lett.* **102** (2009) 146805 [arXiv:0810.2998] [INSPIRE].

[335] D.M. Nenno et al., *Axion physics in condensed-matter systems*, *Nature Rev. Phys.* **2** (2020) 682 [INSPIRE].

[336] A. Sekine and K. Nomura, *Axion Electrodynamics in Topological Materials*, *J. Appl. Phys.* **129** (2021) 141101 [arXiv:2011.13601] [INSPIRE].

[337] M.M. Otrokov et al., *Prediction and observation of an antiferromagnetic topological insulator*, *Nature* **576** (2019) 416 [arXiv:1809.07389] [INSPIRE].

[338] C.P. Hofmann, *Spin wave scattering in the effective Lagrangian perspective*, *Phys. Rev. B* **60** (1999) 388 [cond-mat/9805277] [INSPIRE].

[339] J. Schütte-Engel et al., *Axion quasiparticles for axion dark matter detection*, *JCAP* **08** (2021) 066 [arXiv:2102.05366] [INSPIRE].

[340] A.I. Kakhidze and I.V. Kolokolov, *Antiferromagnetic axions detector*, *Sov. Phys. JETP* **72** (1991) 598 [INSPIRE].

[341] D.J.E. Marsh et al., *Proposal to Detect Dark Matter using Axionic Topological Antiferromagnets*, *Phys. Rev. Lett.* **123** (2019) 121601 [arXiv:1807.08810] [INSPIRE].

[342] S. Chigusa, T. Moroi and K. Nakayama, *Axion/hidden-photon dark matter conversion into condensed matter axion*, *JHEP* **08** (2021) 074 [arXiv:2102.06179] [INSPIRE].

[343] A.J. Millar, G.G. Raffelt, J. Redondo and F.D. Steffen, *Dielectric Haloscopes to Search for Axion Dark Matter: Theoretical Foundations*, *JCAP* **01** (2017) 061 [arXiv:1612.07057] [INSPIRE].

[344] S.P. Bayrakci et al., *Lifetimes of Antiferromagnetic Magnons in Two and Three Dimensions: Experiment, Theory, and Numerics*, *Phys. Rev. Lett.* **111** (2013) 017204.

[345] C. O'Hare, *cajohare/AxionLimits: AxionLimits*, https://cajohare.github.io/AxionLimits/, (2020) [DOI:10.5281/zenodo.3932430].

JCAP07(2026)060